

FREEDOM

Fast Response Enemy Emulating Defense Operations Missile
Providing Superior Emulation Aiding the DoD to Keep
America and its Allies Safe and Free



AIAA Graduate Missile Systems Design Competition 2019-2020



Nicholas Stefan

AIAA Member Number: 1025302



Mehdi Pedari

AIAA Member Number: 595097



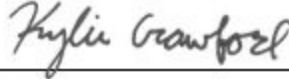
Jacquelyn Rech

AIAA Member Number: 1025489



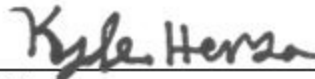
Kylie Crawford

AIAA Member Number: 1025472



Kyle Herda

AIAA Member Number: 808574



Faculty Advisor:

Dr. Ronald Barrett

AIAA Member Number: 022393



Acknowledgment

The authors wish to thank Dr. Saeed Farokhi, Dr. Ray Taghavi, Dr. Shawn Keshmiri, Lauren Schumacher, and Arno Prinsloo for their advisement on the design of the FREEDOM. The designers thank Eugene L. Fleeman for his consultation and for sharing his design spreadsheet. A special thank you is extended to Dr. Ronald Barrett-Gonzalez for his advisement, teaching, and insight through the entire process of the design of the FREEDOM.

Abstract

The goal of the following report was to demonstrate the preliminary design of the FREEDOM. The FREEDOM is a technologically advanced target drone designed to aid the military in defense training. These target drones simulate enemy aerial threats that they can practice taking out, so they are prepared to protect their citizens at any moment. The design of the FREEDOM was based on the mission requirements from the RFP (Ref. 1). This target drone has two stages using an Orion 50XL solid rocket booster and a Launcher E2 rocket engine. The FREEDOM features small fins at a cant angle of 2.7 degrees for a constant roll rate, which the team designed to execute a complicated system to take down. The FREEDOM has a takeoff weight of 19,000 pounds. Without including the booster, the FREEDOM has a diameter of 3 feet and a length of 40 feet.

Table of Contents

<u>Section</u>	<u>Page #</u>
ACKNOWLEDGMENT.....	ii
LIST OF SYMBOLS	vii
1. MISSION SPECIFICATION AND PROFILES.....	1
1.1 MISSION SPECIFICATION	2
1.2 MISSION PROFILE, PERFORMANCE, PAYLOAD-RANGE REQUIREMENTS	3
1.3 OVERALL DESIGN METHODS AND PROCESS	4
1.4 CONCLUSIONS AND RECOMMENDATIONS.....	4
2. HISTORICAL REVIEW.....	5
2.1 HISTORY OF MISSILES AND TARGET DRONES	5
2.2 CONCLUSIONS AND RECOMMENDATIONS.....	6
3. DESIGN VECTOR AND WEIGHTS ESTABLISHMENT.....	7
3.1 EXPERT DESIGN INPUT FOR OBJECTIVE FUNCTION VERIFICATION	7
3.2 OBJECTIVE FUNCTION	7
3.3 CONCLUSIONS AND RECOMMENDATIONS.....	7
4. STAMPED ANALYSIS	8
4.1 THE STAMPED ANALYSIS TECHNIQUE	8
4.2 ESTIMATION OF MAJOR DESIGN VARIABLES	8
4.3 CONCLUSIONS AND RECOMMENDATIONS.....	12
5. WEIGHT SIZING.....	13
5.1 AAA WEIGHT ESTIMATION.....	13
5.2 EMPTY TO TAKEOFF WEIGHT RATIO	13
5.3 PRELIMINARY DESIGN WEIGHTS SIZING	14
5.4 CONCLUSIONS AND RECOMMENDATIONS.....	15
6. WING AND POWER PLANT SIZING	16
6.1 DRAG POLAR ESTIMATION	16
6.2 SIZING CHARTS ANALYSIS.....	17
6.4 CONCLUSIONS AND RECOMMENDATIONS.....	18
7. CLASS I CONFIGURATION MATRIX AND INITIAL DOWNSELECTION.....	20
7.1 MAJOR IMPACT ON THE DESIGN	20
7.2 COMPARATIVE STUDY OF A MISSILE WITH A SIMILAR PERFORMANCE.....	20
7.3 CONFIGURATION SWEEP AND SELECTION.....	20
7.3.1 CONCEPT OPERATIONS	20
7.3.2 SELECTION OF THE OVERALL CONFIGURATION.....	21
7.4 CONCLUSIONS AND RECOMMENDATIONS.....	22
8. LAYOUT OF THE COCKPIT AND THE FUSELAGE.....	23
8.1 LAYOUT OF THE INTERIOR COMPONENTS.....	23
8.2 LAYOUT DESIGN OF THE FUSELAGE	24
8.3 CONCLUSIONS AND RECOMMENDATIONS.....	24
9. LAYOUT DESIGN OF THE PROPULSION INSTALLATION	25
9.1 SELECTION AND LAYOUT OF THE PROPULSION INSTALLATION.....	27
9.2 CONCLUSIONS AND RECOMMENDATIONS.....	27
10. CLASS I LAYOUT DESIGN OF THE WING	28
10.1 BODY LIFT VALIDATION	28
10.2 CONCLUSIONS AND RECOMMENDATIONS.....	28
11. CLASS I DESIGN OF HIGH LIFT DEVICES.....	29
11.1 DESIGN OF HIGH LIFT DEVICES	29
11.2 CONCLUSIONS AND RECOMMENDATIONS.....	29
12. CLASS I DESIGN OF THE EMPENNAGE.....	30
12.1 EMPENNAGE DESIGN PROCEDURE	30
12.2 SUMMARY OF EMPENNAGE DESIGN AND CHARACTERISTICS	31
12.3 CONCLUSIONS AND RECOMMENDATIONS.....	32
13. CLASS I DESIGN OF THE LAUNCH AND RECOVERY SYSTEM	33
13.1 LAUNCH SYSTEM	33
13.2 RECOVERY	34
13.3 CONCLUSIONS AND RECOMMENDATIONS.....	34
14. CLASS I WEIGHT AND BALANCE ANALYSIS	35
14.1 PRELIMINARY THREE-VIEW	35

14.2 CLASS I WEIGHTS BREAKDOWN	36
14.3 CLASS I WEIGHT AND BALANCE CALCULATION	36
14.4 CLASS I C.G. EXCURSION DIAGRAM	37
14.5 CONCLUSIONS AND RECOMMENDATIONS.....	38
15. V-n DIAGRAM.....	39
15.1 V-n CALCULATIONS AND DIAGRAM	39
15.2 GUST SPECTRUM ANALYSIS, DYNAMIC LOADING, AND FLIGHT PATH DEVIATIONS	40
15.3 CONCLUSIONS AND RECOMMENDATIONS.....	41
16. CLASS I STABILITY AND CONTROL ANALYSIS	42
16.1 STABILITY AND CONTROL ANALYSIS	42
16.2 CONCLUSIONS AND RECOMMENDATIONS.....	42
17. CLASS I DRAG POLAR AND PERFORMANCE ANALYSIS	43
17.1 WETTED AREA BREAKDOWN.....	43
17.2 DRAG POLAR ANALYSIS	44
17.3 CONCLUSIONS AND RECOMMENDATIONS.....	45
18. ANALYSIS OF WEIGHT AND BALANCE, STABILITY AND CONTROL, AND L/D	46
18.1 IMPACT OF WEIGHT AND BALANCE AND STABILITY AND CONTROL RESULTS.....	46
18.2 ANALYSIS OF CRITICAL L/D RESULTS.....	46
18.3 DESIGN ITERATIONS PERFORMED	47
18.4 CONCLUSIONS AND RECOMMENDATIONS.....	47
19. PRELIMINARY THREE-VIEW	48
19.1 TABLE OF CLASS I AIRCRAFT CHARACTERISTICS	48
19.2 CLASS I AIRCRAFT DESCRIPTION	48
19.3 ACTION VIEWS.....	50
20. LIST OF MAJOR SYSTEMS AND GHOST VIEWS.....	52
20.1 LIST OF MAJOR SYSTEMS.....	52
20.2 DESCRIPTION OF FLIGHT CONTROL SYSTEM.....	52
20.3 DESCRIPTION OF FUELS SYSTEM	54
20.4 DESCRIPTION OF THE ELECTRICAL SYSTEM	56
20.5 DESCRIPTION OF THE HYDRAULIC SYSTEM	57
20.6 STAGING SYSTEM.....	57
20.7 CONFLICT ANALYSIS.....	58
20.8 CONCLUSIONS AND RECOMMENDATIONS.....	58
21. CLASS II SIZING OF RECOVERY SYSTEMS.....	59
21.1 DESCRIPTION OF MAJOR RECOVERY SYSTEM COMPONENTS AND DISPOSITION.....	59
21.2 CAD OF RECOVERY SYSTEM.....	61
21.3 CONCLUSIONS AND RECOMMENDATIONS.....	61
22. INITIAL STRUCTURAL ARRANGEMENT.....	62
22.1 LAYOUT OF STRUCTURAL COMPONENTS.....	62
22.2 CAD DRAWINGS OF STRUCTURAL LAYOUT.....	65
22.3 CONCLUSIONS AND RECOMMENDATIONS.....	65
23. CLASS II WEIGHT AND BALANCE.....	66
23.1 CLASS II WEIGHT AND BALANCE CALCULATIONS.....	66
23.2 CLASS II CG POSITIONS ON THE AIRFRAME, CG EXCURSION.....	66
23.3 CONCLUSIONS AND RECOMMENDATIONS.....	67
24. CLASS II WEIGHT AND BALANCE.....	69
24.1 CLASS II WEIGHT AND BALANCE ANALYSIS.....	69
24.2 CONCLUSIONS AND RECOMMENDATIONS.....	69
25. UPDATED 3-VIEW AND AIRCRAFT FAMILY SUMMARY	70
25.1 UPDATED 3-VIEW AND SALIENT CHARACTERISTICS	70
25.2 THE FREEDOM MISSILE FAMILY.....	70
25.3 CONCLUSIONS AND RECOMMENDATIONS.....	70
26. ADVANCED TECHNOLOGIES.....	72
26.1 ADVANCED TECHNOLOGY SWEEP.....	72
26.2 CONCLUSIONS AND RECOMMENDATIONS.....	72
2.....	72
27. RISK MITIGATION	73
27.1 RISK MITIGATION SUMMARY.....	73
27.2 CONCLUSIONS AND RECOMMENDATIONS.....	73
28. MANUFACTURING PLAN.....	74

28.1 EXPLODED VIEW	74
28.2 BILL OF MATERIALS	74
28.3 FABRICATION AND ASSEMBLY PROCESS	75
28.4 FUTURE VARIANT ASSEMBLY CONSIDERATIONS.....	76
28.4 CONCLUSIONS AND RECOMMENDATIONS	76
29. COST ANALYSIS	77
29.1 COST ANALYSIS SUMMARY	77
29.2 CONCLUSIONS AND RECOMMENDATIONS.....	77
30. CLASS II STABILITY AND CONTROL	78
30.1 CLASS II STABILITY AND CONTROL ANALYSIS.....	78
30.2 CONCLUSIONS AND RECOMMENDATIONS.....	78
31. ADVANCED PERFORMANCE	79
31.1 ADVANCED PERFORMANCE ANALYSIS.....	79
31.2 CONCLUSIONS AND RECOMMENDATIONS.....	82
32. SPECIFICATION COMPLIANCE.....	83
33. MARKETING PLAN AND PATH FORWARD.....	84
33.1 MARKETING PLAN.....	84
33.2 PATH FORWARD	84
33.3 CONCLUSIONS AND RECOMMENDATIONS.....	84
REFERENCES.....	85

List of Figures

Figure 1.1: High Altitude Flight Profile.....	3
Figure 1.2: Low Altitude Flight Profile.....	3
Figure 1.3: Payload Range Diagram.....	4
Figure 2.1: V-2 Missile (Ref. 13).....	5
Figure 2.3: BQM-34A Firebee (Ref. 18)	5
Figure 2.2: SM-64 Navaho (Ref. 16).....	5
Figure 2.4: GQM-163A Coyote (Ref. 21).....	6
Figure 4.1: STAMPED Empty to Takeoff Weight Trends.....	9
Figure 4.2: STAMPED Parasite Drag Coefficient Trends	9
Figure 4.3: STAMPED Thrust to Takeoff Weight Coefficient Trends	10
Figure 4.4: STAMPED Primary Wing Area Trends.....	11
Figure 4.5: STAMPED Wing Loading Trends.....	11
Figure 4.6: STAMPED Maximum Lift to Drag Ratio Trends	12
Figure 6.1: Drag Polar Graph.....	17
Figure 6.2: Sizing Chart of the FREEDOM Design	19
Figure 7.1: High Profile Operation (Refs. 31 and 32).....	21
Figure 7.2: Low Profile Operations (Refs. 31 and 32).....	21
Figure 7.3: Configuration Sweep (Not to Scale).....	22
Figure 8.1: Payload Component Layout: 3-View and Isometric All Dimensions in Inches (Scale: 1:20)	23
Figure 8.2: Payload Integration: 3-View and Isometric All Dimensions in Inches (Scale: 1:200).....	24
Figure 8.3: Missile Fuselage: 3-View and Isometric All Dimensions in Inches (Scale: 1:125)	24
Figure 9.1: Orion 50 XL (Ref. 27).....	25
Figure 9.2: Launcher E-2 engine testing (Ref. 36)	26
Figure 9.3: Missile Powerplant Layout: 3-View and Isometric All Dimensions in Inches (Scale: 1:125).....	27
Figure 9.4: SRM Booster: 3-View and Isometric All Dimensions in Inches (Scale: 1:200).....	27
Figure 12.1: Empennage Cross Section with Booster (Scale 1:125).....	30
Figure 12.2: Empennage Cross Section without Booster (Scale 1:100).....	30
Figure 12.4: Integrated Fin Layout: 3-View and Isometric All Dimensions in Inches (Scale: 1:100)	32
Figure 12.3: Fin Layout: Detail View	32
Figure 13.1: Vertical Launch System: 3-View and Isometric. All Dimensions in Inches (Scale 1:500).....	33
Figure 13.2: Stored Launch System: 3-View and Isometric. All Dimensions in Inches (Scale 1:250).....	34
Figure 13.3: Mid-Angled Launch System: 3-View and Isometric. All Dimensions in Inches (Scale 1:500).....	34

Figure 14.1: Three View of the Freedom: All Dimensions in Inches (Scale 1:125).....	35
Figure 14.2: Component C.G. Locations: Side and Front Views (Scale 1:200).....	36
Figure 14.3: Weight C.G. Excursion Diagram: Booster Phase.....	37
Figure 14.4: Weight C.G. Excursion Diagram: Rocket Engine Phase.....	38
Figure 15.1: V-n Diagram.....	39
Figure 15.2: Gust Loading: Vertical Acceleration.....	40
Figure 15.3: Gust Loading: Lateral Acceleration.....	40
Figure 15.5: Gust Loading: Lateral Displacement.....	41
Figure 15.4: Gust Loading: Vertical Displacement.....	41
Figure 17.2: Perimeter Plot without Booster.....	43
Figure 17.1: Perimeter Plot with Booster.....	43
Figure 17.3: Fuselage Cross Sections: All Dimensions in Inches (Scale 1:125).....	44
Figure 17.4: Class I Drag Polar at Sea Level.....	45
Figure 17.5: Class I Drag Polar at 65,000 Feet.....	45
Figure 19.1: Class I Design: 3-View and Isometric. All Dimensions in Inches (Scale 1:80).....	49
Figure 19.3: The FREEDOM in Flight.....	50
Figure 19.5: Propellant Loading of the FREEDOM.....	50
Figure 19.2: Transportation of the Launch System.....	50
Figure 19.4: The Launch of the FREEDOM.....	50
Figure 19.7: Termination of the FREEDOM.....	51
Figure 19.8: Storage of the FREEDOM and its Launch Systems.....	51
Figure 19.6: U.S. Artillery Firing at the FREEDOM.....	51
Figure 19.9: Recovering the FREEDOM and SRM.....	51
Figure 20.1: Thrust Vectoring Options (Ref. 33).....	52
Figure 20.3: Booster Gimbal Oblique View (Not to Scale).....	53
Figure 20.2: Flight Control System: 3-View and Isometric (Scale 1:200).....	53
Figure 20.4: Gimbal Oblique View (Not to Scale).....	53
Figure 20.6: SRM Insulation (Ref. 33).....	54
Figure 20.5: Orion 50 XL: Thrust versus Time.....	54
Figure 20.7: Fuel System Ghost Views: 3-View and Isometric (Scale 1:200).....	55
Figure 20.9: Radar Location (Not to Scale).....	56
Figure 20.8: Electrical System: 3-View and Isometric (Scale 1:200).....	56
Figure 20.10: Explosive Bolt Array Location (Not to Scale).....	56
Figure 20.11: Hydraulic Launch System: 3-View and Isometric (Scale 1:200).....	57
Figure 20.12: Staging System (Not to Scale).....	57
Figure 21.2: Recovery Position Flight Profile.....	59
Figure 21.1: Short Period Mode (Red) and Long Period/Phugoid Mode (Blue).....	59
Figure 21.3: The Recovery Storyboard.....	60
Figure 21.5: Deflagration Line: 3-View and Isometric (Scale 1:200).....	61
Figure 21.4: Impact Velocity to Weight.....	61
Figure 22.1: Frame and Bulkhead Spacing: Side View All Dimensions in Inches (Scale 1:100).....	62
Figure 22.3: Exterior and Interior Fin (Not to Scale).....	63
Figure 22.2: Nose to Bulkhead (Not to Scale).....	63
Figure 22.6: Fuse-adapter Ring (Not to Scale).....	64
Figure 22.4: Engine Bulkhead (Not to Scale).....	64
Figure 22.5: Ring Frame Bolts (Not to Scale).....	64
Figure 22.7: Structure Schematic: 3-View and Isometric (Scale 1:200).....	65
Figure 23.1: Class II C.G. Excursion Diagram: Booster Phase.....	67
Figure 23.2: Class II C.G. Excursion Diagram: Rocket Engine Phase.....	67
Figure 23.3: FREEDOM C.G.: 3-View and Isometric (Scale 1:80).....	68
Figure 25.1: The FREEDOM Family (Not to Scale).....	70
Figure 25.2: Updated 3-View: All Dimensions in Inches (Scale 1:80).....	71
Figure 28.1: FREEDOM Exploded View (Not to Scale).....	74
Figure 28.2: FREEDOM Assembly Facility Layout (Not to Scale).....	75

Figure 28.3: Assembly Flow (Not to Scale)..... 76
 Figure 29.1: Cost vs. the Number of Target Drones Produced 77
 Figure 31.1: Rate of Climb of the FREEDOM..... 79
 Figure 31.2: Altitude vs. Mach: The FREEDOM and GQM-163 Coyote 80
 Figure 31.3: Thrust vs. Speed: The Freedom and GMQ-163 Coyote..... 80
 Figure 31.4: Turn Rate vs. Calibrated Air Speed..... 82

List of Tables

Table 1.1: Supersonic Aerial Target Mission Specifications and Requirements (Ref. 1) 2
 Table 2.1: Weight and Performance Characteristics of Historical Aircraft (Refs. 11-21)..... 6
 Table 4.1: STAMPED Analysis Data 12
 Table 5.1: High and Low Profile Fuel Fractions..... 14
 Table 5.2: Roskam Weight Sizing..... 14
 Table 5.3: Final Preliminary Weight Sizing..... 15
 Table 6.1: Sized Design Parameters..... 18
 Table 7.1: Downselecton Reasoning..... 22
 Table 8.1: Payload Components 23
 Table 10.1: Required Angle of Attack..... 28
 Table 12.1: Fin Set Design Characteristics 31
 Table 12.2: Fin and Body Lift: Angle of Attack 31
 Table 14.2: Component Weight and C.G. Locations 36
 Table 14.1: Weight Fractions and Component Weight..... 36
 Table 14.3: C.G. Excursion Values 38
 Table 16.1: Stability and Control Values 42
 Table 17.1: Calculated and Measured Wetted Area Values..... 44
 Table 17.2: Cruise Zero-Lift Drag Coefficients 44
 Table 17.3: Cruise Zero-Lift Drag Coefficients 45
 Table 18.1: Class I $(L/D)_{max}$ and Preliminary Drag Polar Values..... 46
 Table 18.2: Rotational Frequency Values 47
 Table 19.1: Class I Fuselage Characteristics..... 48
 Table 19.2: Class I Fin Characteristics 48
 Table 21.1: Impact Speeds 61
 Table 22.1: Structural Components..... 65
 Table 23.1: C.G. Excursion Results 67
 Table 25.1: Salient Characteristics..... 71
 Table 29.1: Cost Analysis Value 77
 Table 30.1: Class II Stability and Control Results..... 78
 Table 31.1: FREEDOM Rate of Climb..... 79
 Table 31.2: : FREEDOM Cruise Data 81
 Table 31.3: Dive Profile Calculations 81
 Table 31.5: Cruise and Dive Profile Results 82
 Table 31.4: Climb Rate Results 82
 Table 32.1: RFP Specifications Compliance..... 83

List of Symbols

Symbol	Description	Units
a	Speed of Sound, Acceleration Major Diameter	ft/s, ft/s ² , ft
A	Aspect Ratio, Area	~, ft ²
AR	Aspect Ratio	~
b	Span, Minor Diameter	ft, ft
c	Chord	ft
c _j	Thrust Specific Fuel Consumption	lbf/lbf/hr
\bar{c}	Mean Geometric Chord	ft, in
C _D	Drag Coefficient	~
C _{D0}	Parasite Drag Coefficient, Zero Lift Drag Coefficient	~, ~
C _{DU}	Drag Coefficient With Respect to Velocity Along X Axis	s/ft
C _f	Equivalent Skin Friction Coefficient	~
C _L	Lift Coefficient	~
C _{Lα}	Lift Coefficient With Respect To Angle of Attack	rad ⁻¹
C _{mq}	Pitching Moment Coefficient With Respect to Pitch Rate	~
C _{mα}	Pitching Moment Coefficient With Respect to Angle of Attack	~
C _N	Normal Force Coefficient	~
C _{Nα}	Normal Force Coefficient With Respect to Angle of Attack	rad ⁻¹
C _T	Thrust Coefficient	~
C _{TXU}	Thrust Coefficient With Respect to Velocity Along X Axis	s/ft

C _{T$X1$}	Steady State Thrust Coefficient	~
d	Diameter, Distance of Gust Length	in, ft
D	Drag Force	lbf
DS _{wet}	Incremental Change in Wetted Area	in ² , ft ²
Dx	Incremental Change in Length	in, ft
e	Oswald Efficiency Factor	~
f	Equivalent Parasite Area	ft ²
F	Force	lbf
g	Acceleration of Gravity	ft/s ²
g _o	Sea Level Acceleration of Gravity	ft/s ²
h	Altitude	ft
i	Incidence Angle, i th Item in Sequence	degrees, ~
I _{sp}	Specific Impulse	s
l	Length	in, ft
L	Lift Force, Scale of Turbulence	lbf, ft
L/D	Lift to Drag Ratio, length ratio	~, ~
L/W	Lift to Weight Ratio	~
m	Mass	lbm, slug
M	Mach Number, Mission, Pitching Moment	~, ft-lbf
M _q	Pitching Moment With Respect to Pitch Rate	sec ⁻¹
M _{α}	Pitching Moment With Respect to Angle of Attack	sec ⁻¹
M _{$\dot{\alpha}$}	Pitching Moment With Respect to Angle of Attack Rate	sec ⁻²

M_{ALE}	Mach Number Normal to Leading Edge Sweep Angle	~
n	Load Factor, nth Item in Sequence, Number of Items	g's, ~
N	Normal Force	lbf
N_{α}	Normal Force With Respect to Angle of Attack	~
P	Occurance Probability, Pressure	~, psf
Perim	Perimeter	in, ft
q	Dynamic Pressure	psf
\bar{q}	Dynamic Pressure	psf
r	Recovery Factor	~
R	Fluid Gas Constant, Range	ft-lbf/slug-°R, nmi
R_t	Turn Radius	ft
S	Area	ft ²
S_{wet}	Wetted Area	ft ²
t	Time, Thickness	Seconds, ft
t/c	Thickness Ratio	~
T	Temperature, Thrust	°R, lbf
T/W	Thrust Loading	~
U	Velocity Along X Axis	ft/s
U_{DE}	Vertical Gust Intensity	ft/s
\dot{U}	Accleration Along X Axis	ft/s ²
V	Speed, Velocity Along Y Axis	ft/s, kts
\bar{V}	Volumetric Coefficient	~
W	Weight, Velocity Along Z Axis	lbf, ft/s
W/S	Wing Loading	psf

W_e/W_{TO}	Empty to Takeoff Weight Ratio	~
X	Distance Along X Axis	ft
$\frac{-}{X}$	Distance Along X Axis Normalized by MAC	~
Y	Side Force,	lbf
Z_{α}	Vertical Acceleration due to Angle of Attack	ft/s ²
\$	United States Dollar	U.S Dollars
%	Percentage	~
<u>Greek Symbols</u>	<u>Description</u>	<u>Units</u>
α	Angle of Attack	degrees
β	Sideslip Angle	degrees
γ	Dive Angle, Specific Heat Ratio	~, ~
Γ	Dihedral Angle	degrees
δ	Fligh Path Deviation, Deflection	ft, degrees
δ_{LE}	Leading Edge Angle	degrees
Δ	Change in Value	~
ϵ	Twist Angle	degrees
ζ	Damping Ratio	~
η_p	Propeller Efficiency	~
λ	Taper Ratio	~
Λ	Sweep Angle	degrees
ρ	Air Density	slug/ft ³
σ	RMS Gust Velocity	ft/s
Σ	Summation	~
Φ	Roll	degrees
Φ_T	Thrust Inclination Angle	degrees
ψ	Turn Rate	deg/s
ω_n	Natural Frequency	Hz
Ω	Open-Loop Motion Frequency	Hz
<u>Subscripts</u>	<u>Description</u>	<u>Units</u>

abs	Absolute	~
assumed	Assumed	~
av	Average	~
A	Correspondent to Design Maneuver Point	~
AC	Aerodynamic Center	~
base	Base	~
body	Body	~
boosted	Boosted Missile Configuration	~
burnout	Powerplant Fuel Exhausted	~
B	Body, Maximum Gust Intensity	~, ~
cl	Climb Condition	~
component	Component	~
cr	Cruise	~
CG	Center of Gravity	~
D	Dive	~
e	Empty, Nozzle Exit	~
E	Empty	~
ETent	Tentative Empty	~
f	Final	~
fin	Fin	~
friction	Friction	~
fus	Fuselage	~
F	Fuel	~
FF	Fuel Fraction	~
g	Gust	~
gust	Gusts	~
h	Horizontal Fin	~
i	Initial, i th Item in Sequence	~
lim	Limit	~
LE	Leading Edge	~
mac	Mean Aerodynamic Chord	~

mac	Mean Aerodynamic Chord	~
maneuver	Maneuver	~
max	Maximum Value	~
n	Nose, n th Item in Sequence	~
neg	Negative	~
nose	Nose	~
oe	Operating Empty	~
OETent	Tentative Operating Empty	~
p	Phugoid Mode	~
pos	Positive	~
powered	Powered Flight Conditions	~
Payload	Payload	~
PL	Payload	~
r	Root	~
ref	Reference	~
sp	Short Period Mode	~
S	Stall	~
t	Tip	~
thrust	Thrust	~
total	Total	~
T	Tail	~
TFO	Trapped Fuel and Oil	~
TO	Takeoff	~
u	Along Direction of Longitudinal Velocity	~
unboosted	Unboosted Missile Configuration	~
v	Along Direction of Lateral Velocity	~
w	Along Direction of Vertical Velocity	~
wave	Wave	~
wing	Wing	~
x	Longitudinal Axis of Missile Body Frame	~

y	Lateral Axis of Missile Body Frame	~
z	Vertical Axis of Missile Body Frame	~
1	First Point	~
2	Second Point	~
<u>Acronyms</u>	<u>Description</u>	<u>Units</u>
3D	Three Dimensional	~
AIAA	American Institute of Aeronautics and Astronautics	~
AN	Army-Navy Standard Bolt	~
B.L.	Butt Line	in
CEP	Circular Error Probable	~
CFD	Computational Fluid Dynamics	~
C.G.	Center of Gravity	~
CY	Calendar Year	Years
DARCorp	Design Analysis Research Corporation	~
DATCOM	Digital Compendium	~
DoD	Department of Defense	~
EPGA	Enhanced Pointing Gimbal Assembly	~
FREE-DOM	Fast Response Enemy Emulating Defense Operations Missile	~
F.S.	Fuselage Station	in
GNC	Guidance, Navigation, and Control	~
GW	Ground Weight	lbf

IOC	Initial Operational Capability	~
KCAS	Claibrated Air Speed in Knots	kts
KEAS	Knots Equivalent Air Speed	kts
NATOPS	Naval Air Training and operating Procedures Standard	~
LOX	Liquid Oxygen	~
No.	Number	~
Qty.	Quantity	~
RC	Rate of Climb	ft/min
RC ₀	Maximum Rate of Climb at Sea Level	ft/min
RMS	Root Mean Squared	~
RP	rocket propulsion/refined petroleum	~
RTM	Resin Transfer Molding	~
SRM	Solid Rocket Motor	~
USAF	United States Air Force	~

1. MISSION SPECIFICATION AND PROFILES

The American Institute of Aeronautics and Astronautics (AIAA) distributed the specifications for the design of the system. Found [here](#), AIAA states these specifications in the form of a Request for Proposal (RFP).



As technology advances, there are more possibilities of advanced aerial threats against the United States (U.S.) and its allies. To keep citizens safe, the U.S. and its allies must be ready for these threats by having the technology to take the threat out before it has the chance to harm. For the U.S. and its allies to be effective at protecting themselves, new and existing systems must be tested to prove effectiveness and success rate. To make sure that these success rates are not false confidence against foreign adversaries, realistic emulation of enemy aerial targets must be developed (Ref. 1).

The RFP (Ref. 1) is interested in a new aerial target to provide this superior emulation of multiple different aerial threats. This unmanned target will be shot at in an attempt to test new defense systems as well as train and confirm the use of existing systems. This system will enter service by the end of the year 2026. With initial production starting in October of 2021 for testing and development, the technology and materials used will be projected to be available by this 2021 time-frame (Ref. 1).

The U.S. Department of Defense (DoD) and its allies are looking to initially purchase 350 of these targets along with an additional 15 for development and system testing before put into service (Ref. 1). The following report illustrates the design process of this mission specification.

1.1 MISSION SPECIFICATION

The RFP (Ref. 1) distributed by AIAA for the 2019-2020 Graduate Team Missile System Design Competition is shown as Reference 1. Table 1.1 outlines the general design requirements and flight profiles to complete the supersonic aerial target mission.

Table 1.1: Supersonic Aerial Target Mission Specifications and Requirements (Ref. 1)

General Design Requirements	
Altitude Flight Envelope	0-65,000 ft
Threshold Range	60 nmi
Objective Range	150 nmi
Cruise Course Error Distance	±1500 ft
Circular Error Probable for End of Life	50 ft
Launch Systems Requirements	
Launch Altitude	0-3,500 ft
Azimuth Angle	360 degrees
Launch Elevation Angle	0-90 degrees
Payload Requirements	
Minimum Length	3.5 ft
Minimum Diameter	10 in
Maximum Payload Weight	500 lbs
Low Altitude Profile	
Cruise Altitude	15-200 ft
Cruise Velocity	Mach 2.0-3.5
Terminal High G Maneuvering Distance from end of life	20 nmi
Lateral Back and Fourth Turns	15-g
Vertical Climb and Dives	7-g
Time Requirement of Maximum G's	45 s
Terminal Impact Velocity	Mach 2.0-3.5
High Altitude Profile	
Cruise Altitude	5,000-65,000 ft
Cruise Velocity	Mach 2.0-4.5
Terminal Dive Angle	10-75 degrees
Terminal Impact Velocity	Mach 0.9-3.5

1.2 MISSION PROFILE, PERFORMANCE, PAYLOAD-RANGE REQUIREMENTS

The RFP (Ref. 1) splits the mission profile up into high altitude and low altitude flight profiles. Each flight profile consists of three phases: launch, mid-course cruise, and terminal. The launch phase occurs from the ignition of the engine(s) on the launch rail to when the flight levels out at cruise condition. The target drone will initiate this phase at an elevation between sea level and 3,500 feet above sea level. The design team will determine the launch rail length. This will set the recommended limit of the elevation angle for a safe deployment (Ref. 1). Figure 1.1 and Figure 1.2 show a visual representation of the two flight profiles.

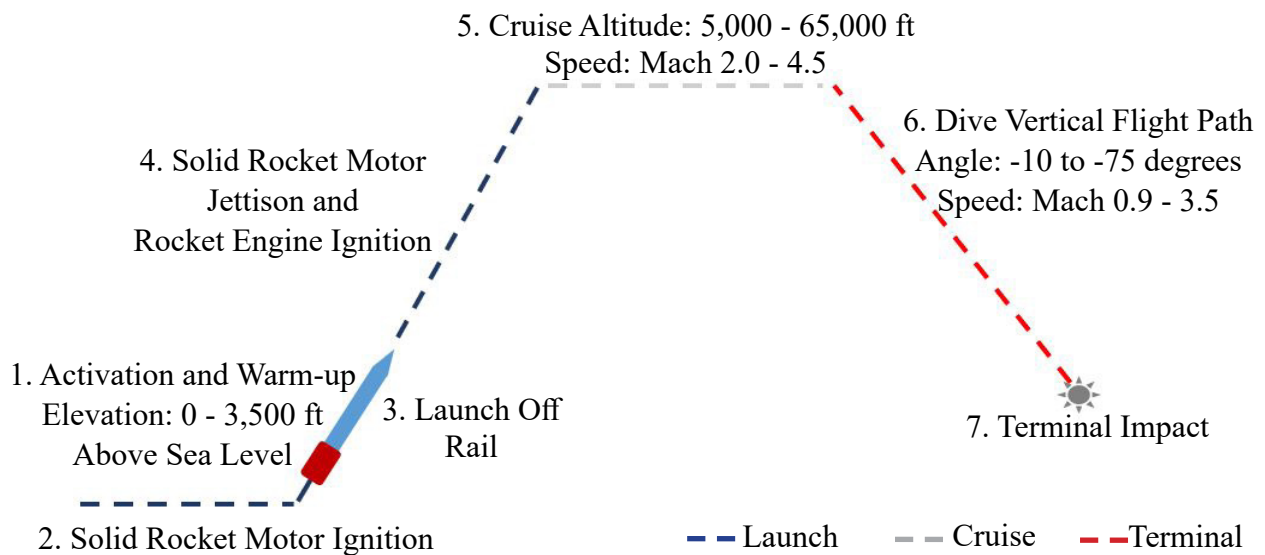


Figure 1.1: High Altitude Flight Profile

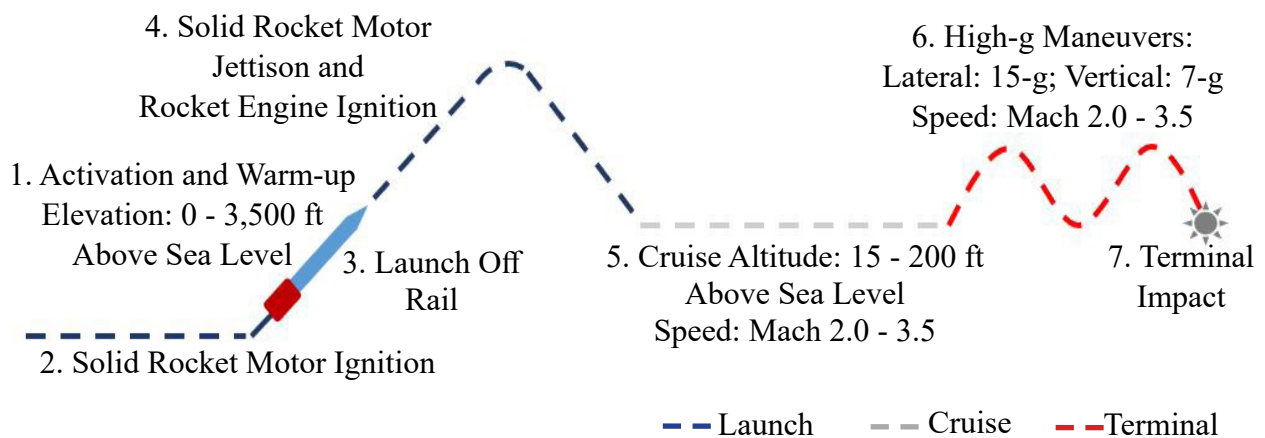


Figure 1.2: Low Altitude Flight Profile

Figure 1.3 shows the payload range diagram for the mission. The target must maintain a course within 1,500 feet of its planned trajectory with a 50 feet Circular Error Probable (CEP) at the end of the terminal phase. Guidance, navigation, and control

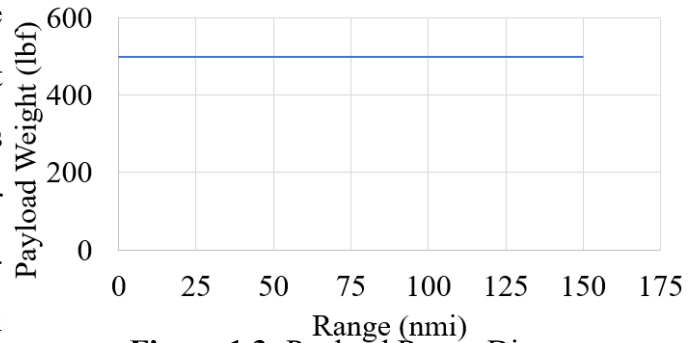


Figure 1.3: Payload Range Diagram

(GNC) systems will equip the target drone. A transponder beacon and telemetry module transmit data for tracking while acting as a flight termination system. These components combined with additional payloads total a maximum payload weight of 500 lbs (Ref. 1).

1.3 OVERALL DESIGN METHODS AND PROCESS

The authors performed the process for the development of this target with Aircraft Design Parts I through VIII (Refs. 2-9). Dr. Jan Roskam wrote and developed this book series. The program Advanced Aircraft Analysis (AAA) (Ref. 10) was based on Dr. Roskam's books. With this program, the authors analyzed the design of the target. The design process steps are as follows:

1. Identified the mission specifications for both profiles
 - Completed a historical review for a baseline design
2. Statistical Time and Market Predictive Engineering Design (STAMPED) Analysis
 - Analyzed past trends to get design parameters based on market forecast
3. Class I Design
 - Designed a variety of configurations to analyze the best target configuration
4. Class II Design and Evaluation of Final Design
 - Analyzed Class II calculations based on cost and amount of emulated aerial threats

1.4 CONCLUSIONS AND RECOMMENDATIONS

The authors conclude that:

- i.) The design should cruise at 0 to 65,000 ft at a Mach range of 2 to 4.5 throughout the mission.

The authors recommend that:

- i.) The design meets all requirements in the RFP (Ref. 1) before adding extra elements.

2. HISTORICAL REVIEW

The following chapter will present the inspirations for the FREEDOM with the milestones throughout history of guided missiles and target drones.

2.1 HISTORY OF MISSILES AND TARGET DRONES



Figure 2.1: V-2 Missile (Ref. 13)

During WWII, Wernher von Braun developed the first rocket-powered missile: the V-2 missile shown in Figure 2.1. The Germans had an advantage with this weapon because a mixture of ethyl alcohol and liquid oxygen fuel powered the missile. The V-2 also carried an explosive payload and was nearly impossible to throw off course (Ref. 11). In contempt of the devastation during WWII, the V-2 missile sparked other world powers to pour their efforts into the development of cruise missiles and intercontinental ballistic missiles (Ref. 12).

Entering into the Cold War, the U.S. decided to invest in contracts to develop guided missiles with inspiration from the V-2.

A contract from the U.S. Air Force for a supersonic missile led to the development of the North American Aviation's SM-64 Navaho shown in Figure 2.2. In ten years (1946-1957), the Navaho program provided the first turbojet-powered aircraft to achieve Mach 2.0 and use inertial guidance to complete a mission (Ref. 14). The Navaho power-plant consisted of two Wright XRJ47-W-7 ramjets with a XLR83-NA-1 liquid-fueled rocket booster. Similar



Figure 2.2: SM-64 Navaho (Ref. 16)

to the specifications of the RFP (Ref. 1), the Navaho reached a speed of Mach 3.25 and ceiling of 80,000 feet (Ref. 15). Although the Navaho was not in service long because of the development of intercontinental ballistic missiles, this project laid the foundation for modern-day missiles.



Figure 2.3: BQM-34A Firebee (Ref. 18)

During the 1960s, Ryan Aeronautical Company manufactured the BQM-34A Firebee as an aerial target system. The Firebee, shown in Figure 2.3, trained the military for defense readiness by emulating aerial threats. Consistent with the RFP (Ref. 1) specifications, the BQM-34A Firebee went as low as 10 feet above sea level and had a ceiling of 60,000

feet. It had the ability to maintain 7-g turns along with an endurance of 115 minutes and maximum speed of Mach 0.97. A General Electric J-85-100 engine furnished its propulsion system (Ref. 17).

In 2005, Northrop Grumman developed the GQM-163A Coyote as a supersonic anti-ship cruise missile. It helped the U.S. Navy with ship defense training exercises shown in Figure 2.4 (Ref. 19). Similar to the RFP (Ref. 1), the high altitude profile of the Coyote had an altitude range of 5,000 to 52,000 feet and a cruise speed range of Mach 3.0 to 4.0. The terminal phase impacted at a speed range of Mach 0.7 to 3.0 from a dive angle range of 15 to 55 degrees. The low altitude profile of the Coyote has an altitude of 50 feet and cruise speed of Mach 2.6. The terminal phase maneuvers for the low altitude profile included a 12-g maximum lateral maneuver and 5.0-g maximum vertical maneuver. The GQM-163A Coyote had a MARC-R282 ramjet engine and solid propellant rocket booster (Ref. 20). Table 2.1 displays the weight and performance characteristics of the mentioned historical aircraft.



Figure 2.4: GQM-163A Coyote (Ref. 21)

Table 2.1: Weight and Performance Characteristics of Historical Aircraft (Refs. 11-21)

Missile	W_e (lbf)	W_{TO} (lbf)	W_e / W_{TO} (lbf)	Ceiling (ft)	Range (nmi)	Mach Cruise Speed (~)	Engine Thrust (lbf)	Booster Thrust (lbf)
V-2	10,000	25,600	0.39	264,000	174	4.5	-	60,000
SM-64 Navaho	23,500	63,000	0.48	80,000	5,500	3.3	11,300	405,000
BQM-43A Firebee	1,500	2,060	0.73	60,000	690	0.97	1,700	-
GQM-163A Coyote	850	3,300	0.26	52,000	45	3.0-4.0	-	-

2.2 CONCLUSIONS AND RECOMMENDATIONS

The authors conclude that:

- i.) The GQM-163 A Coyote has a high profile cruise speed of Mach 4.0; this is similar to the maximum cruise speed of the RFP (Ref. 1) of Mach 4.5;
- ii.) The 45 nmi range of the GQM-163 A Coyote is close to the 60 nmi range requirement (Ref. 1);
- iii.) Future missile designs strive to outperform historical systems.

The authors recommend that:

- i.) A higher fidelity research take place of more historical missiles.

3. DESIGN VECTOR AND WEIGHTS ESTABLISHMENT

The team created an objective function based on the RFP (Ref. 1). They gathered inputs from aerospace pundits such as Dr. Shahriar Keshmiri and aerospace graduate students including Meihua Zhang, Thomas Le Pichon and Rohith Gindihar. The team verified the objective function and maximized it to determine the ideal design candidate. Finally, the FREEDOM design maximized the objective function. This indicates its functionality throughout the mission profile.

3.1 EXPERT DESIGN INPUT FOR OBJECTIVE FUNCTION VERIFICATION

The team communicated with Dr. Keshmiri regarding the validity of the objective function due to his specific knowledge on missile dynamics and previously published papers (Refs. 22 and 23). He guided the team to “investigate the sensitivity of each objective by using different variable ranges (e.g. W_{TO}/W_{TOmax}).” Ultimately Dr. Keshmiri commented on the objective function by stating “Your function looks good.” In addition, aforementioned graduate students verified the most recent modified objective function to allow the authors distinguish the most ideal design case.

3.2 OBJECTIVE FUNCTION

The team constructed the following objective function to quantify various design candidates. The reference price is based on the cost of a GQM-163A Coyote (Ref. 24). Maneuverability, cruising, and terminal conditions within the envelope as well as adequate GNC equipment are defined in Sections 1.1 and 1.2. Reference 8 outlines the safety and airworthiness standards of military airplanes before they are accepted into service. The objective function is displayed as a pop-up image.

3.3 CONCLUSIONS AND RECOMMENDATIONS

The authors conclude that:

- i.) The objective function meets RFP (Ref. 1) requirements like a maximum speed of Mach 4.5 in the high altitude profile and Mach 3.5 in the low altitude profile.

The authors recommend that:

- i.) More experts on missile design should be consulted regarding the design of the FREEDOM.

Objective Function
(Click)

4. STAMPED ANALYSIS

The authors utilized the Statistical Time and Market Predictive Engineering Design (STAMPED) analysis to estimate different design variables based on market trends. The STAMPED analyses provided the designers the means to choose competitive design drivers over selecting values within a given range.

4.1 THE STAMPED ANALYSIS TECHNIQUE

STAMPED techniques are based on market research of aircraft similar to the RFP (Ref. 1) over time. The team plotted and extended the trend-lines of the historical data to the date of initial operational capability (IOC). These plots also include one standard deviation above and one standard deviation below the trend-lines. These will represent aggressive and conservative design philosophies. The designers repeated this process for all significant design variables.

4.2 ESTIMATION OF MAJOR DESIGN VARIABLES

For the supersonic aerial target, the primary design variables were empty to takeoff weight, zero-lift drag coefficient, thrust to takeoff weight ratio, wing area, wing loading, and maximum lift to drag ratio. The authors conducted research of supersonic aerial target missiles and drones, high subsonic aerial target missiles and drones, surface-to-surface missiles, air-to-air missiles, and cruise missiles. Although some of these vehicle categories do not match the RFP (Ref. 1), they provide insight into how to design for certain aspects of the RFP (Ref. 1). These aspects include high supersonic Mach numbers at high altitudes and high-g maneuvers.

The designers analyzed the empty and gross weights of the aircraft. They investigated data either provided in the available public data or estimated using methods from John B. Norwell Jr.'s Master's Thesis (Ref. 25) on missile weight and size estimation. Figure 4.1 displays the results of the analysis. A vertical line at the year 2026 depicts the requested entry year of the FREEDOM. A conservative design approach results in a W_e/W_{TO} of 0.7. The designers chose this design approach because the strength and thermal capabilities of affordable materials will result in high structural weight for this flight profile.

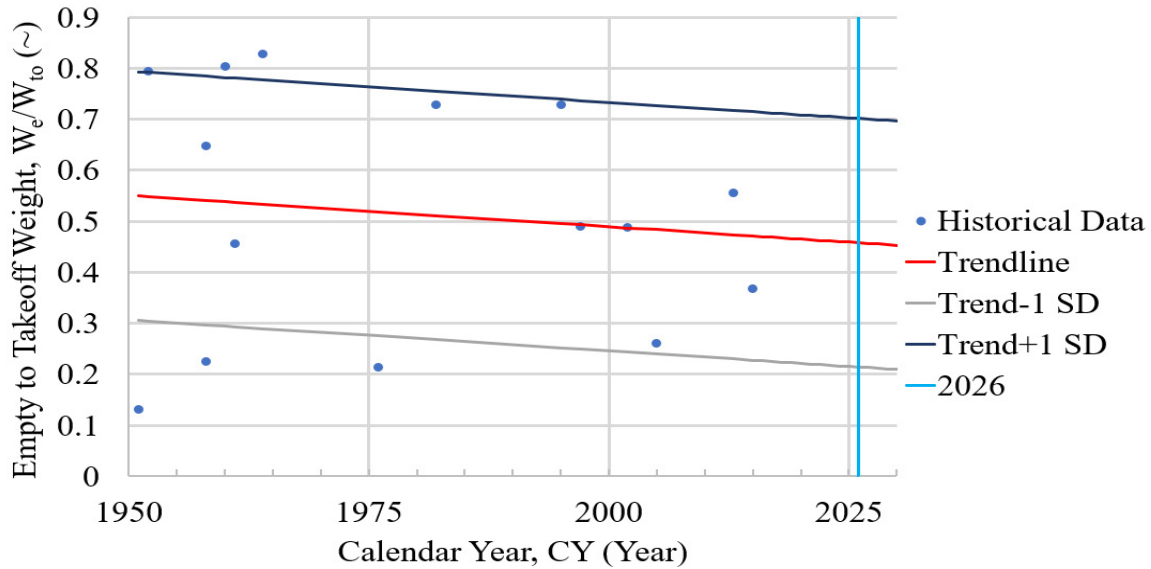


Figure 4.1: STAMPED Empty to Takeoff Weight Trends

The team found the equations and methods from Section 3.4.1 of Reference 2 to calculate the zero-lift drag coefficient. Figure 4.2 shows the historical data and trends of the zero-lift drag coefficient. A vertical line at the year 2026 depicts the requested entry year of the FREEDOM. The authors decided to take this aggressive approach because it will aid the overall performance of the target by reducing drag, resulting in a design goal of 0.021 for C_{D_0} .

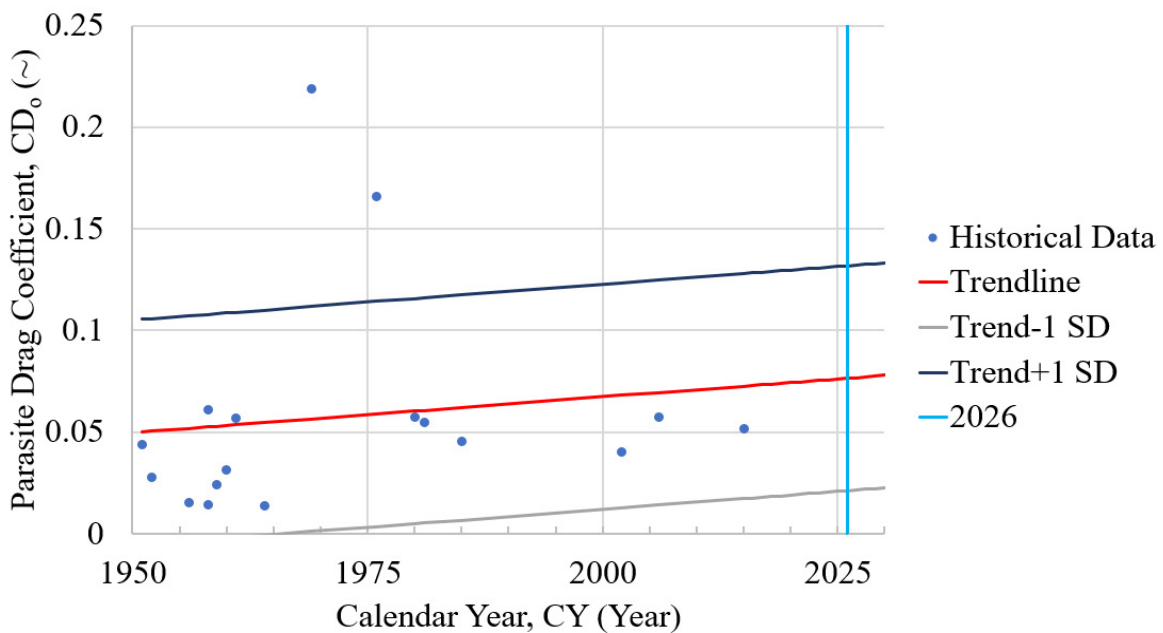


Figure 4.2: STAMPED Parasite Drag Coefficient Trends

The team found the thrust to takeoff weight ratios for the historical aircraft by summing the thrust of the first stage engines of each aircraft and dividing by the takeoff weight. Figure 4.3 presents the trends and historical data of T/W_{TO} . A vertical line at the year 2026 depicts the requested entry year of the FREEDOM. For an aggressive design approach, the target T/W_{TO} is 7.6. The team took an aggressive design approach because this will result in a larger power plant, which will assist with reaching the RFP cruise Mach numbers and final maneuvers.

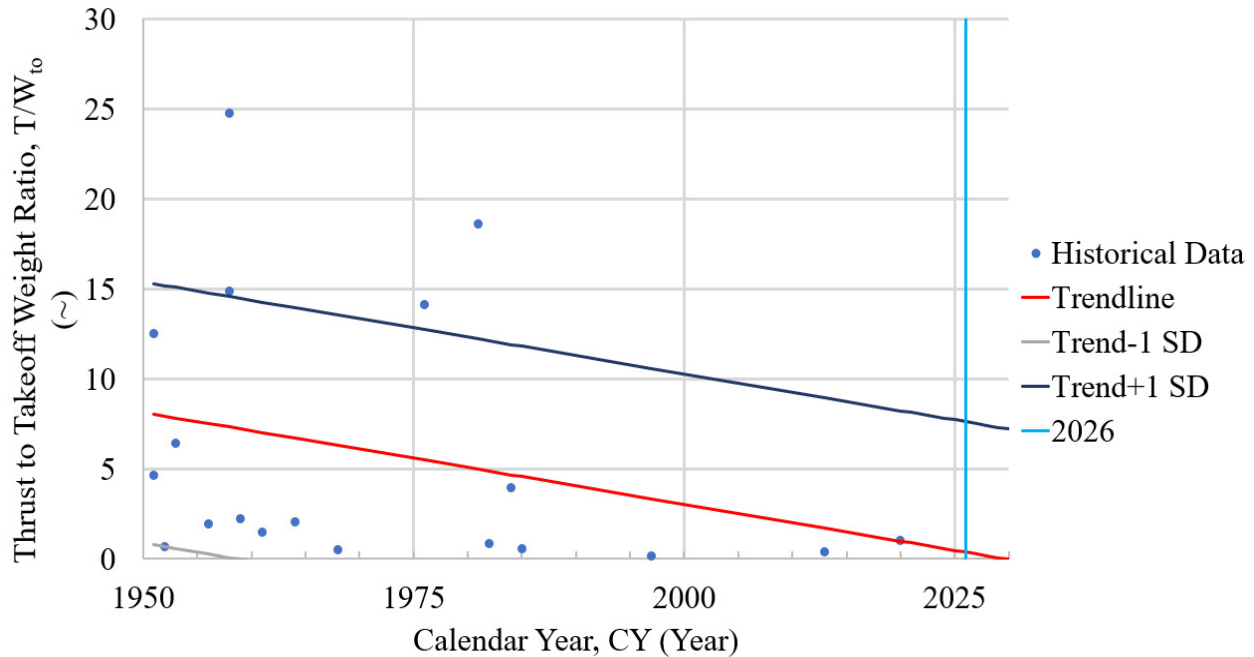


Figure 4.3: STAMPED Thrust to Takeoff Weight Coefficient Trends

Measuring scaled three-views of the target missiles helps the team estimate the primary wing/fin area. Figure 4.4 displays the results of the historical analysis. A vertical line at the year 2026 depicts the requested entry year of the FREEDOM. The team dictated the wing area to be 15 ft² evenly distributed across two wings by using a conservative design approach. This value is lower than the trend minus one standard deviation line. However, this action results in a value that better matches the historical missiles found. A conservative design approach allows this value to result in more weight and aerodynamic forces acting on the missile during flight.

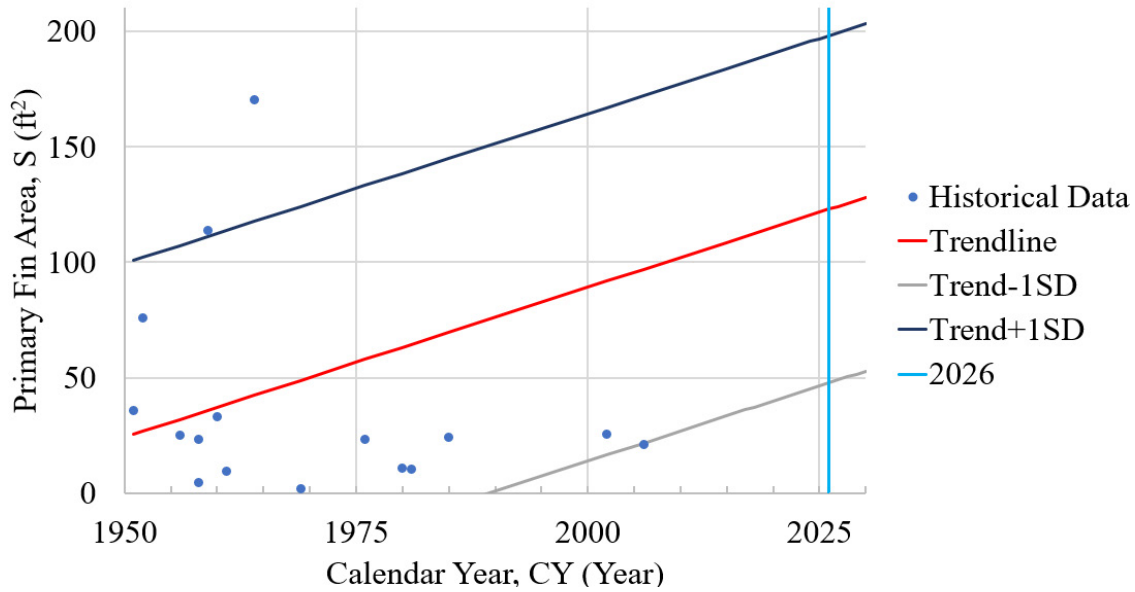


Figure 4.4: STAMPED Primary Wing Area Trends

Figure 4.5 below shows the wing loading trends. A vertical line at the year 2026 depicts the requested entry year of the FREEDOM. An aggressive design philosophy demands the design goal for wing loading to be 266 psf. An aggressive design value gives the most likely achievable value for the IOC date of 2026 and aligns with previous historical data.

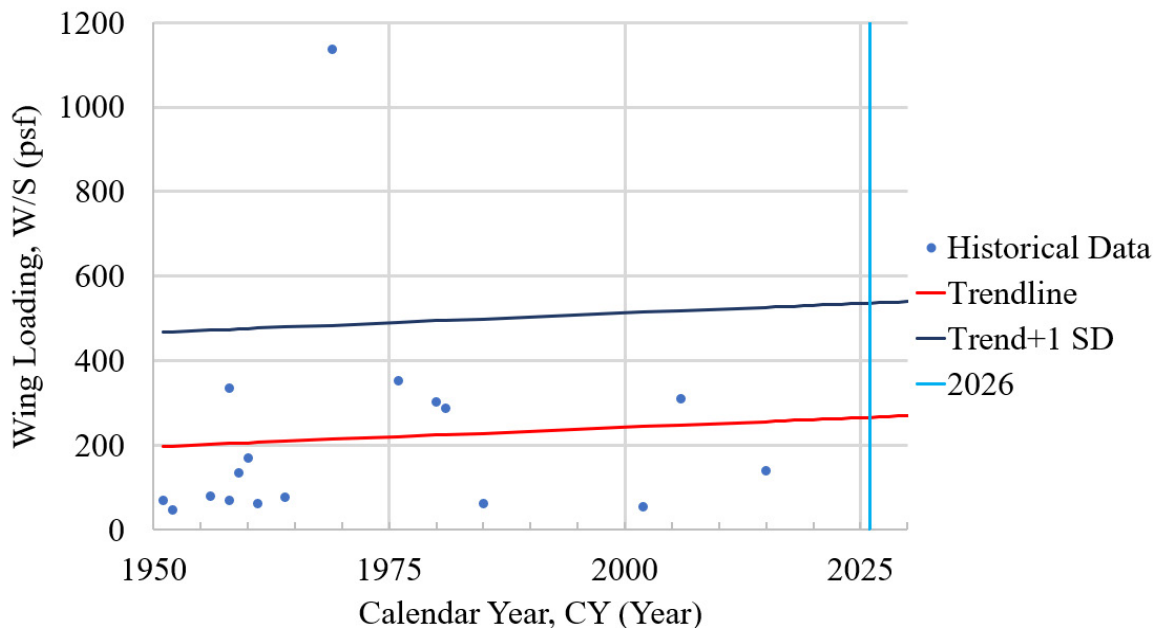


Figure 4.5: STAMPED Wing Loading Trends

By continuing the calculations from Section 3.4.1 (Ref. 2), the designers found the $(L/D)_{max}$ values for the historical aircraft. They made estimations for the Oswald Efficiency Factor based on primary wing/fin geometry. Figure 4.6 below displays the trends for this design driver. A vertical line at the year 2026 depicts the requested entry year of the FREEDOM. For a balanced design philosophy, the design goal for maximum lift to drag ratio is 4.97. The team chose a balanced design philosophy for this design parameter because this value was most in line with historical data on supersonic target missiles. Table 4.1 presents all results from these analyses.

Table 4.1: STAMPED Analysis Data

W_e/W_{TO}	0.70 (~)
C_{D_0}	0.021 (~)
T/W_{TO}	7.6 (~)
S	15 ft ²
W/S	266 psf
$(L/D)_{max}$	4.97 (~)

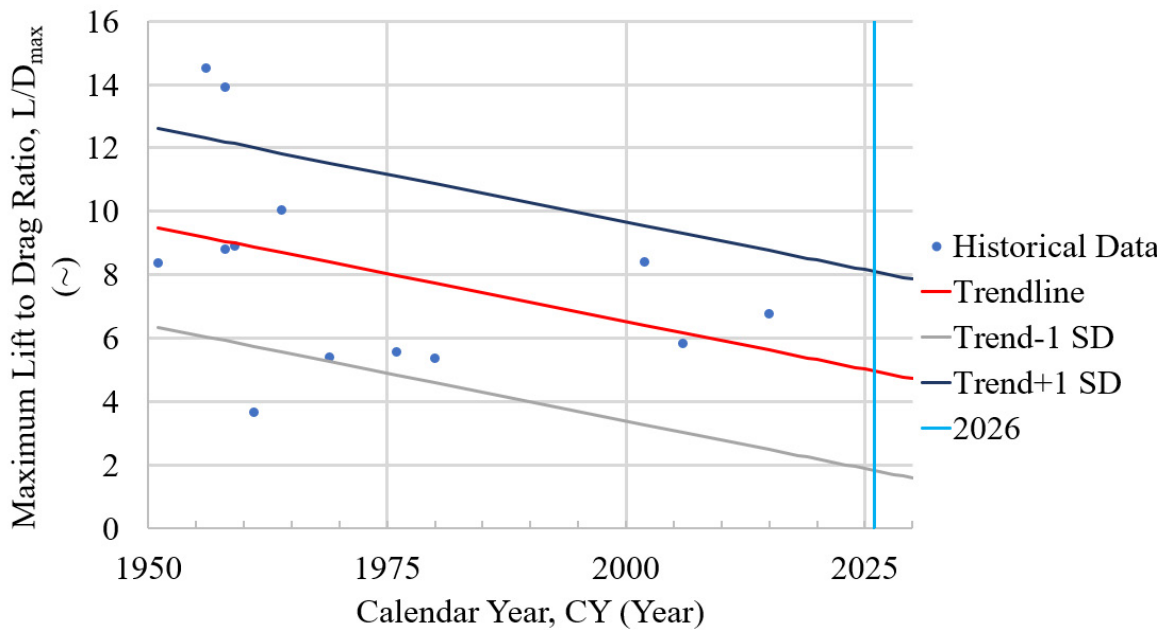


Figure 4.6: STAMPED Maximum Lift to Drag Ratio Trends

4.3 CONCLUSIONS AND RECOMMENDATIONS

The authors conclude that:

- i.) An aggressive design approach yields the following design parameters: W_e/W_{TO} is 0.70, C_{D_0} is 0.021, T/W_{TO} is 7.6, S is 15 ft², W/S is 266 psf, and $(L/D)_{max}$ is 4.97.

The authors recommend that:

- i.) A further analysis into historical trends is done for this class of missiles.

Sample Calculation
(Click)

5.3 PRELIMINARY DESIGN WEIGHTS SIZING

The RFP (Ref. 1) defined the total payload weight as 500 pounds. Using Dr. Roskam's method, the authors selected an initial takeoff weight of 4000 pounds. This estimated weight is similar to the GQM-163A Coyote, a supersonic target missile with comparable flight and performance profiles (Ref. 20). The next step determines the fuel fractions based on the flight profile stages for both the high and low profiles. The cruise fuel fraction in both profiles uses the Breguet Range Equation (Ref. 2). The Breguet Endurance Equation (Ref. 2) finds the fuel fraction for the terminal maneuver in the low

profile. The other stages use fuel fraction values found in Table 2.1 and Figure 2.2 from Reference 2. Table 5.1 shows the high and low profile fuel fractions of each stage found using data from Chapter 2 in Reference 2.

Table 5.1: High and Low Profile Fuel Fractions

High Altitude Profile			Low Altitude Profile		
Phase	Ratio	Value (~)	Phase	Ratio	Value (~)
Engine Start-up	W_1/W_{TO}	0.990	Engine Start-up	W_1/W_{TO}	0.990
Takeoff	W_2/W_1	0.995	Takeoff	W_2/W_1	0.995
Climb to Cruise	W_3/W_2	0.900	Climb to Cruise	W_3/W_2	0.900
Cruise	W_4/W_3	0.986	Cruise	W_4/W_3	0.986
Terminal Dive	W_5/W_4	0.985	Terminal Maneuver	W_5/W_4	0.999
	M_{FF}	0.861		M_{FF}	0.873

Found from the takeoff weight, a tentative value for empty weight was compared to an empty weight found from STAMPED values. The takeoff weight changes in this iterative process to find the error between the tentative empty weight and STAMPED empty weight until the error is within 0.5%. Table 5.2 shows the final payload, empty, fuel, and takeoff weights obtained from the method in Reference 2.

Table 5.2: Roskam Weight Sizing

Profile:	High	Low
Takeoff Weight	6,770 (lbf)	5,400 (lbf)
Empty Weight	4,740 (lbf)	3,790 (lbf)
Payload Weight	500 (lbf)	500 (lbf)
Fuel Weight	1,500 (lbf)	1,100 (lbf)

Using the method in Reference 26, the length and diameter of the missile provided a rough estimate of the takeoff weight. With this rough estimate for takeoff weight, the authors calculated the empty weight of the missile from the empty to takeoff ratio of

**Roskam
Method 2**
(Click)

**Roskam
Method 3**
(Click)

0.2. The rough estimate for takeoff weight and a function of the velocity and specific impulse of the engine estimated the fuel weight needed for the target drone. The payload of 500 pounds given in the RFP (Ref. 1) still applied for the payload weight in this method. The final takeoff weight for the missile combined the empty, fuel, and payload weight similar to Dr. Roskam’s method. This takeoff weight does not include the booster or adapter needed to launch the target drone off the rail.

The Orion 50 XL booster (Ref. 27) launches the missile off the rail. The following weights obtained the final takeoff weight when added to the

Table 5.3: Final Preliminary Weight Sizing

Profile:	High	Low
Takeoff Weight	23,900 (lbf)	23,600 (lbf)
Empty Weight	6,580 (lbf)	6,580 (lbf)
Payload Weight	500 (lbf)	500 (lbf)
Fuel Weight	16,800 (lbf)	16,500 (lbf)

missile empty and fuel weight: the empty weight of the booster, the weight of the adaptor, and fuel weight of the booster. The adaptor weight was found using the method described in Chapter 2

from Reference 28. The takeoff weights for both the high and low profiles used this method. Table 5.3 shows the values for the empty, fuel, and takeoff weights for the high and low profiles using the method in Reference 26.

The values from Reference 2 were undersized for the amount of fuel and empty weight that was considered for the final takeoff weight. Based on the final weights calculated from both methods, the method from Reference 26 proved to have reasonable values for takeoff weight in each flight profile. Sample calculations show the final weight sizing estimated from both methods.

Final Weight Sizing
(Click)

5.4 CONCLUSIONS AND RECOMMENDATIONS

The authors conclude that:

- i.) The preliminary takeoff weight, empty weight, payload weight, and fuel weight are 23,900 lbf, 6,580 lbf, 500 lbf, and 16,800 lbf for the high profile mission;
- ii.) The preliminary takeoff weight, empty weight, payload weight, and fuel weight are 23,600 lbf, 6,580 lbf, 500 lbf, and 16,500 lbf for the low profile mission.

The authors recommend that:

- i.) The conduction of a more detailed weight sizing analysis of STAMPED data will yield more accurate fuel fractions.

6. WING AND POWER PLANT SIZING

The purpose of this section is to determine the suitable design point through creating a Performance Sizing Chart that ultimately is capable of complying with RFP mission requirements. The right and bottom area within the allowable region shows the most preferred design point. Chapter 3 from Reference 2 shows all the equations used to estimate the drag polar as well as wing and power plant sizing.

6.1 DRAG POLAR ESTIMATION

The designers estimated the drag polar to determine the coefficient of drag based off of coefficient of lift. Only the clean condition drag polar was calculated because the target drone does not have flaps or landing gear.

The first step to estimate the drag polar includes calculating the wetted area based on the takeoff weight determined in Chapter 5. To help reduce drag for supersonic conditions, the designers assumed a small skin friction coefficient of 0.0025. The designers use the skin friction coefficient and wetted area to calculate the equivalent parasite area. The zero-lift drag coefficient comes from the wing area derived from the STAMPED analysis and the equivalent parasite area. Using a clean condition, the coefficient of drag did not increase due to compressibility effects and because the Oswald Efficiency Factor is 0.85. With all of the parameters known, an equation can be derived for the coefficient of drag dependent on the coefficient of lift. Equation 6.1 shows the drag polar used to find the coefficient of drag from a coefficient of lift range of zero to two.

$$C_D = 0.171 + 0.374 C_L^2 \quad (\text{Eq. 6.1})$$

Figure 6.1 displays the clean condition drag polar graph and the location of the maximum lift to drag ratio point. The coefficient of drag obtained from this point is 0.342.

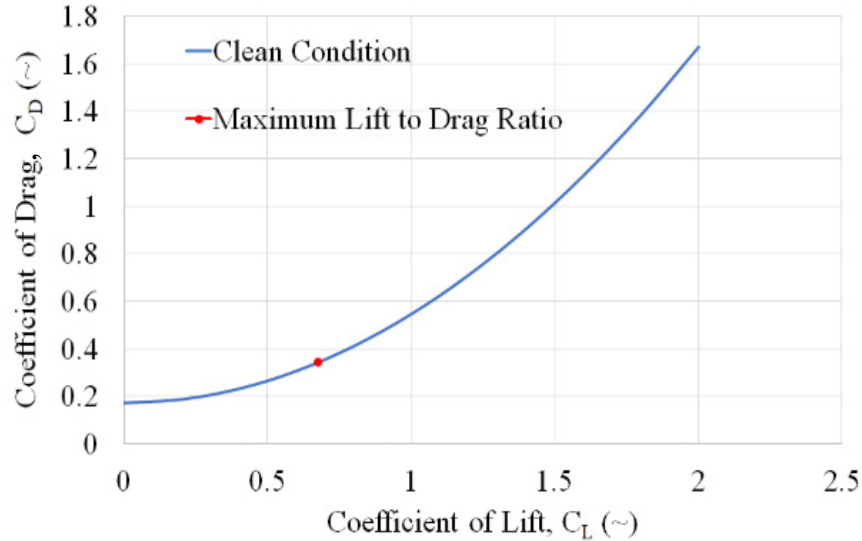


Figure 6.1: Drag Polar Graph

6.2 SIZING CHARTS ANALYSIS

Chapter 3 of Reference 2 discusses the methods used to determine the wing loading and thrust to weight ratio of the FREEDOM. The authors assumed that the maximum lift coefficient the missile fins would attain for stall sizing was the C_L at $(L/D)_{max}$. The FREEDOM uses this assumption because it will always fly at a clean configuration with minimal operation in the subsonic flight regimes.

Figure 6.2 displays the sizing chart for the different performance constraints. The 15-g sea level maneuvers are not shown in the sizing chart because the method assumes the aircraft achieves constant speed throughout the entire maneuver. However, the power increases to maintain this constant speed. This results in an extremely high value for the thrust to weight ratio, which would be an unrealistic parameter for the design. The hash marks show the boundaries of the design. The intersection between the stall wing loading point and the maximum cruise thrust to weight ratio value represents the final design point. The authors chose small fins for the primary purpose of roll control, so the small fins do not generate the majority of the lift for the missile. The body of the missile generates the majority of the lift for the missile; however, the sizing chart only considered the generation of lift from fins. This design point allows the FREEDOM to complete all cruise and climb maneuvers with the smallest planform size. Table 6.1 summarizes major design parameters sized for the FREEDOM.

Additionally, the authors used AAA to generate another sizing chart to compare with the manual calculations. Because of the lack of launch modeling, only two lines are shown. This chart assumes that AAA calculated

Table 6.1: Sized Design Parameters

Design Parameter	Value	Units
Planform Area, S	15.00	ft ²
Wetted Area, S _{wet}	1,050.00	ft ²
Aspect Ratio, A	1.00	~
Max Takeoff Lift Coefficient, CL _{maxTO}	0.68	~
Max Lift Coefficient CL _{max}	0.68	~
Wing Loading, W/S	1,590.00	psf
Thrust to Weight Ratio	2.12	~

takeoff weight; whereas, the team determined it was easier to use another method for calculating the takeoff weight. Therefore, the chart shown in the pop-up window below does not demonstrate realistic results.

6.4 CONCLUSIONS AND RECOMMENDATIONS

The authors conclude that:

- i.) The preliminary sizing design parameters are as follows: S is 15 ft², S_{wet} is 1050 ft², A is 1.0, CL_{maxTO} and CL_{max} are 0.68, W/S is 1,590 psf, and the Thrust-to-Weight Ratio is 2.12.

The authors recommend that:

- i.) The power plant sizing method to use more accurate aerodynamic analysis techniques for a broad range of altitudes.

AAA Sizing Chart
(Click)

Wing and Powerplant Sizing
(Click)

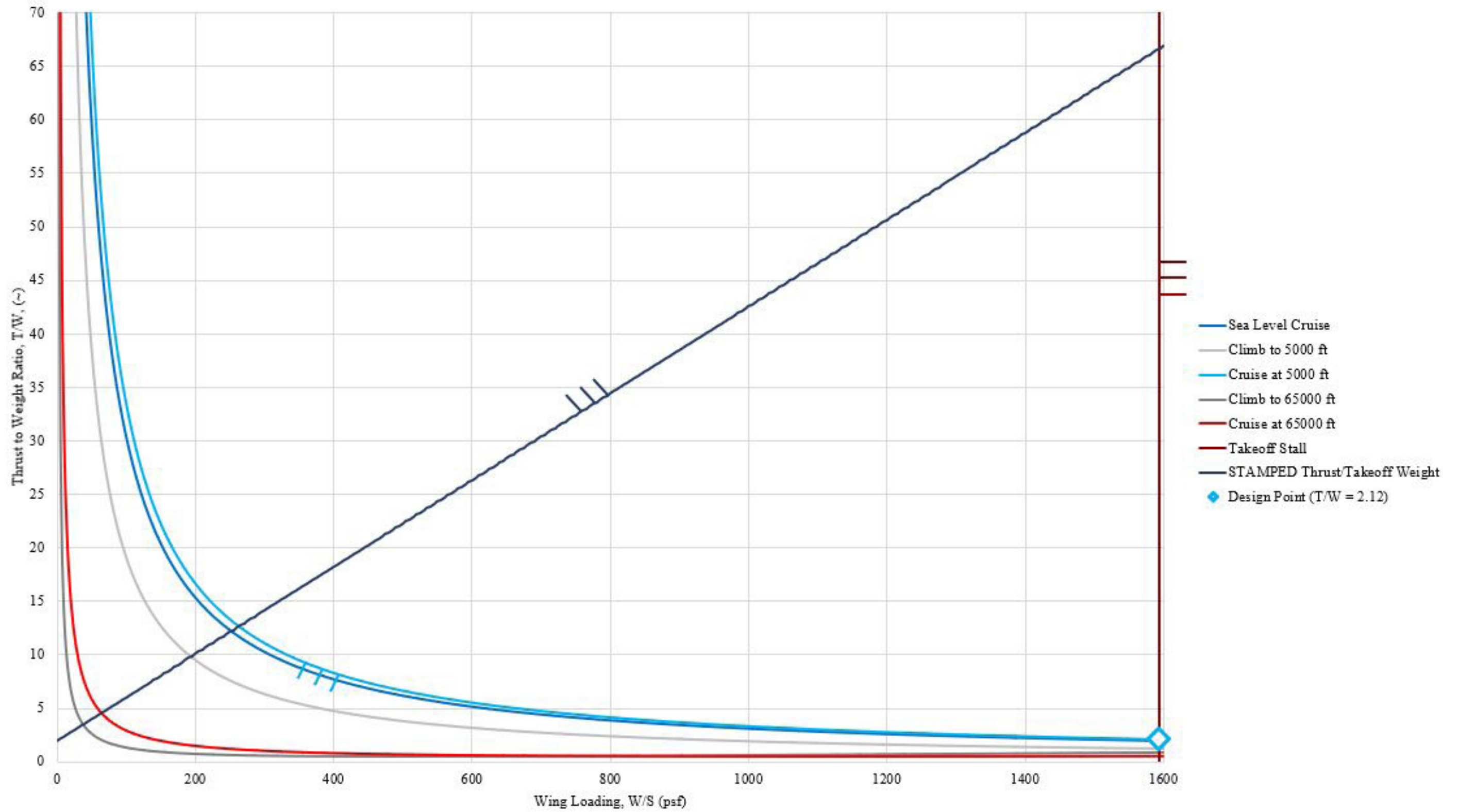


Figure 6.2: Sizing Chart of the FREEDOM Design

7. CLASS I CONFIGURATION MATRIX AND INITIAL DOWNSELECTION

The primary goal of this chapter is to document the selecting process for the desired configuration of the supersonic aerial target based on the process outlined in Reference 3.

7.1 MAJOR IMPACT ON THE DESIGN

The authors considered many different design factors when selecting a final configuration, including the requirements from the RFP (Ref. 1) and preliminary sizing trends. The designers decided that these factors include:

- Range of 150 nmi
- Mach 3.5 flight at sea level
- Mach 4.5 flight 15,000-65,000 ft above sea level
- 15-g maneuvering capability
- High thrust-to-weight ratio
- Low acquisition and maintenance costs
- Ability to mimic other missile threats
- 75° dive capability for "high diver" cruise

7.2 COMPARATIVE STUDY OF A MISSILE WITH A SIMILAR PERFORMANCE

As stated in Chapter 2, the GQM-163A Coyote is a supersonic cruise missile with similar high and low profiles to the RFP (Ref. 1). The Coyote cruises just under the maximum altitude of the FREEDOM for both profiles. The cruising and terminal speeds of the Coyote also follow this trend. The Coyote begins the high profile terminal phase by diving at an angle between 15 and 55 degrees. The FREEDOM also dives into this phase, but with a larger angle range outlined in Reference 1. The low profile terminal phases of the RFP (Ref. 1) and Coyote are similar in that both missiles complete longitudinal and lateral maneuvers. The maximum g-loading on the FREEDOM is higher than on the Coyote (Ref. 20). Although the FREEDOM must outperform the Coyote, the design of the Coyote provides a recent and similar example of a supersonic target.

7.3 CONFIGURATION SWEEP AND SELECTION

7.3.1 CONCEPT OPERATIONS

The configuration for this supersonic aerial target concept must reach the maximum speed, altitude, and maneuvering requirements specified in the RFP (Ref. 1). The on-board systems allow the missile to fulfill the mission requirements found in Section 1.2. These systems include the capability to navigate over a terrain in the low-altitude cruise, detecting the target intended to shoot the missile down; a fail-safe to self-destruct equips the missile for range safety. This missile

mimics the maneuverability and radar observability of threats during both high and low altitude cruise trajectories.

Launched from a rail mounted on the back of a semi-truck flatbed, the missile provides training for U.S. armed forces in intercepting potential enemy aerial threats. Although the operating conditions put it at risk of damage, the designers have considered possibly recovery systems such as parachutes when the missile is not intercepted. Figure 7.1 and Figure

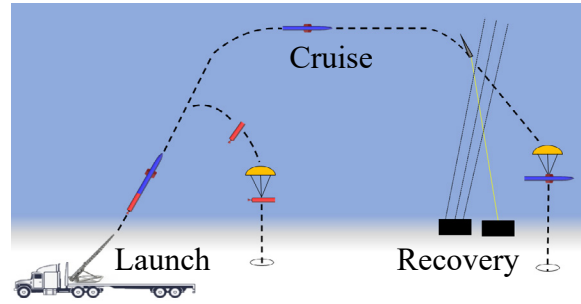


Figure 7.1: High Profile Operation (Refs. 31 and 32)

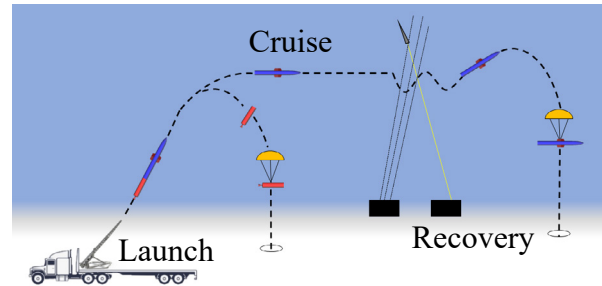


Figure 7.2: Low Profile Operations (Refs. 31 and 32)

7.2 displays this concept for high and low profiles. This gives the FREEDOM a chance to reuse a majority of the parts in a future launch, reducing the cost (Ref. 29). With a liquid-fueled rocket engine as the power plant, the parachute system could allow for more than 80% system recovery and reuse in a future flight (Ref. 30).

7.3.2 SELECTION OF THE OVERALL CONFIGURATION

7.3.2.1: Missile Category and Historical Configurations

Chapter 3 from Reference 3 illustrates the 12 categories of existing configurations for aircraft design. Since missiles are not included in these categories, the FREEDOM closest falls under category 12 as a supersonic cruise vehicle. The historical missiles and supersonic targets from Section 2.1 offered more detail examples of possible configurations. Due to similar flight profiles, the GQM-163A (Ref. 20) provided a baseline configuration for the FREEDOM.

7.3.2.2: Configuration Sweep

The following configurations were designed in OpenVSP and Siemens NX. Figure 7.3 displays the configuration sweep where configuration 10 was selected to continue in the design process.

7.3.2.3: Configuration Downselection

Because of time constraints, only one configuration was selected for Class I sizing. As described in Section 3.2, the authors considered the configuration sweep based on the objective function. Table 7.1 explains the reasoning behind the each downselection. Configuration 10 was selected as the advancing configuration for the FREEDOM.

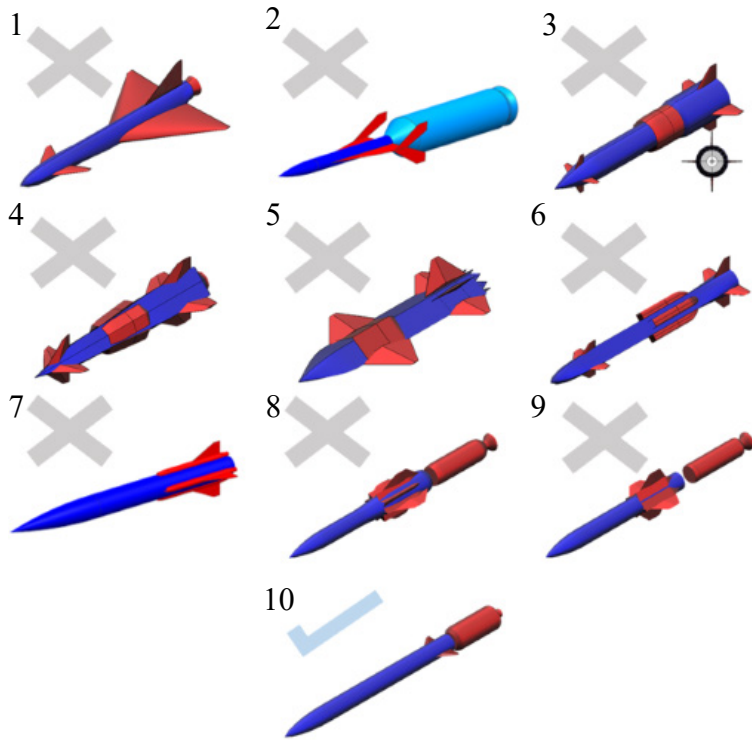


Figure 7.3: Configuration Sweep (Not to Scale)

Table 7.1: Downselection Reasoning

Configuration	Reasons for Downselection
1	High drag; complex controls; large planforms for desired maneuvers
2	Complex controls; large planform for desired maneuvers
3	High drag at inlet; mechanical complexities with multiple ramjets
4	Structural and aerodynamic concerns with all-faceted surfaces
5	Complex controls; structural and aerodynamic concerns with all-faceted surfaces
6	High RCS
7	Higher profile drag with external ramjets; interrupts flow around fins
8	Mechanical complexities of 8 inlets
9	Ramjets

7.4 CONCLUSIONS AND RECOMMENDATIONS

The authors conclude that:

- i.) The advancing configuration is a two stage missile with a thrust vectoring rocket engine;
- ii.) The terminal stage of the missile will be designed with low observability and recovery in mind.

The authors recommend to:

- i.) “Fly off” multiple designs and determine the configuration using quantitative measures.

8. LAYOUT OF THE COCKPIT AND THE FUSELAGE

This chapter consists of the design process for the interior components and the fuselage. The fuselage design process follows the methods found in Chapters 2 and 4 of Reference 26. These guided the design of the fuselage shape and the locations of primary interior components.

8.1 LAYOUT OF THE INTERIOR COMPONENTS

The RFP (Ref. 1) requires an unspecified payload module that is a 10-inch diameter, 3.5 feet long cylinder that weighs up to 500 pounds. Reference 1 also includes a GNC package that is capable of maneuvering and accuracy requirements in the payload. A radar emitting device to mimic potential threat missiles, a fail-safe self-destruct device, and a battery to power the avionics also equips the missile. Table 8.1 shows the components and the color of each component in the model. The designers placed the payload module in the front end of the nose and the internal layout of components in the payload bay follows the example configuration in Figure 4.7 from Reference 26. This configuration allowed for easy access for maintenance and loading additional payload. The layout of the components is shown in Figure 8.2 and Figure 8.1.

Table 8.1: Payload Components

Component	Color
GNC system	Light Blue
GNC Battery	Light Red
Payload Module	Dark Blue
Range Safety Device	Dark Red
Transponder	Light Gray
Emitter	Dark Gray
Unspecified Payload	Black

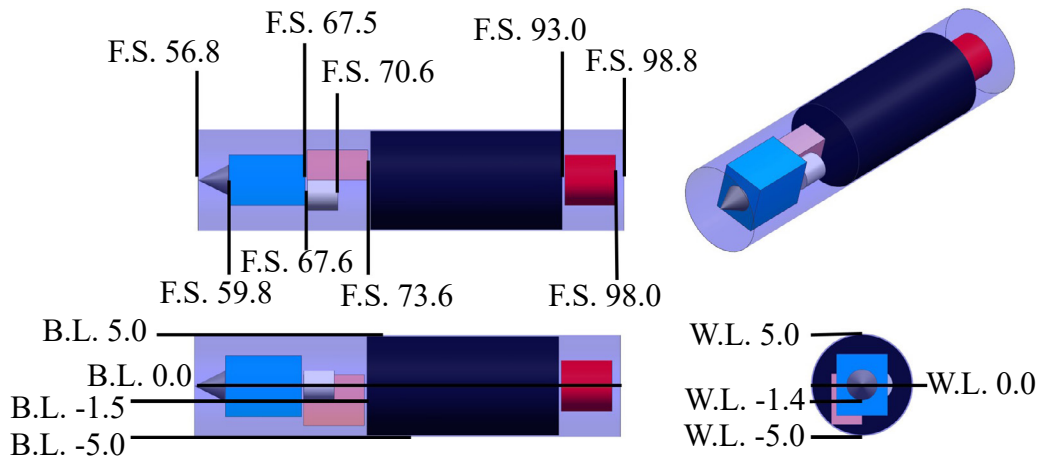


Figure 8.1: Payload Component Layout: 3-View and Isometric
All Dimensions in Inches (Scale: 1:20)



Figure 8.2: Payload Integration: 3-View and Isometric
All Dimensions in Inches (Scale: 1:200)

8.2 LAYOUT DESIGN OF THE FUSELAGE

The recommendations in Chapter 2 of Reference 26 drove the fuselage layout. It featured a sharp tangent ogive nose cone and a cylindrical body. The length of the nose cone and body was 180 inches and 300 inches, for a total length of 480 inches. The maximum body diameter was 36 inches. To reduce drag, the designers selected lengths that would increase the fineness ratios of the nose cone and body. Reference 26 shows this

in the zero-lift drag coefficient equations.

The fuel and oxidizer volumes required for the liquid fuel rocket determine the fuse-

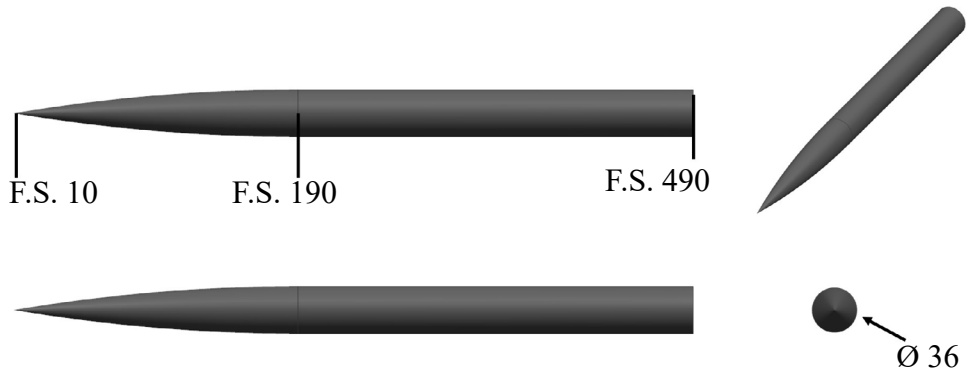


Figure 8.3: Missile Fuselage: 3-View and Isometric
All Dimensions in Inches (Scale: 1:125)

lage diameter and length. Figure 8.3 displays a three-view of the missile fuselage.

8.3 CONCLUSIONS AND RECOMMENDATIONS

The authors conclude that:

- i.) The fuselage has a tangent ogive nose cone and a cylindrical body with a total length of 480 in;
- ii.) The 3.5 ft long payload cylinder was placed at the front end of the nosecone.

The authors recommend:

- i.) Sourcing off-the-shelf components for the interior of the fuselage;
- ii.) Adding a missile and booster recovery system.

9. LAYOUT DESIGN OF THE PROPULSION INSTALLATION

An initial selection for the propulsion system was an integral rocket ramjet. The designers chose to explore other power plant options because of the overall complexity of the dual purpose engine (Ref. 33). This engine has issues bonding the solid propellant to the engine casing when transforming from rocket to ramjet. Challenges in the nozzle lead to thermal abnormalities and make the system more complex. The authors scrutinized the implications of employing an aft ramjet with four inlets in a cruciform configuration. The missile performance results were presented in various flight profiles within the flight envelope to Professor Farokhi. He advised the team to rule out ramjet propulsion and utilize a rocket engine instead, due to the high Mach speeds in low altitudes (Ref. 34). The simplicity design intention of the system dictated the use of a separate solid rocket motor (SRM). This SRM jettisons after burnout at the cruising altitude.

The team performed a comparative analysis to select an ideal booster off the shelf to reach the cruise altitude. For the low profile altitude, the booster must augment with the descent to reach as low as 15 ft. As stated in Chapter 5, the SRM chosen for the initial launch and climb is the Northrop Grumman Orion 50 XL. The Orion 50 XL (displayed in Figure 9.1) contained a vectoring nozzle with

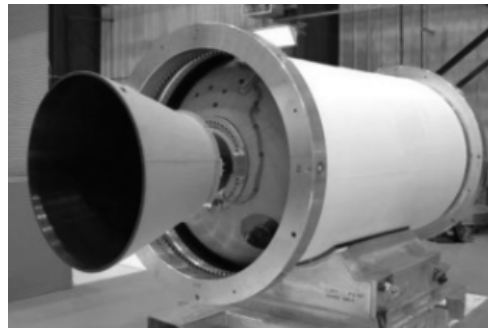


Figure 9.1: Orion 50 XL (Ref. 27)

a specific impulse (I_{sp}) of 292 seconds. Because the specific impulse did not suffer from any ram drag penalty, it was independent of the vehicle speed. According to Chapter 12 from Reference 35, the environmental conditions did not affect the combustion. The authors chose this because of the high efficiency compared to other SRM in the same category. This SRM also fell within the sizing and thrust ranges needed for both flight profiles.

The team selected the Launcher Engine-2 rocket as the main powerplant upon reaching the cruise altitude. This decision was based on efficiency, thrust production, and operational performance throughout the flight envelope. The 3D printed engine made the manufacturing process simple, cost-effective, and highly adaptable to improvements and modifications. As a closed cycle staged-combustion engine, this engine produced up to 24,800 pounds of thrust in a vacuum top-

ping out at 22,000 pounds at sea level. The rocket was mounted inside the fuselage towards the aft.

Figure 9.2 displays an engine test at the Launcher Space facility in Long Island, New York (Ref. 36). Below is a schematic drawing from Ref-



Figure 9.2: Launcher E-2 engine testing (Ref. 36)

erence 36 with specifications in the pop-up.

The authors decided to follow the conventional cylindrical design for adapters connecting the missile to the booster. The diameter of the adapter increases progressively from the rocket diameter to the booster diameter (Ref. 37). Transition ducts are characterized by a cross-sectional geometry that transitions from round to rectangular (Ref. 35). Professor Farokhi stated: “a rectangular, high aspect ratio nozzle makes the missile low observable.” Subsequently, the team designed a round-to-rectangular cross-section within the exhaust system. The authors sought to verify a Silicon dioxide duct design to eliminate separation bubbles and minimize corner vortices from previously done computational studies. Bernhard Anderson’s findings with benchmark experimental data validated the features of a transition duct that are listed in Table 9.1 and demonstrated in the pop-up window below (Ref. 38).

Table 9.1: Three-dimensional Transition Duct Characteristics

Exit-to-inlet Area Ratio (~)	Length Ratio, L/D (~)	Aspect Ratio, AR (~)
1	2	3

The team achieved thrust vector control using a gimbaled

nozzle with liquid propellant (Ref. 39). The control authority using this approach ranged from -7 to 7 degrees, according to chapter 12 of (Ref. 35). The hole-type nozzle was capable of increasing the thrust vectoring efficiency in smaller scales (Ref. 40). The authors examined the insight above in higher fidelity; which scaled the results mentioned above into a larger scale.

Launcher Engine-2 Schematic (Ref. 36)
(Click)

Transition Duct Design Point (Ref. 38)
(Click)

9.1 SELECTION AND LAYOUT OF THE PROPULSION INSTALLATION

Figure 9.3 and Figure 9.4 display the powerplant installation layout of the FREEDOM.

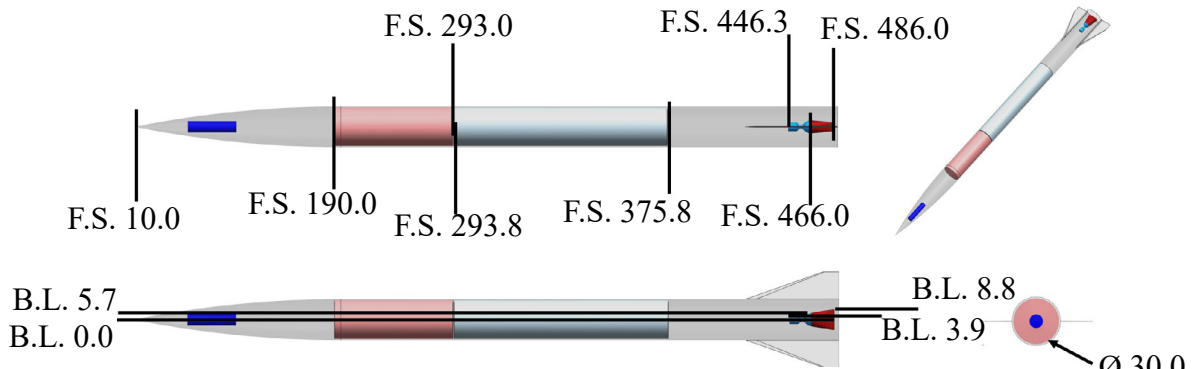


Figure 9.3: Missile Powerplant Layout: 3-View and Isometric All Dimensions in Inches (Scale: 1:125)

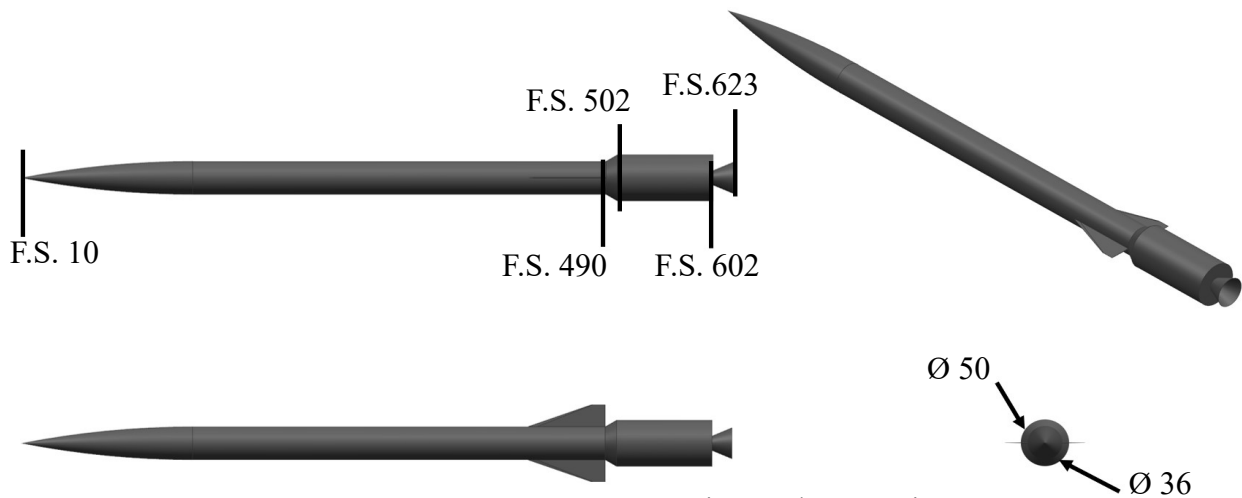


Figure 9.4: SRM Booster: 3-View and Isometric All Dimensions in Inches (Scale: 1:200)

9.2 CONCLUSIONS AND RECOMMENDATIONS

The authors conclude that:

- i.) The Orion 50XL SRM was selected because it has an I_{sp} of 292 s with no ram drag penalties;
- ii.) The Launcher Engine-2 was selected as the main propulsion system because it has 22,000 lbs of thrust and an I_{sp} of 291 s.

The authors recommend that:

- i.) A further in depth analysis of SRM engines takes place;
- ii.) More research should be conducted on non-cryogenic oxidizer engines and non-toxic hypergolic propellants.

11. CLASS I DESIGN OF HIGH LIFT DEVICES

The purpose of this chapter analyzes the possible need for high lift devices on the target drone using a method discussed by Dr. Barrett (Ref. 41). This method consisted of determining the required angle of attack for each phase of the mission to achieve the desired load factor. For the maneuver phase, this load factor is 15-g's. In all other phases, this is 1-g. By the recommendation of Dr. Barrett (Ref. 41), an angle of attack less than 10 degrees will not require high lift devices. The lift of the missile was determined using the equations presented in Chapter 2 of (Ref. 26).

11.1 DESIGN OF HIGH LIFT DEVICES

Resulting from Chapter 10, The highest angle of attack required for the flight was 9.25 degrees for dive condition in the high-altitude mission. Per Reference 41, this angle of attack is low enough for the in-flight missile not to require high lift devices. Table 10.1 shows the angle of attack and lift to weight for each flight phase, demonstrating that no high lift devices were needed for this design. The hand calculations for the critical flight condition are displayed in Section 10.1. The lift needed for the booster flight segment was much lower than the calculated lift because the launch required a steep flight path angle. This flight segment had excess thrust from the booster, which helped counteract the weight. This allows for the FREEDOM to have the ability to rely on body lift alone. The selected configuration from Chapter 7 also includes a fin set for stability and control. Chapter 12 presents the sizing and lift effects of the fins.

11.2 CONCLUSIONS AND RECOMMENDATIONS

- The authors conclude that:
- i.) From Chapter 10, Table 10.1 shows the angles of attack required in all mission phases and lift-to-weight ratios;
 - ii.) The missile will not require high lift devices during any phase of the flight.

The authors recommend that:

- i.) A CFD analysis is completed for further proof that no high lifting devices are necessary.

Table 10.1: Required Angle of Attack

Flight Profile	Flight Condition	Angle of Attack (degrees)	L/W (~)
High Profile	Booster Climb	7.88	1.00
	Rocket Climb	8.63	1.01
	65,000 ft. Cruise	9.00	1.04
	Dive	9.25	1.03
	Terminal Impact	0.75	1.03
Low Profile	Sea Level Boost	1.30	1.02
	Sea Level Cruise	1.38	1.02
	Maneuvers	7.30	15.02

12. CLASS I DESIGN OF THE EMPENNAGE

This chapter of the report documents the initial design of the empennage. The authors designed the empennage to maintain roll stability and control and generate lift in flight. The empennage design followed the procedure documented in Section 8.1 of Reference 2.

12.1 EMPENNAGE DESIGN PROCEDURE

The empennage of the FREEDOM was a single fin set. This gave the FREEDOM roll control. The authors based the empennage sizing on historical volumetric coefficients from past missiles. From these models, the authors determined the wingspan, mean geometric chord, planform areas, and an approximate center of gravity (C.G.) location.

To calculate the volumetric coefficient for a missile with a booster, the booster section was considered a subsection of the empennage. The authors assumed the side view cross sectional areas as the horizontal stabilizer planform area. From these cross sections, the centroid was assumed as the aerodynamic center to calculate the volumetric coefficient (Ref. 42). Figure 12.1 and Figure 12.2 show the horizontal stabilizer planform areas for the boosted and unboosted configurations of the FREEDOM. The historical cross sectional areas combined with the cross sectional areas of the FREEDOM (with and without the boosters) established a scale factor between the historical missiles and the FREEDOM. Using the scale factor, the designers calculated the X_h and C.G. location for the FREEDOM. The values for X_h and C.G. determined the planform area. Since the angle of attack is less than 10 degrees, the mono-wing configuration provides sufficient inherent stability for all flight conditions; therefore, the booster does not require additional fins.

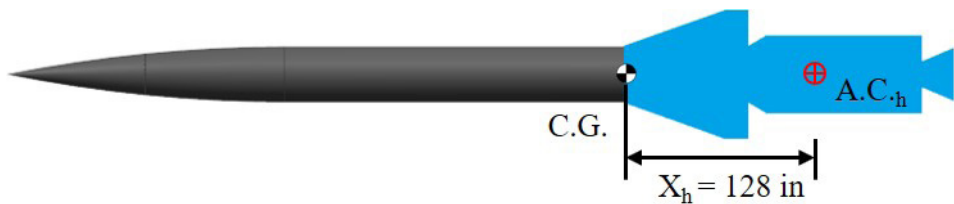


Figure 12.1: Empennage Cross Section with Booster (Scale 1:125)



Figure 12.2: Empennage Cross Section without Booster (Scale 1:100)

12.2 SUMMARY OF EMPENNAGE DESIGN AND CHARACTERISTICS

Table 12.1 shows the primary values for the fin set of the FREEDOM. The planforms generate additional lift, reducing the required angle of attack for each cruise condition. Table 12.2 displays the angle of attacks produced with the fin set.

Table 12.1: Fin Set Design Characteristics

Geometric Parameters	Value
S_{fin}	15.50 (ft ²)
A	1.00 (~)
b/2	1.97 (ft)
λ	0.18 (~)
C_r	6.71 (ft)
C_{mac}	4.59 (ft)
L.E. Thickness Angle	5.00 (degrees)
t/c	1.00 (~)
Λ	70.40 (degrees)
i	0.00 (degrees)
ε	0.00 (degrees)
Γ	0.00 (degrees)

Table 12.2: Fin and Body Lift: Angle of Attack

Flight Profile	Flight Condition	Angle of Attack: Body Lift and Fins (degrees)
High Profile	Booster Climb	7.88
	Rocket Climb	8.63
	65,000 ft. Cruise	9.00
	Dive	9.25
	Terminal Impact	0.75
Low Profile	Sea Level Boost	1.30
	Sea Level Cruise	1.38
	Maneuvers	7.30

The designers chose a thin flat plate with a sharpened leading edge for the fin set airfoil. The authors determined a thickness ratio of 0.01 to reduce the wave drag (Ref. 26). The designers estimated a 0.175 taper ratio based on the a trapezoidal wing assumption. Other wing shapes considered include triangular and square. These configurations were ruled out since a triangular wing has a taper ratio of 0, and a square wing has a taper ratio of 1 (Ref. 43). The designers chose a leading-edge thickness of 5 degrees to reduce wave drag. For structural purposes, the leading edge should not be a perfectly sharp corner because it would fail under high loading. The geometry of the planform and taper ratio estimated the sweep angle of the fins. Figure 12.3 and Figure 12.4 show the locations of crucial fin components.

Fin Sizing 1
(Click)

Fin Sizing 2
(Click)

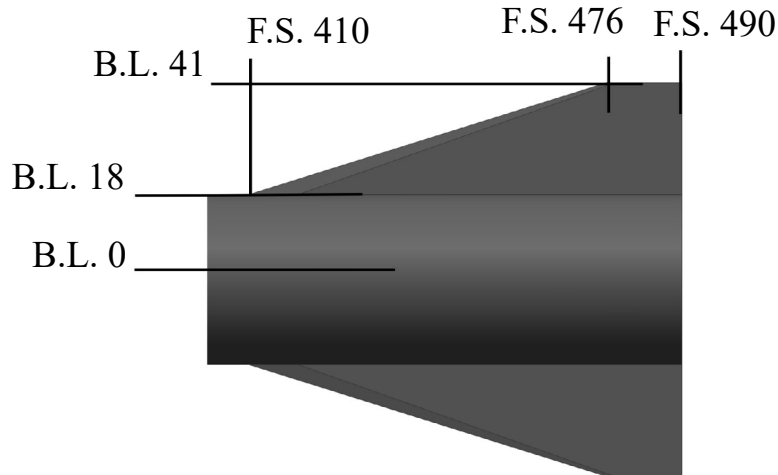


Figure 12.3: Fin Layout: Detail View
All Units in Inches (Scale: 1:40)

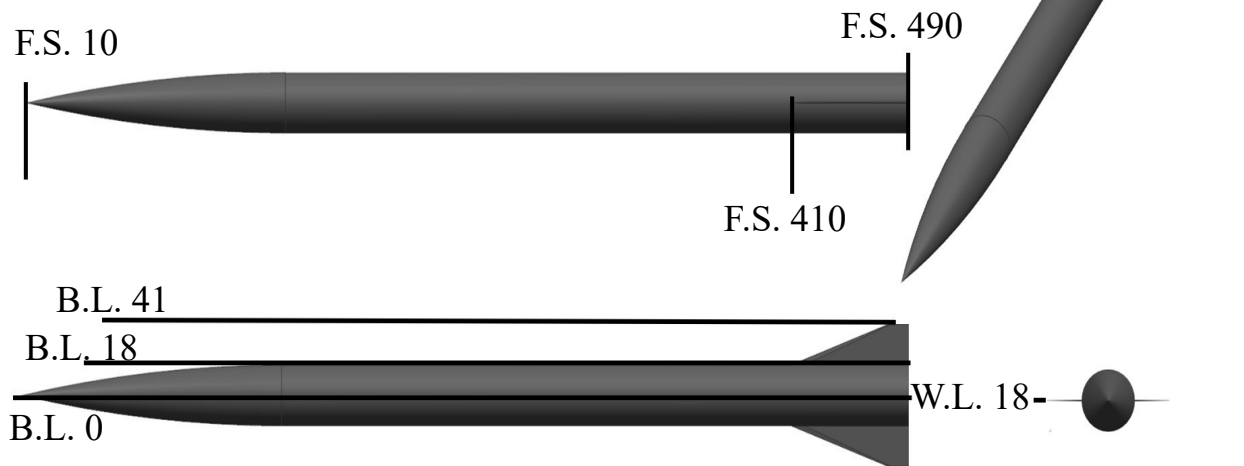


Figure 12.4: Integrated Fin Layout: 3-View and Isometric
All Dimensions in Inches (Scale: 1:100)

12.3 CONCLUSIONS AND RECOMMENDATIONS

The authors conclude that:

- i.) The sized fins have the following characteristics: S_{fin} of 15.5 ft², A of 1.00, b/2 of 1.97 ft, λ of 0.18, C_r of 6.71 ft, C_{mac} of 4.95 ft, L.E. thickness angle of 5.00 degrees, t/c of 1, Λ of 70.40 degrees, i of 0 degrees, ϵ of 0 degrees, and Γ of 0 degrees;
- ii.) The critical angle of attack with the addition of fins is 9.25 degrees during the high profile dive.

The authors recommend that:

- i.) A larger group of historical missiles models be utilized for estimating the C.G. position;
- ii.) A CFD analysis is completed to verify the required angles of attack of each profile.

13. CLASS I DESIGN OF THE LAUNCH AND RECOVERY SYSTEM

This chapter discusses the preliminary considerations of a launch and recovery system for the FREEDOM. Based on the concept of operations discussed in Chapter 7 and the geometry of the missile, the team designed a vertical launch system. The procedures used for the following sections are from Chapter 6 of Reference 26.

13.1 LAUNCH SYSTEM

Due to the long length of the FREEDOM, a static launch rail system would be unreasonably large. With guidance from Reference 29, the authors chose to launch from a mobile semi-truck trailer for launch location versatility. The designers created this launch system because a standard 53-foot trailer can store the missile and be modified to launch the missile. The mass production of the semi-trailer reduced the acquisition and maintenance costs of the launch system. The U.S. Department of Transportation limits the semi-truck and cargo weight to 80,000 pounds. The launcher system, FREEDOM without liquid propellant, and semi-truck weighed less than this limit (Ref. 44). Off of the semi-trailer, the team designed the FREEDOM to launch from a tube in a sabot. Tube launching requires minimal mounting hardpoints and assists with absorbing vibrations during transit to the launch site. For the material of the sabot, a lightweight foam could break away from the missile after launch (Ref. 29).

Figure 13.1 - Figure 13.3 depict the FREEDOM in vertical launch, mid-angle launch, and transport configurations. The designers chose geared motors to move two tracks across the trailer to raise the missile. In the center of the trailer, a blast plate and two ducts diverted the booster exhaust away from critical systems. Prior to launch, the FREEDOM would elevate into the launch position without any liquid fuel on board for safety and efficiency reasons.

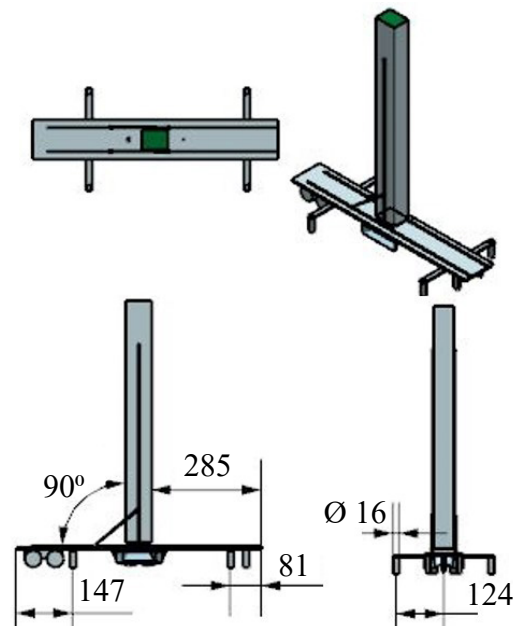


Figure 13.1: Vertical Launch System: 3-View and Isometric. All Dimensions in Inches (Scale 1:500)

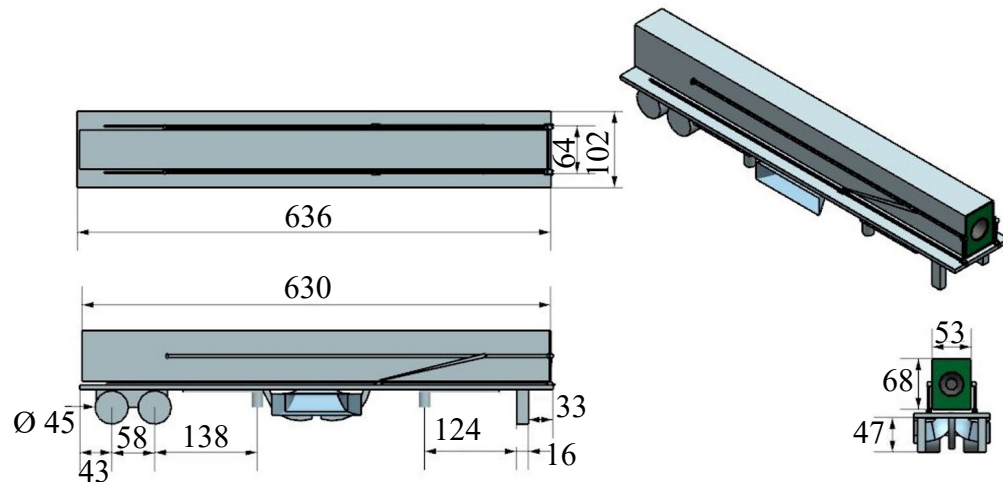


Figure 13.2: Stored Launch System: 3-View and Isometric. All Dimensions in Inches (Scale 1:250)

13.2 RECOVERY

A goal of the FREEDOM was to maximize the reusability of various components, including the booster and main body. A large parachute would act as the recovery system for the booster. If the defense system designed to destroy the FREEDOM fails, a supersonic drogue parachute would be deployed to decelerate the fuselage for the main parachute to deploy safely. The main parachute would reduce the vertical speed to 1,700 feet per minute which allows for the refurbishment and reuse of 80% of the FREEDOM (Ref. 34).

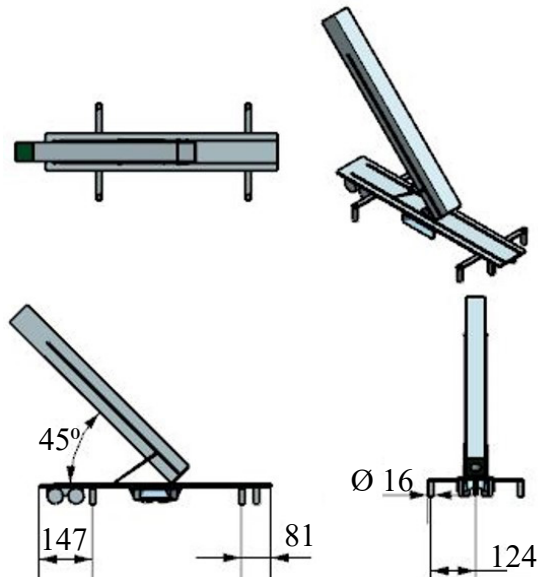


Figure 13.3: Mid-Angled Launch System: 3-View and Isometric. All Dimensions in Inches (Scale 1:500)

13.3 CONCLUSIONS AND RECOMMENDATIONS

The authors conclude that:

- i.) The FREEDOM is launched vertically on a modified trailer of a truck;
- ii.) 80% of the FREEDOM is reusable with a sufficient parachute system.

The authors recommend that:

- i.) A detailed CFD analysis is performed to confirm the parachute recovery systems;
- ii.) A full structural analysis of the trailer launcher be performed to confirm no failure occurs.

14. CLASS I WEIGHT AND BALANCE ANALYSIS

The authors performed preliminary weight and balance analysis using Roskam’s method laid out in Chapter 2 of Reference 6. An iterative process calculated the weight fractions for specific components of the FREEDOM and the center of gravity position for each configuration. An excursion diagram shows the C.G. position of the target drone throughout the mission profile.

14.1 PRELIMINARY THREE-VIEW

Figure 14.1 shows the preliminary three view of the FREEDOM.

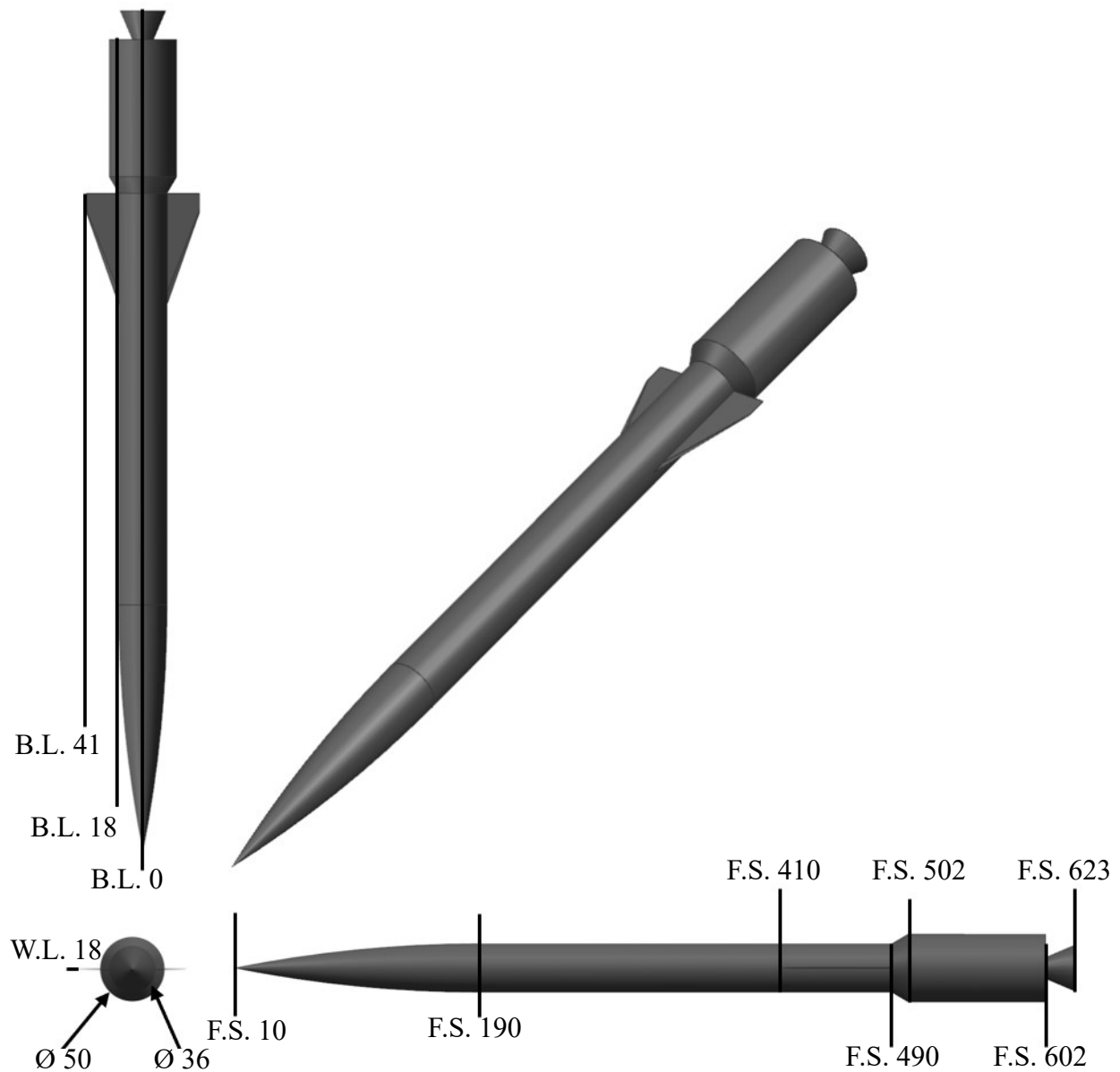


Figure 14.1: Three View of the Freedom: All Dimensions in Inches (Scale 1:125)

14.2 CLASS I WEIGHTS BREAKDOWN

To obtain the individual weights of the major components in the target drone, the authors calculated the weight fractions of each component. The values necessary to determine the weight fractions for each component were the component volumes and material density of the component. Reference 26 shows the material densities for typical target drone components. Table 14.1 shows the weight fractions, and individual component weights found using Chapter 2 of Reference 6.

Table 14.1: Weight Fractions and Component Weight

Component	Weight Fraction (~)	Component Weight (lbf)
Structure Group	0.102	2,430
Powerplant Group	0.102	2,540
Fixed Equipment Group	0.088	2,110
Propellant Group	0.704	16,800

14.3 CLASS I WEIGHT AND BALANCE CALCULATION

After calculating the individual component weights, the designers found the location of the C.G. for the entire target drone. Using Roskam’s method in Chapter 10 of Reference 3, the authors found the locations in the x-axis for each individual location of C.G. The y-axis and z-axis C.G. location were not included in the analysis because the target drone was axis-symmetric and all of the C.G. locations were placed along the x-axis. The designers calculated the C.G. location for the entire target drone with the summation of all of the individual component weights multiplied by the C.G. locations and divided by the total weight. Table

Table 14.2: Component Weight and C.G. Locations

	Component	Weight (lbf)	F.S. (in)	W.L. (in)
1	Structures Group	2,430	333	0
2	Powerplant Group	2,540	510	0
3	Fixed Equipment Group	2,110	196	0
4	Propellant Group	16,800	460	0
5	Take-off Weight	23,900	428	0

14.2 shows the individual component weights and C.G. locations. Figure 14.2 shows the side and front view of the location of C.G. for the individual components and the entire target drone.

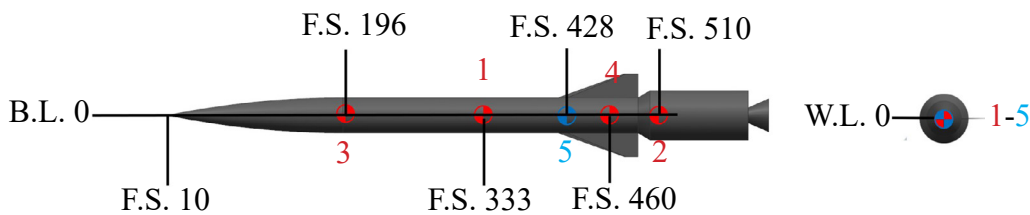


Figure 14.2: Component C.G. Locations: Side and Front Views (Scale 1:200)

14.4 CLASS I C.G. EXCURSION DIAGRAM

The C.G. excursion diagram provides a visual for the change of the C.G. location for the target drone. Figure 14.3 and Figure 14.4 show the C.G. excursion diagrams for the target drone during the booster and rocket engine phases. The designer’s goal for this diagram was to have as little change of the C.G. location as possible throughout the mission profile. Because of the booster drop off phase, however, the C.G. location changed drastically. Therefore, the C.G. excursion for the booster phase obtained a massive value because a significant amount of fuel burned in a short amount of time. The first phase was the takeoff with the booster through the booster burnout. The other stage was the booster drop off through the rocket engine burnout. Because of the significant change in weight between these two phases, the authors analyzed these two different phases. For simplicity, the target drone could fly both mission profiles because, at launch, the it contained the maximum amount of fuel. The C.G. excursion diagram for both profiles was the same because the weight remains the same. Therefore, Figure 14.3 and Figure 14.4 are valid for all mission profiles of the target drone.

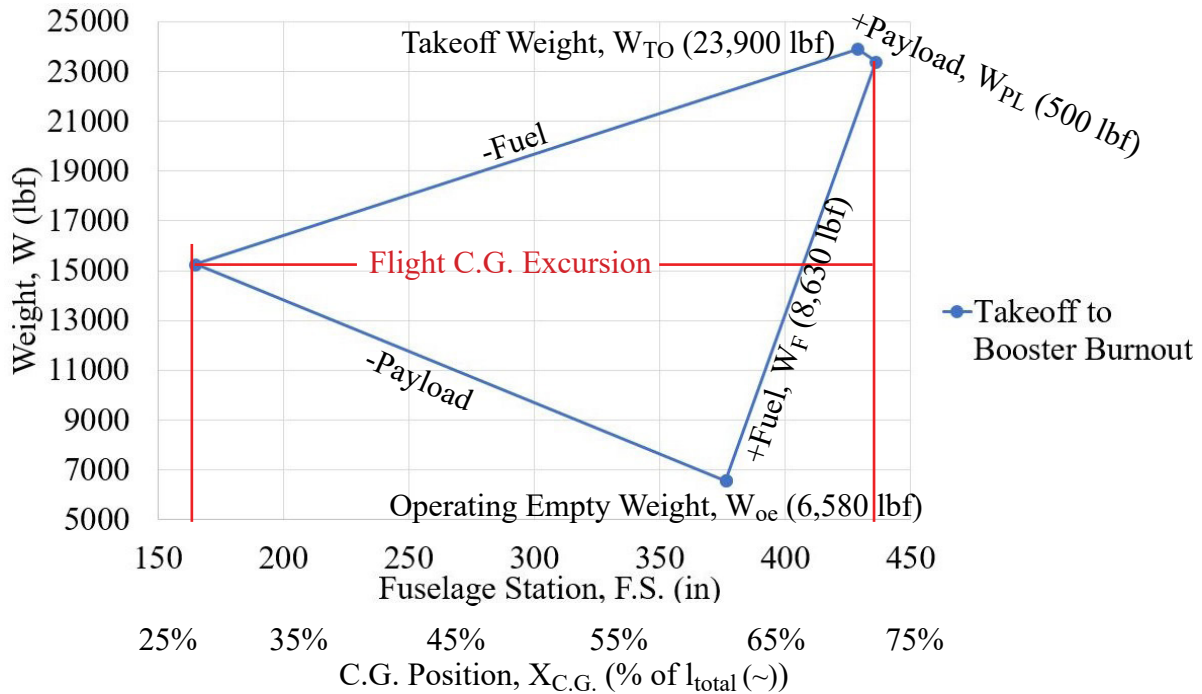


Figure 14.3: Weight C.G. Excursion Diagram: Booster Phase

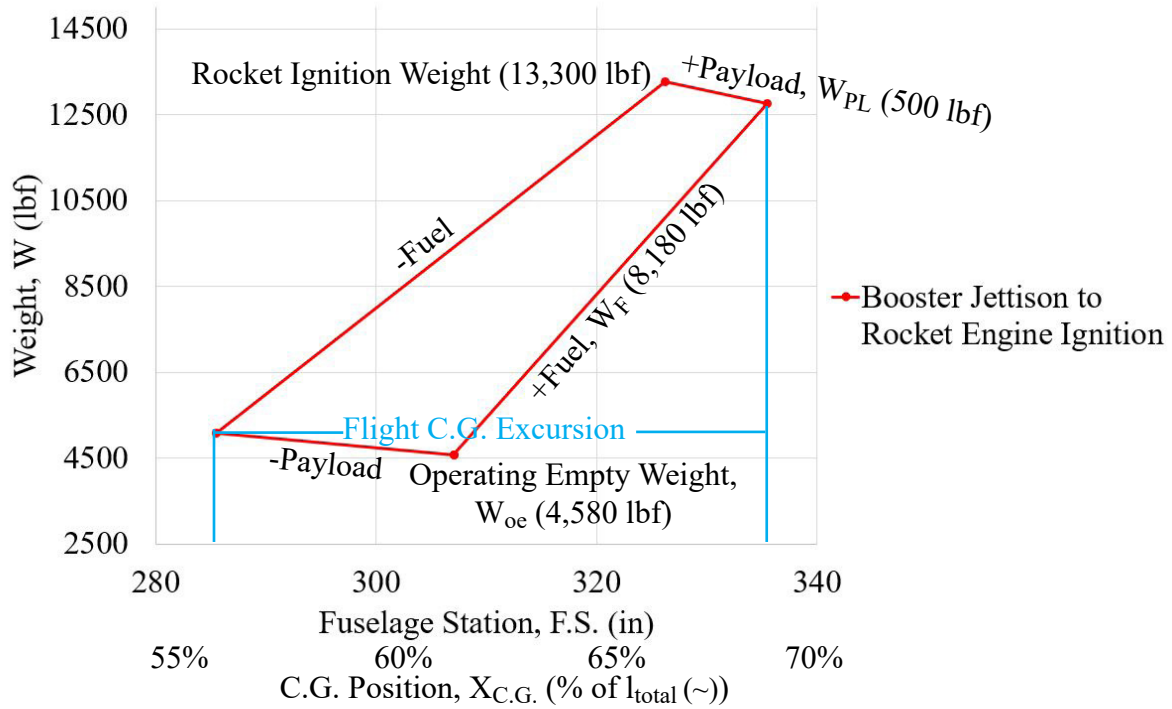


Figure 14.4: Weight C.G. Excursion Diagram: Rocket Engine Phase

Table 14.3 shows the values calculated for the C.G. excursion for both the booster and rocket engine phase. The booster phase (Figure 14.3) only accounts

Table 14.3: C.G. Excursion Values

Flight Condition	C.G. Excursion (in)	C.G. Excursion (%)
Booster Phase	271	44
Rocket Engine Phase	50	10

for a small portion of the mission profile, so it does not represent the typical loading condition for the FREEDOM. The designers decided that the rocket engine phase (Figure 14.4) best represents the loading condition for the FREEDOM because the target drone spends the majority of the mission profile in this phase. This phase also produces a smaller C.G. excursion.

14.5 CONCLUSIONS AND RECOMMENDATIONS

The authors conclude that:

- i.) For the booster phase, the C.G. excursion is 271 in and 44 %;
- ii.) The C.G. excursion for the rocket engine phases are 50 in and 10%.

The authors recommend that:

- i.) More iterations are performed to mitigate the C.G. excursion.

15. V-n DIAGRAM

This chapter describes the process and displays the result of the V-n diagram construction. The authors utilized the Roskam method to complete this process (Refs. 3 and 6).

15.1 V-n CALCULATIONS AND DIAGRAM

A V-n diagram determines the design limits and ultimate load factors at corresponding speeds used for aircraft structure design (Ref. 6). The load factors were set to ± 15 g's based on Reference 1. To create the V-n diagram, the authors considered the induced loading values from maneuvering and gust conditions. They utilized the FAR-25 certification approach from Reference 6 to calculate the induced gust load factors. The procedure lacks the vertical gust intensity data in high altitudes. Subsequently, the team consulted with Dr. Barrett (Ref. 45) regarding the shortage. It was advised that the team to utilize values at lower altitudes of the mission profile. The team concluded the insignificant effect of gust loads during high flight speeds. Figure 15.1 depicts the combination effects of maneuver and gust loading values. The FREEDOM missile reaches the limit loading factors by the dive stage. This diagram shows that the missile was structurally strong enough to endure these loads throughout the speed spectrum.

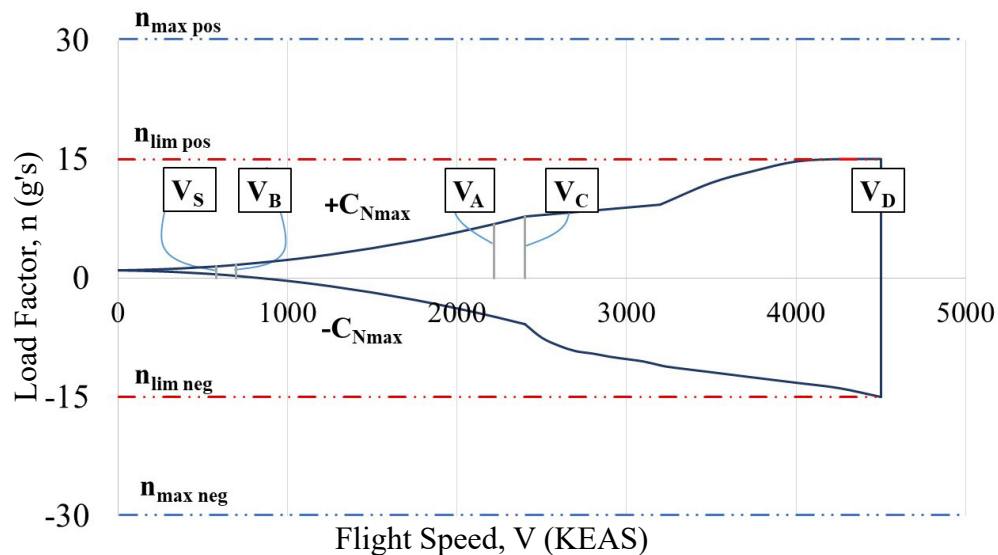


Figure 15.1: V-n Diagram

V-n Calculations 1
(Click)

V-n Calculations 2
(Click)

15.2 GUST SPECTRUM ANALYSIS, DYNAMIC LOADING, AND FLIGHT PATH DEVIATIONS

This section determines the number of g's the FREEDOM experiences, the frequency content, and the resulting open-loop spatial flight path deviations. The process mentioned above was completed by following the Roskam method from Reference 46.

The authors analyzed the effect of the gust spectrum through dynamic loading and 3D flight path deviation in the longitudinal, lateral, and vertical directions. The change in longitudinal gust loading was two orders of magnitude less than lateral and vertical gust loadings due to a high forward speed. The changes in the angle of attack and sideslip angle determined the up/down and left/right flight path deviations. The Root Mean Square (RMS) values of the gust velocities were obtained from Figure 9.60 of Reference 46.

The following figures demonstrate the values of acceleration the FREEDOM will experience for the gust frequency and flight path deviation in the vertical and lateral directions. The FREEDOM was structurally strong enough to withstand the gust loading throughout the mission profile. Also, this missile was dynamically capable of overcoming the gust-induced flight path deviations for different values of open-loop motion frequency. Hand calculations are shown below as pop-up windows.

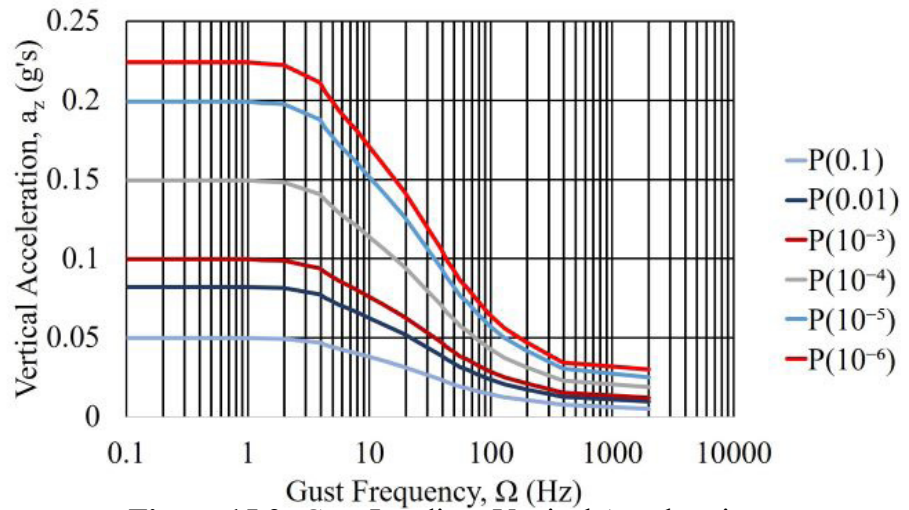


Figure 15.2: Gust Loading: Vertical Acceleration

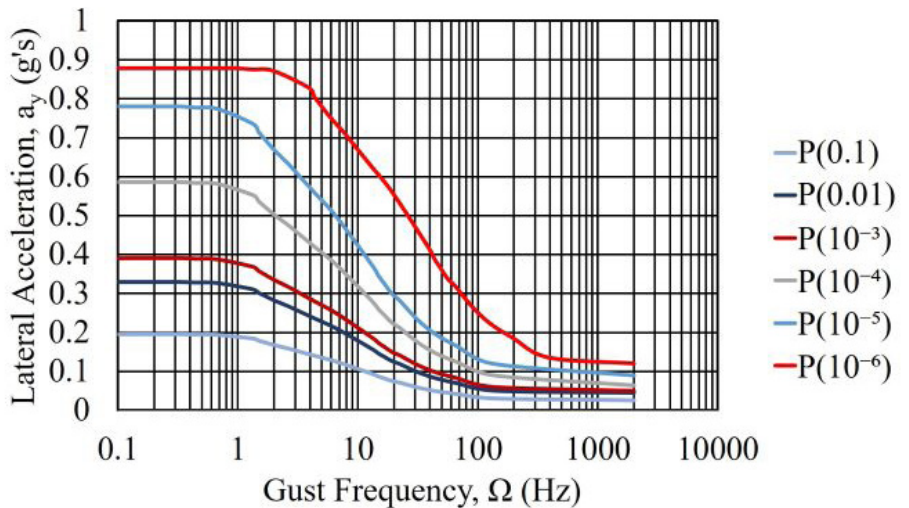


Figure 15.3: Gust Loading: Lateral Acceleration

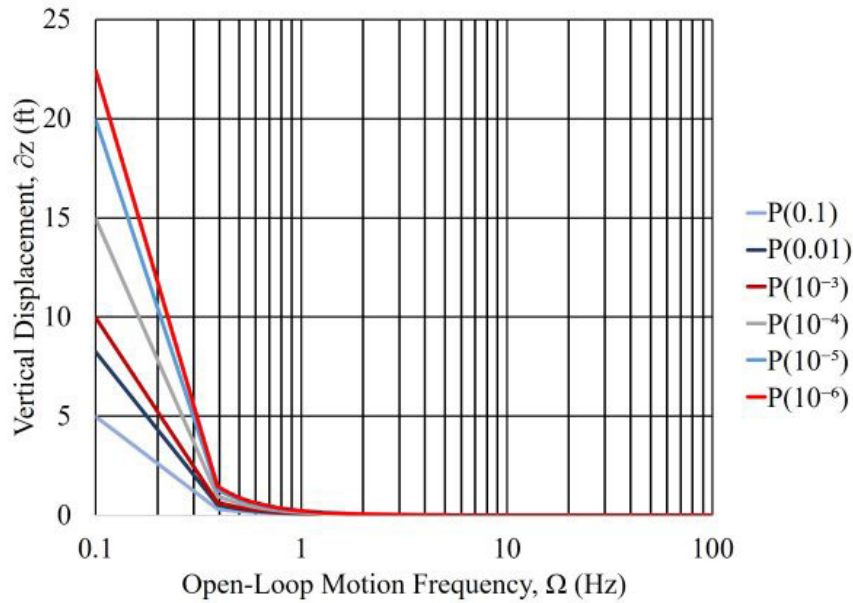


Figure 15.4: Gust Loading: Vertical Displacement

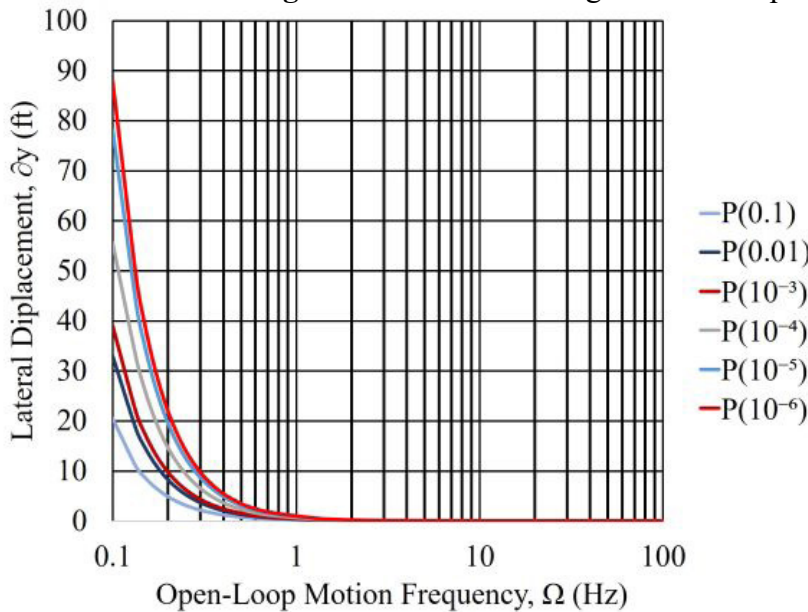


Figure 15.5: Gust Loading: Lateral Displacement

Gust Calculations 2
(Click)

15.3 CONCLUSIONS AND RECOMMENDATIONS

At the worst case scenario, the authors conclude that:

- i.) The vertical flight path deviation attenuates linearly from 22.4 to 0.1 ft and lateral flight path deviation decreases exponentially from 73.2 ft to 1.2 ft within the range of 0.1 and 1 Hz;
- ii.) The missile experiences a 0.224-g vertical acceleration and 0.878-g lateral acceleration within 0.1 and 2 Hz.

The authors recommend that:

- ii.) A study for the longitudinal gust loading effects on the FREEDOM should be completed.

17. CLASS I DRAG POLAR AND PERFORMANCE ANALYSIS

The goal of Chapter 17 was to generate Class I drag polars with the missile geometry and aerodynamics designed in Chapters 8 through 12. These values verified that the aerodynamic efficiency of FREEDOM meets the sizing goals, as outlined in Chapter 6. This method used the processes outlined in Reference 3, Reference 5, and Chapter 2 of Reference 26.

17.1 WETTED AREA BREAKDOWN

The designers used two methods to find the wetted area. The first method calculated the fuselage wetted area using a perimeter plot and fin wetted area using Equation 12.1 from Reference 3. The second method measured the surface area of the missile model in Siemens NX. To capture the curvature of the tangent ogive nose cone for the perimeter plot, the designers used 30 evenly spaced cross sections. Because the cross sections of the missile body, adaptor ring, and SRM either changed linearly or remained constant, only the cross sections at the beginning and ending of each component made up the rest of the perimeter plot. Figure 17.1 and Figure 17.2 show the perimeter plots of the FREEDOM in both boosted and unboosted configurations.

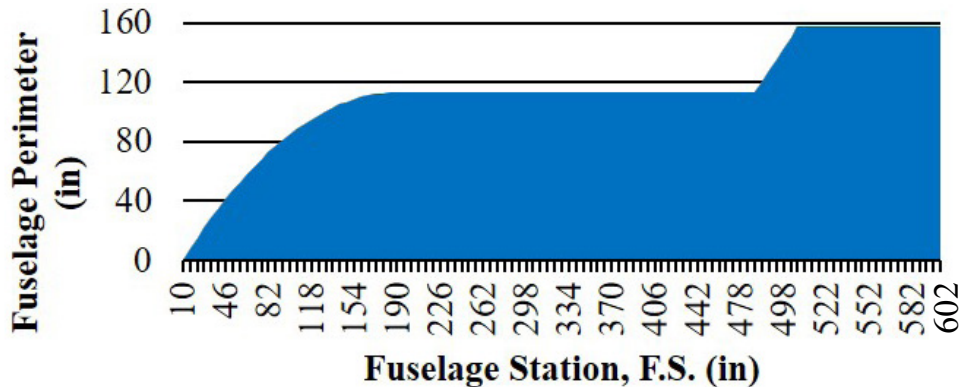


Figure 17.1: Perimeter Plot with Booster

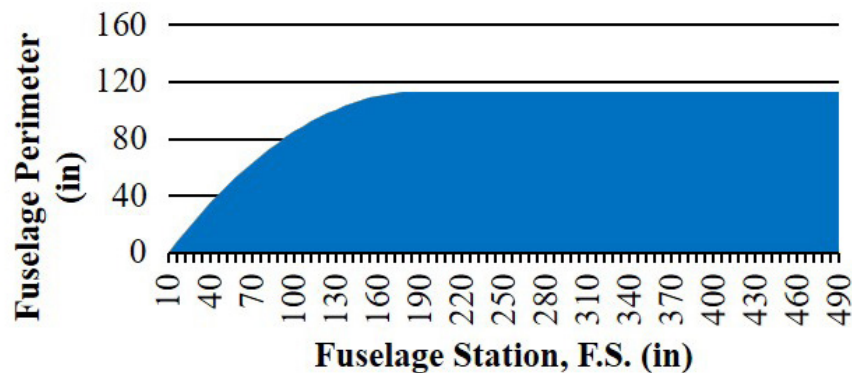


Figure 17.2: Perimeter Plot without Booster

Figure 17.3 shows the cross-sections used for the generation of these plots. Due to space constraints, only three of 30 nose cone cross-sections are present in Figure 17.3. When combined with the fin wetted area results from Equation 12.1 of Reference 3, the total wetted area of the FREEDOM in both boosted and unboosted configurations were found. Table 17.1 compares these values with the surface area measurements found in NX.

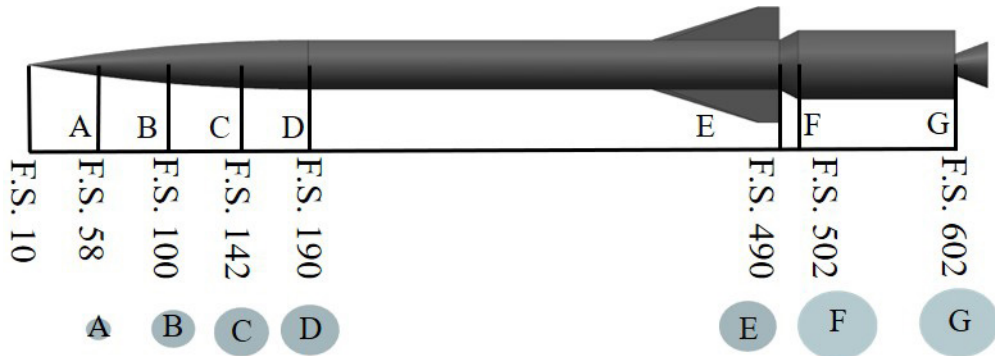


Figure 17.3: Fuselage Cross Sections: All Dimensions in Inches (Scale 1:125)

Table 17.1: Calculated and Measured Wetted Area Values

Component	Calculated Value	CAD Measurement
Missile Body	332.0 ft ²	330.0 ft ²
Fins	31.5 ft ²	32.1 ft ²
Missile Body, Boosted	453 ft ²	453 ft ²

17.2 DRAG POLAR ANALYSIS

The drag polars for the FREEDOM were calculated using equations from Chapter 2 of Reference 26. The pop-up win-

dows below show the hand calculations used to determine these values. Figure 17.4 and Figure 17.5 show the drag polar graphs at the cruise conditions. Because the FREEDOM spends the most time in the these conditions, the cruise conditions represent the critical mission phases. Table 17.2 shows the calculated zero-lift drag coefficients.

Table 17.2: Cruise Zero-Lift Drag Coefficients

Profile:	Mach (~)	C _{D0} (~)
Sea Level	2.00	0.21
	3.50	0.16
High Altitude, 65,000 ft	3.00	0.23
	4.50	0.19

[Class I Drag Polar 2 \(Click\)](#) [Class I Drag Polar 3 \(Click\)](#)

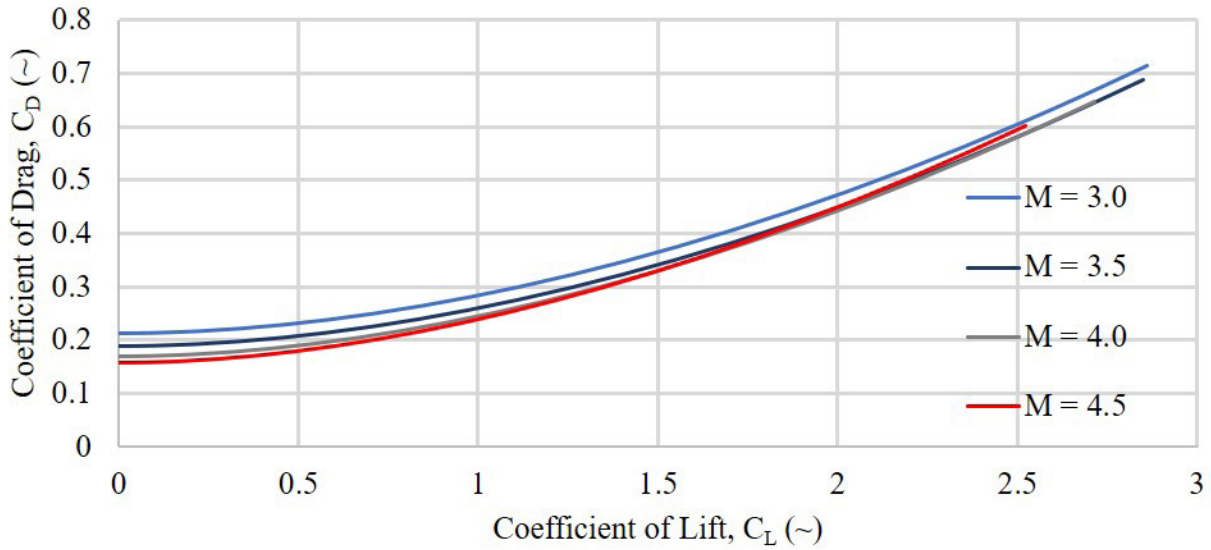


Figure 17.4: Class I Drag Polar at Sea Level

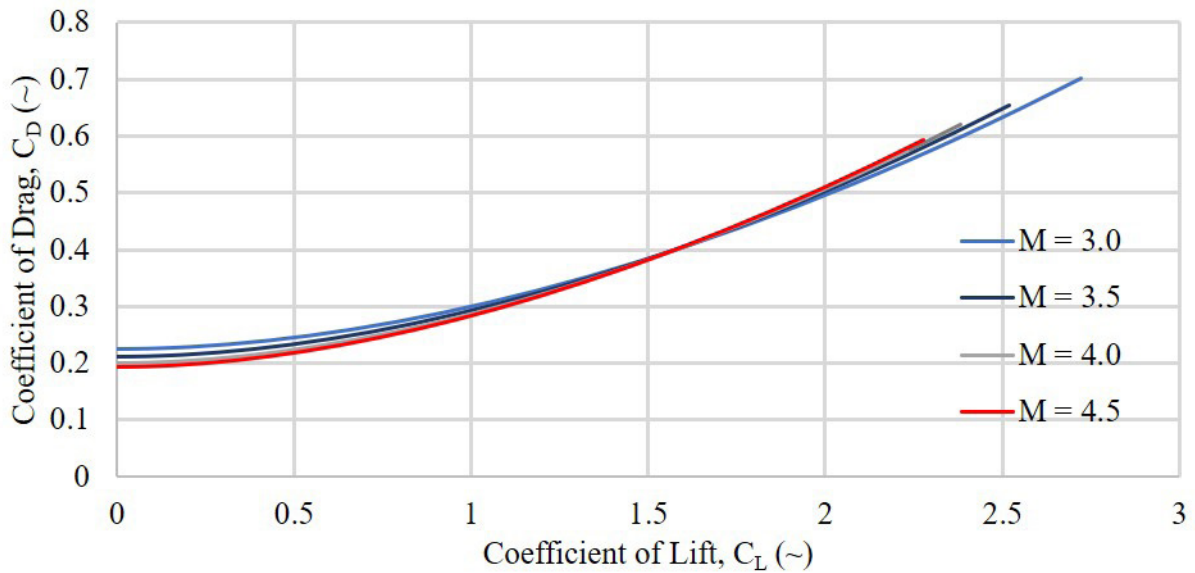


Figure 17.5: Class I Drag Polar at 65,000 Feet

17.3 CONCLUSIONS AND RECOMMENDATIONS

The authors conclude that:

- i.) Table 17.3 displays the resulting drag coefficients.

The authors recommend that:

- i.) A CFD analysis should be performed to calculate a more accurate zero-lift drag coefficient.

Table 17.3: Cruise Zero-Lift Drag Coefficients

Profile:	Mach (~)	C_{D0} (~)
Sea Level	2.00	0.21
	3.50	0.16
High Altitude, 65,000 ft	3.00	0.23
	4.50	0.19

18. ANALYSIS OF WEIGHT AND BALANCE, STABILITY AND CONTROL, AND L/D

The purpose of Chapter 18 consists of showing the design process and decisions made for Class I design. The designers used procedures in Reference 3 for the following design iterations.

18.1 IMPACT OF WEIGHT AND BALANCE AND STABILITY AND CONTROL RESULTS

Based on Chapters 14, the FREEDOM had acceptable weight and balance values. The FREEDOM also resulted in respectable stability and control values for a responsive and maneuverable target drone in Chapter 16. The designers decided to implement a tight feedback loop to allow the missile to be controllable in all flight conditions.

18.2 ANALYSIS OF CRITICAL L/D RESULTS

To validate the calculated weight and balance values of the FREEDOM, the designers compared the preliminary and Chapter 17 Class I lift to drag ratios for each flight condition. Table 18.1 shows the preliminary and Class I lift to drag ratios for each mission phase. The designers found the Class I lift to drag ratios for each flight condition from equations in Reference 26. The Class I lift to drag ratios were smaller than the preliminary ratio. Therefore, the lift over drag decreased from the preliminary values, so the weight of the FREEDOM increased.

Table 18.1: Class I $(L/D)_{max}$ and Preliminary Drag Polar Values

Flight Condition	Mach Number (~)	C_L (~)	C_D (~)	$(L/D)_{Preliminary}$ (~)	$(L/D)_{ClassI}$ (~)	Weight (lb _f)
65,000 ft. Cruise	4.50	1.71	0.43	4.97	3.91	16,000
Sea Level Boost	3.50	1.06	0.27	4.97	3.92	24,600
Sea Level Cruise	3.50	1.62	0.36	4.97	4.50	16,000
Maneuvers	3.50	1.32	0.34	4.97	3.87	16,000

Regarding the environmental impact of the FREEDOM, the RP-1 (rocket propulsion-1/refined petroleum-1) and SRM fuel accumulated to produce 3,080 pounds of carbon dioxide per launch (Ref. 51). According to the Environmental Protection Agency, the initial development of 365 missiles was 99 ten millionths of a percent of the emissions produced by the U.S. each year (Ref. 52). This would not be a large environmental issue but could become one in the future as more missile are produced.

18.3 DESIGN ITERATIONS PERFORMED

The FREEDOM has undergone many iterations to improve the overall design of the vehicle. The designers changed the initial selection of a ramjet to the E-2 rocket engine based on the advisement of Dr. Farokhi (Ref. 34). The extreme range of speeds and altitudes requested by the RFP (Ref. 1) were the reasons for this design change. This engine converts 60% of the fuel mass to carbon dioxide (Ref. 51). The authors intend to work with Launcher Space to create a variant of the E-2 to use liquid methane or liquid hydrogen, which would reduce carbon dioxide emissions by 40% or 44%. The engine selection iteration forced a change in the SRM selection due to the increase in required total impulse and thrust of the booster.

The C.G. of the FREEDOM was shifted forward to reduce the static margin. The designers moved the payload, thermal protection system, structural components, and propellant systems forward in the fuselage. From Chapter 14, the large C.G. excursion of the booster flight phase would increase with this iteration. It would still be an acceptable C.G. excursion because only the wind gust affects the flight path during this phase. Additionally, the fuel and oxidizer tanks were made coaxial to minimize the C.G. excursion of the terminal flight phase.

The design was changed to reduce the fin size (drag) and eliminate the need for fin actuators. This put the FREEDOM in a constant rolling state. The fins were set at opposite incidence angles of 2.73 degrees with a new area of 0.96 square feet. This change significantly reduced the drag with a minimal lift cost. At this incidence angle, the FREEDOM rotated between 8.7 Hertz and 19.5 Hertz. Table 18.2 shows the maximum and minimum rotational frequencies for the high and low profiles.

Table 18.2: Rotational Frequency Values

Mach Number (~)	Altitude (ft.)	Rotational Frequency (Hz)
2.0	0.0	10.0
3.5	0.0	17.5
2.0	65,000.0	8.7
4.5	65,000.0	19.5

18.4 CONCLUSIONS AND RECOMMENDATIONS

The authors conclude that:

- i.) The $(L/D)_{\max}$ of the high altitude cruise is 3.91, sea level cruise is 4.50, sea level maneuvers is 3.87, and sea level booster is 3.92.

The authors recommend that:

- i.) A variant of the E-2 should be developed to minimize the carbon footprint of the FREEDOM.

19. PRELIMINARY THREE-VIEW

This chapter summarizes the major characteristics for the Class I design of the FREEDOM. A three-view depicts the resulting Class I configuration of the FREEDOM. Multiple visuals that show the procedure and capabilities of the FREEDOM are presented at the end of this chapter.

19.1 TABLE OF CLASS I AIRCRAFT CHARACTERISTICS

Table 19.1 and Table 19.2 display the values for the Class I design of the FREEDOM.

Table 19.1: Class I Fuselage Characteristics

Flight Condition	Boosted Flight	Unboosted Flight
Maximum Body Diameter (ft)	4.18	3.00
Body Length (ft)	51.08	40.00

Table 19.2: Class I Fin Characteristics

S_{fin}	0.96 (ft ²)
A	1.46 (~)
b/2	0.59 (ft)
λ	0.03 (~)
C_r	1.67 (ft)
C_{mac}	1.11 (ft)
L.E. Thickness Angle	5.00 (degrees)
t/c	1.00 (~)
Λ	70.00 (degrees)
i	2.73 (degrees)
ϵ	0.00 (degrees)
Γ	0.00 (degrees)

19.2 CLASS I AIRCRAFT DESCRIPTION

The FREEDOM is a two-stage cruise missile with an SRM booster for launch and a vectoring liquid-fueled rocket engine sustainer with a transition duct. It is capable of reaching Mach 4.5 flight at 65,000 feet altitude, Mach 3.5 flight at sea level and the terminal phase, and has a range of 150 nautical miles. At a maximum launch weight of 23,900 pounds, it is designed to be transported and tube-launched from a 53-foot trailer. This launcher configuration makes the missile highly mobile and capable of being launched from most land-based test ranges. In the event the U.S. armed forces fail to shoot down the FREEDOM, it is designed to have recoverable and reusable systems and structures via the use of parachutes. Ablative coatings on the missile prevent overheating of the structure and internal systems. An onboard GNC package and RF emitter are present in the payload bay of the missile to match the flight pattern and RCS of possible enemy threat missiles during flight.

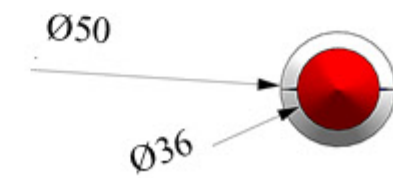
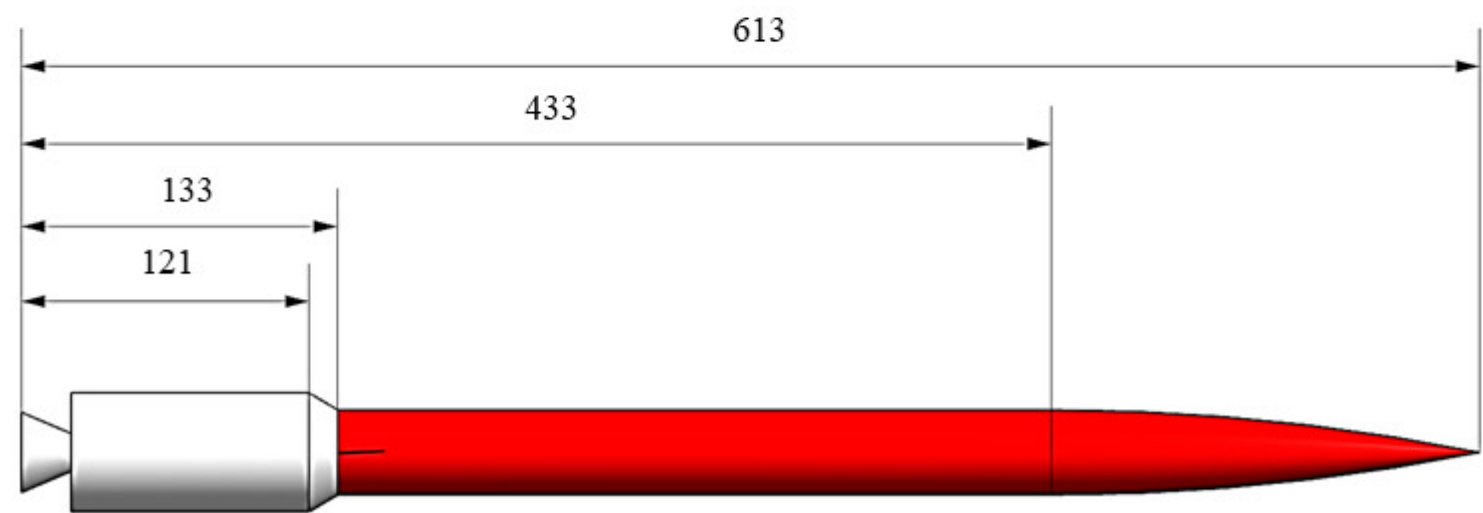
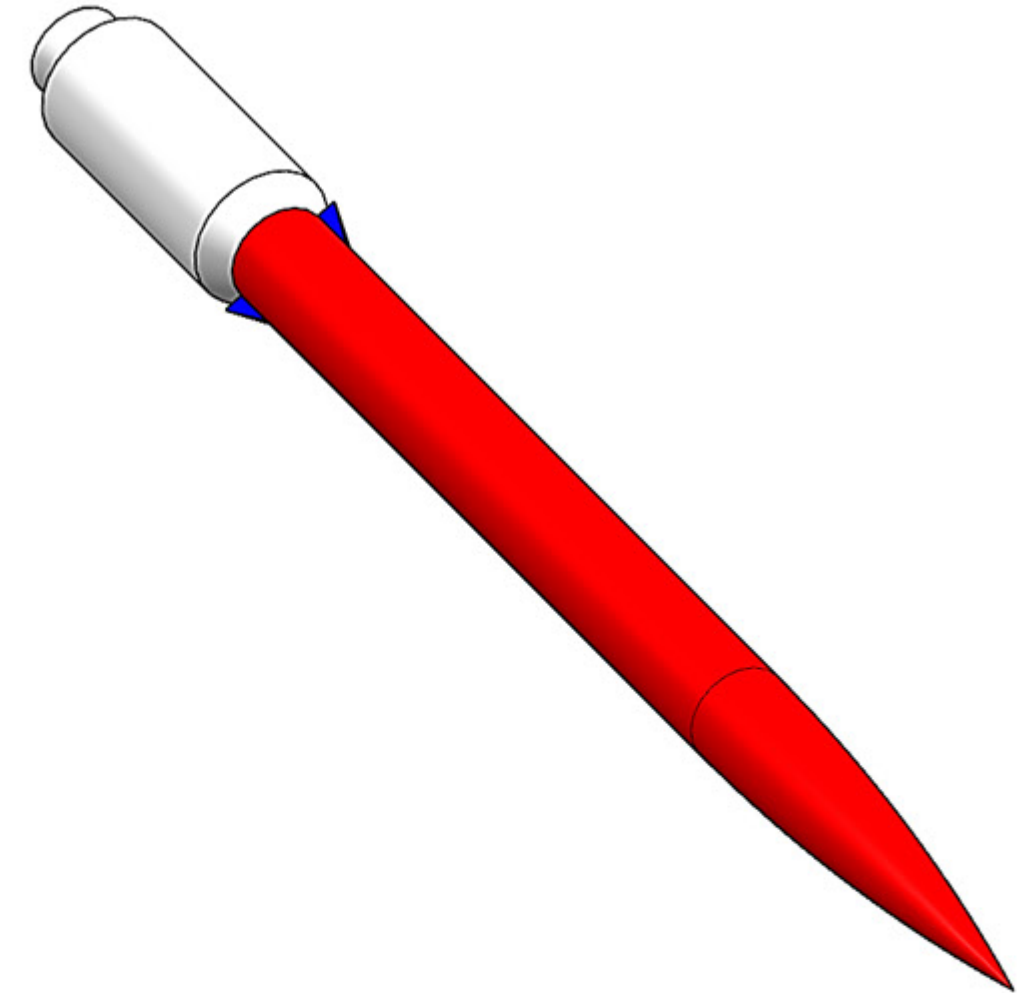
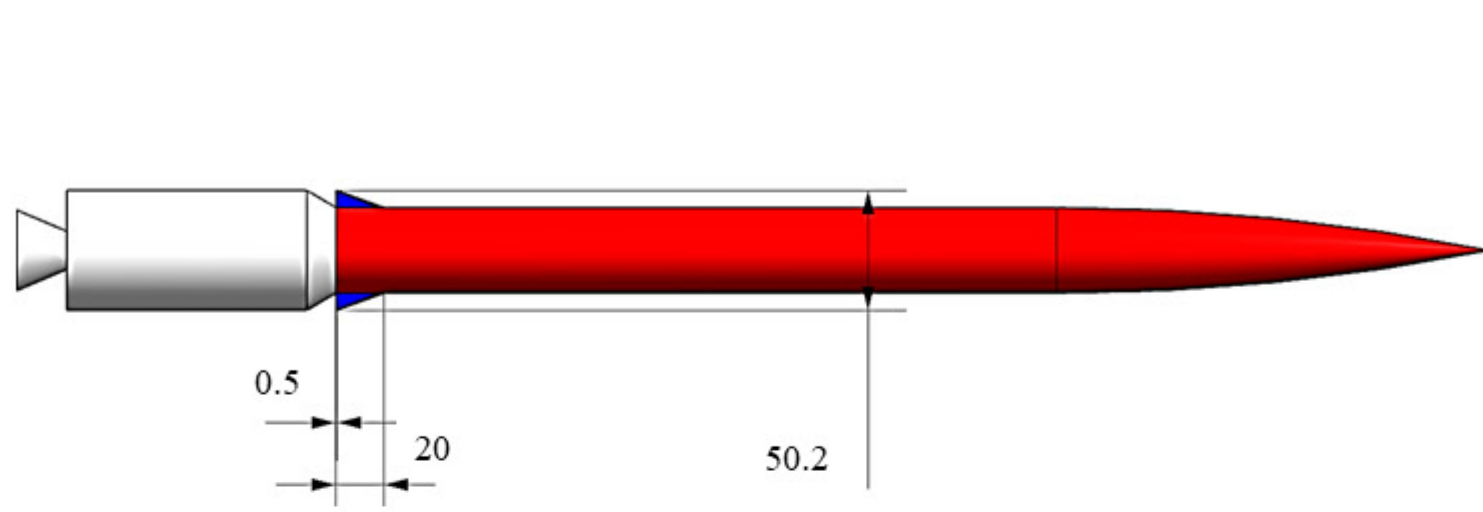


Figure 19.1: Class I Design: 3-View and Isometric.
All Dimensions in Inches (Scale 1:80)

19.3 ACTION VIEWS

Figure 19.2 to Figure 19.9 display different scenes of the FREEDOM in action.

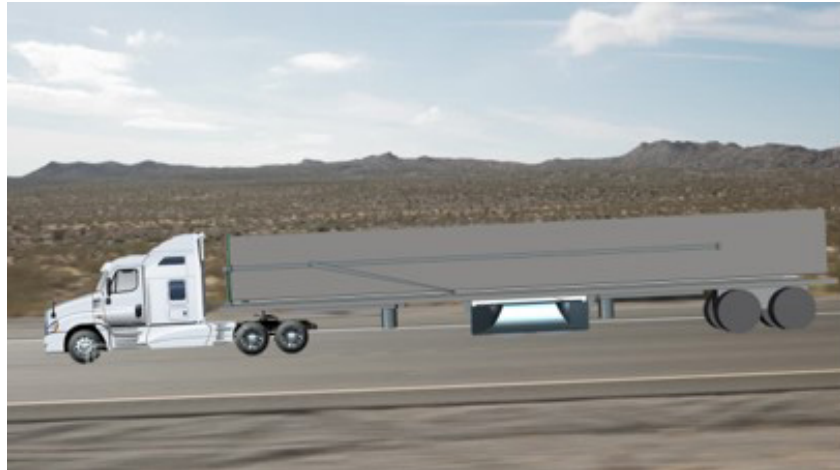


Figure 19.2: Transportation of the Launch System



Figure 19.3: The FREEDOM in Flight



Figure 19.4: The Launch of the FREEDOM

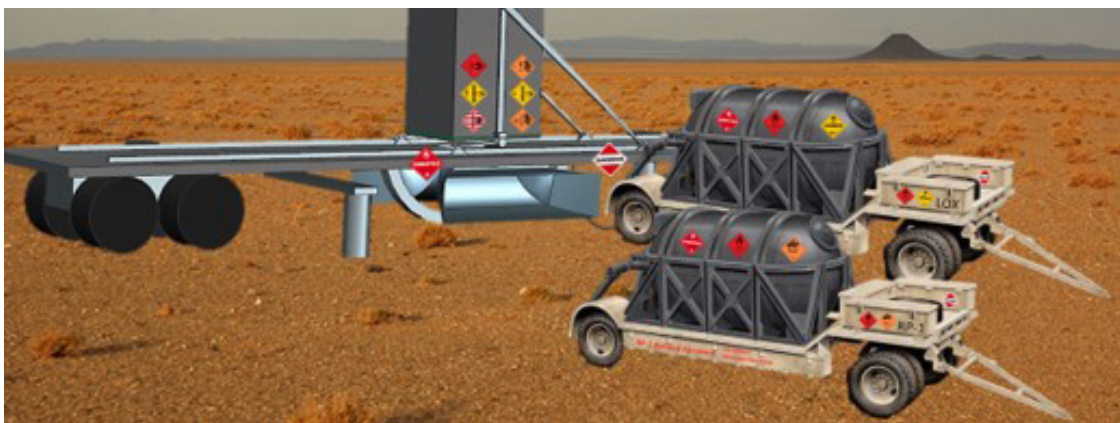


Figure 19.5: Propellant Loading of the FREEDOM



Figure 19.6: U.S. Artillery Firing at the FREEDOM



Figure 19.7: Termination of the FREEDOM



Figure 19.8: Storage of the FREEDOM and its Launch Systems



Figure 19.9: Recovering the FREEDOM and SRM

20. LIST OF MAJOR SYSTEMS AND GHOST VIEWS

This chapter discusses the design and integration of the major systems in the FREEDOM when utilizing Roskam’s method from Reference 5.

20.1 LIST OF MAJOR SYSTEMS

The systems that equip the FREEDOM are as follows:

- **Fight Control:** the system that commands the thrust vectoring control actuators;
- **Fuel:** the system that controls the propellant and oxidizer;
- **Electrical:** the system that controls the power that goes to the other systems;
- **Hydraulic:** the system that controls the launcher position actuators.

20.2 DESCRIPTION OF FLIGHT CONTROL SYSTEM

This section discusses the sizing of the actuators, basic arrangement, and control routing for the flight controls. The FREEDOM employs irreversible actuators, which are commonly applied in missiles. The actuator power stems from an electric system, while the input signal is fiber optic. Lightning environments subject the missile body to experience a range of electric currents. The fibers play a crucial role in minimizing induced-electromagnetic interferences.

Assuming the harshest environmental conditions was at 15 g’s throughout the body determined the maximum induced-lift. The team examined the lifting surface and assumed the FREEDOM is lifting two times its load. Next, the team determined the normal force and stall torque on the fins by assuming that the normal force was acting at 35% of the chord. The authors then determined the deflection, bandwidth, and corner frequency.

Throughout the entire mission profile, it was essential to control the attitude and direction of the FREEDOM. Figure 20.1 displays the different options for thrust vectoring. The



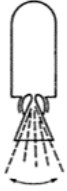
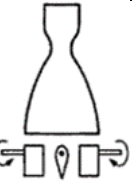
Gimble or Hinge	Flexible Laminated Bearing	Flexible Nozzle Joint	Jet Vanes
			
Universal joint suspension for thrust chamber	Nozzle is held by rings of alternate layers of molded elastomer and spherically formed sheet metal	Sealed rotary ball joint	Four rotating heat resistant aerodynamic vanes in jet

Figure 20.1: Thrust Vectoring Options (Ref. 33)

authors studied the different aspects, which included the mass, inertia, mechanical complexity, and induced torque. Ultimately, the team selected the gimbal (hinge) actuator due to its overall mechanical simplicity, proven technology, low torques, low power consumption, and minimal thrust loss. Although a gimbal actuator requires flexible piping, high inertia, and large actuators for a high slew rate, it depicted ideal outcomes for the FREEDOM (Ref. 33). The team chose the Enhanced Pointing Gimbal Assembly (EPGA) from Moog Inc. The EPGA exceeded the required value for the maximum moment to allow the FREEDOM to stay on path. This gimbal actuator is 5.8 x 6.57 x 11.93 inches in volume (Ref. 53). The team downsized the EPGA to restrict to 2D motion of gimbal and lower the power consumption.

The gimbaling actuators were linear and electrically powered by DC brushless motors, which were selected from the Rutherford engine manufactured by the Rocketlabusa company. The authors placed two of these actuators on the top and the bottom of the nozzle, which will make the exhaust capable of deflecting within -20 and +20 degrees downwards and upwards. The gimbal power requirements are dependent on the gimbal actuation torque and gimbal rotation rate (Ref. 54). The team decided to follow Reference 54 to examine various characteristics of the actuators. Figure 20.2 shows the layout of the flight control system, while Figure 20.3 and Figure 20.4 display magnified views.

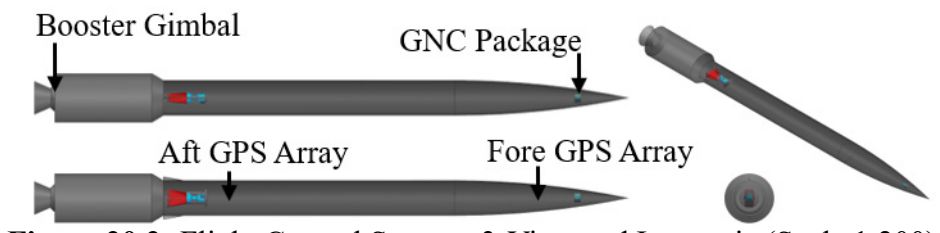


Figure 20.2: Flight Control System: 3-View and Isometric (Scale 1:200)

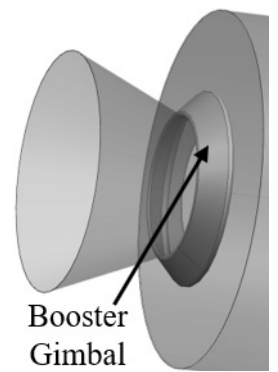


Figure 20.3: Booster Gimbal Oblique View (Not to Scale)

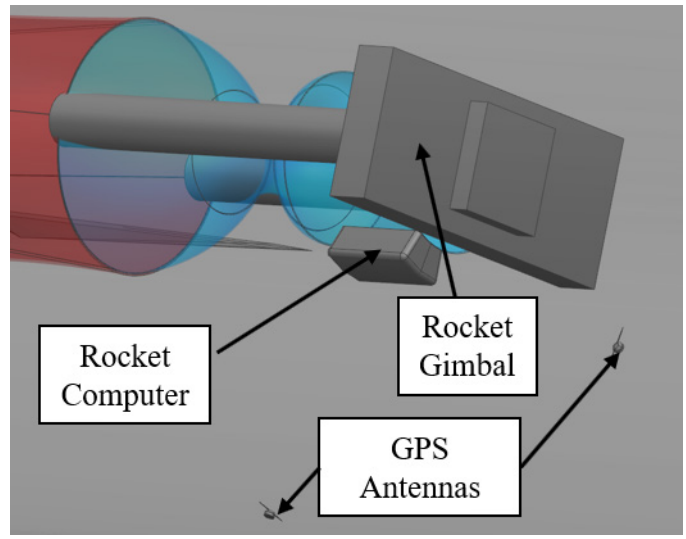


Figure 20.4: Gimbal Oblique View (Not to Scale)

20.3 DESCRIPTION OF FUELS SYSTEM

This section covers the fuel system integration process into the FREEDOM based on the engine and booster selection in Chapter 9. Although the Northrop Grumman Orion 50 XL booster provided sufficient total impulse, the supplied thrust profile does not match what was required for the FREEDOM. A new thrust to time plot was prescribed by the authors to assist in the performance of the FREEDOM. Figure 20.5 shows this plot.

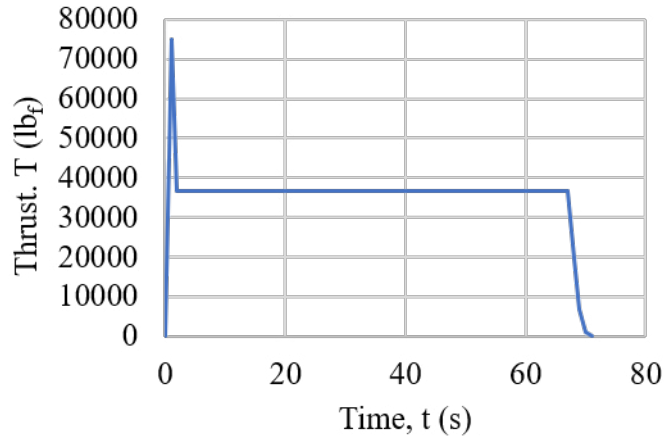


Figure 20.5: Orion 50 XL: Thrust versus Time

The authors also prescribed the booster to be made with an ablative filament insulation layer to make the shell reusable with minimal refurbishment costs. Dr. Ray Taghavi recommended an ablative insulation layer and minimal hardening to make the booster reusable for a minimum of five launches per booster (Ref. 55). Reference 33 also states that with this insulation layer, a cartridge could be added to simplify the refueling of the booster. Figure 20.6 displays this design.

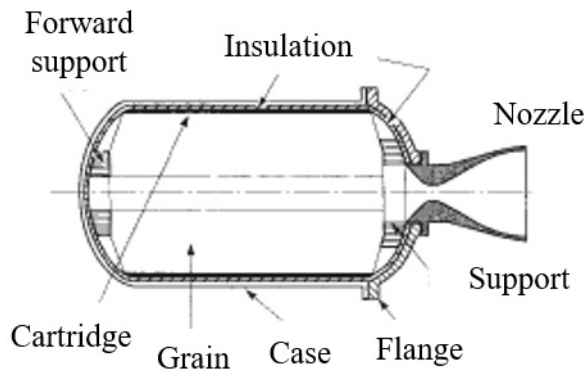


Figure 20.6: SRM Insulation (Ref. 33)

The bipropellant feed system for the liquid-fueled rocket engine used a staged combustion cycle. These subcomponents were already part of the off-the-shelf Launcher Space E-2 engine selected for this stage of flight. This engine already had a startup sequence built into it, minimizing the selection (Ref. 36). The E-2 was fed by two propellant tanks aligned coaxially. The center tank was the liquid oxygen oxidizer (LOX) tank with a thin insulation layer surrounding it. This tank, pressurized consistently at 70 pounds per square inch, required the insulation to minimize the boil-off of the liquid oxygen. To accomplish this, it kept the temperature close to -290 degrees Fahrenheit. Immediately outside of the insulation layer was the liquid fuel RP-1 tank. This tank was continuously pressurized at 30 pounds per square inch at 70 degrees Fahrenheit. Therefore, it did not require any insulation (Refs. 36 and 55).

There was a single compressed helium tank, which provided the pressurant for both the fuel and oxidizer tanks. The oxidizer tank had a foldable metallic diaphragm separating the pressurant and liquid oxidizer. It forced the oxidizer to the bottom of the tank and the location of the line to the engine. This diaphragm was selected due to the frigid temperature of the oxidizer. The fuel tank used an identically shaped piston to separate the pressurant and RP-1. In addition to the interior components, both tanks had the following external components:

- Fueling Lines;
- Defueling line;
- Defueling quick release disconnects;
- Pressure release valve;
- Inlet fuel filter;
- Defueling manual release valve;
- Line from tank to engine inlets;
- Helium pressurant lines;
- Fueling line back-flow check valve;
- Fueling quick release disconnects;
- Engine line back-flow check valve;
- Pressurant solenoids.

As stated in Chapter 18, the FREEDOM does create 3080 pounds of carbon dioxide per launch; however, it is not a considerable amount in comparison to other transportation and power systems. It is desired to change the fuel to hydrogen or methane, which would reduce this carbon dioxide amount by 44% or 40%. Figure 20.7 depicts this fuel system with the missile body while the popups below display detail views of the fuel lines.

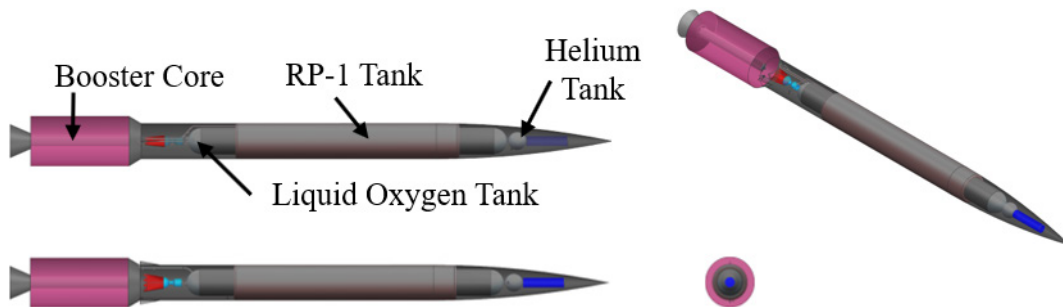


Figure 20.7: Fuel System Ghost Views: 3-View and Isometric (Scale 1:200)

Fuel Lines: Helium (Not to Scale)
(Click)

Fuel Lines: RP-1 (Not to Scale)
(Click)

20.4 DESCRIPTION OF THE ELECTRICAL SYSTEM

This section covers the various electrical elements on the FREEDOM, as well as the corresponding power consumption and interconnections. The team took the approach of externally sourcing off the shelf components.

The FREEDOM contains a triple-redundant electrical system that supplies power to various components throughout the whole configuration. The authors did extensive research to specify all the essential electrical components. Subsequently, the team laid out an overall scheme of the system and depicted the interconnections (shown in Figure 20.8). Figure 20.9 and Figure 20.10 show magnified views of the connections to the system. Three lithium-ion batteries with a total available energy of 1.79 kilowatt-hours powered all of the following components. The two 17 amp-hour batteries weigh 16 pounds each, while the 30 amp-hour battery weighs 27 pounds. The batteries were located at the aft end of the missile to provide adequate cooling and safety for the adjacent components. The popup windows below demonstrate the overall schematic of the three batteries and corresponding interconnections of the electrical components.

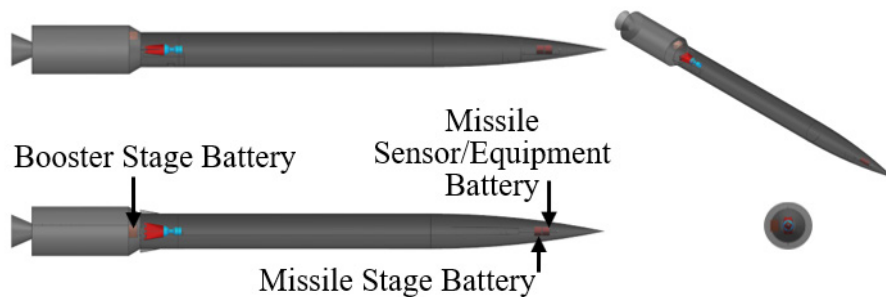


Figure 20.8: Electrical System: 3-View and Isometric (Scale 1:200)

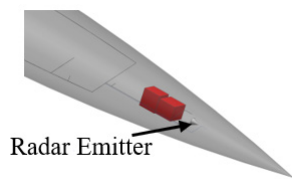


Figure 20.9: Radar Location (Not to Scale)

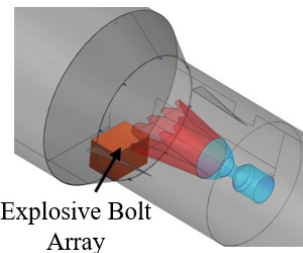


Figure 20.10: Explosive Bolt Array Location (Not to Scale)

Missile Stage Wiring
(Click)

Booster Wiring
(Click)

Sensor Wiring
(Click)

20.5 DESCRIPTION OF THE HYDRAULIC SYSTEM

The FREEDOM launcher used hydraulic actuators to extend and retract outriggers. These outriggers stabilized the launcher as it raised the launch tube into the firing position. Two sets of outriggers were present on the launcher, one ahead and one behind the final launch position. The authors chose a commercially available 72,000 ft-lbf outrigger system from Reference 56. Each outrigger set had an independent reservoir, pump, and relief valve. Independent hydraulic systems were used to avoid routing hydraulic lines near the exhaust vent. The towing vehicle provided power for the hydraulic systems. Figure 20.11 shows the launcher hydraulic system with a pop-up detailed view.

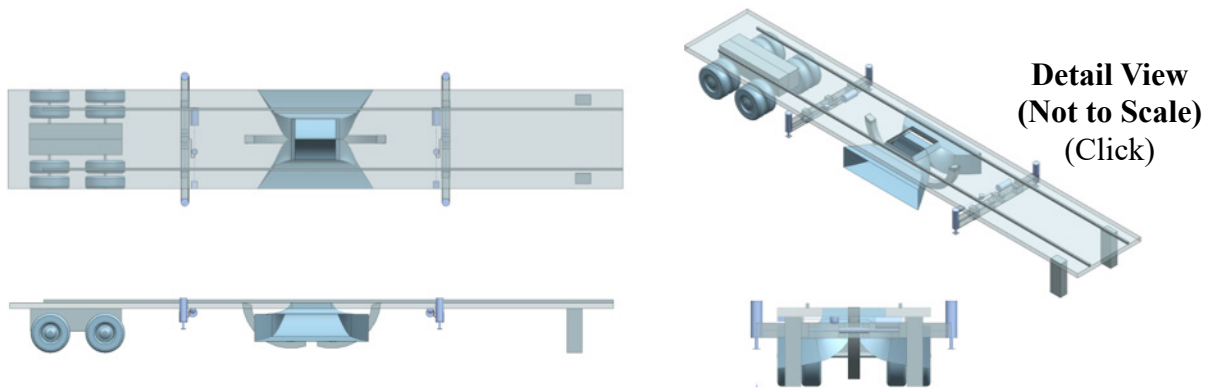


Figure 20.11: Hydraulic Launch System: 3-View and Isometric (Scale 1:200)

20.6 STAGING SYSTEM

Because the FREEDOM is a two-stage missile (a SRM stage and main rocket engine stage), a system was integrated into the body for the staging separation. This system included controlling the row of eight exploding bolts that detach the SRM adapter ring from the main stage. Immediately after SRM burnout, the flight computer would send an electric pulse through a wire that ignites the bolts. The connection fuel lines to the SRM (shown in Figure 20.12) would be sealed to prevent leakage. A pyrotechnic actuator from Ensign-Brickford Aerospace and Defense (Ref. 57) has been specked to close the lines permanently during SRM jettison. At this time, the flight controller would also ignite the main stage engine to start the second stage.

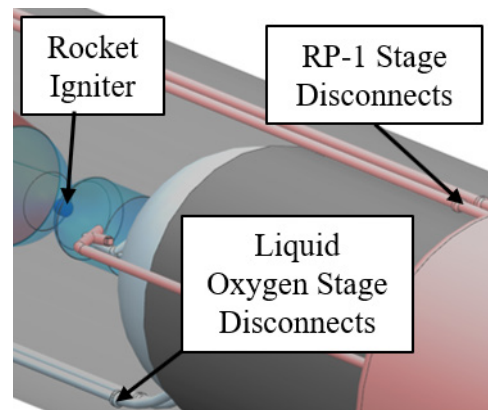


Figure 20.12: Staging System (Not to Scale)

20.7 CONFLICT ANALYSIS

The complexity of the overall electrical configuration leads to conflict points that need to be corrected for the next design iterations. Even though the authors forethought high thermal loading at the nose, space limitations, and distances from power sources to corresponding components resulted in placing two batteries close to the nose. This may bring hazardous consequences, including the degradation of the batteries. In case the incident above occurs, the team must reiterate the design process by enlarging the length of fuselage to place the batteries further aft. The modular design could raise an issue concerning wiring within each section. The current configuration includes wires embedded in the system, which are mainly unreachable for inspection purposes. In case of a wire failure, the entire circuit will be dysfunctional; then, the FREEDOM may require a body substitution.

20.8 CONCLUSIONS AND RECOMMENDATIONS

The authors conclude that:

- i.) The pre-installed gimbal on the Orion 50-XL SRM is used for booster control;
- ii.) Two EPGA actuators that generate 2230 ft-lbf of torque are used for rocket engine control;
- iii.) The engine gimbal operates at a rate of 1.6 degrees per second;
- iv.) Pressurized helium is utilized to initialize fuel flow to the rocket engine;
- v.) The FREEDOM consumes 946 kW-hr of power during the flight;
- vi.) Two 72000 ft-lbf hydraulic outriggers are used for stabilizing the launch trailer during firing;
- vii.) Oversizing the source power is beneficial in supplying power to a damaged segment of the system through parallel back-ups.

The authors recommend that:

- i.) Rotary actuators should be investigated to possibly lower overall power consumption;
- ii.) The authors collaborate with Northrop Grumman to redesign the Orion 50 XL booster grain, so it produces a high-thrust initial kick followed by a constant-thrust burn until burnout;
- iii.) Batteries with higher energy densities than lithium-ion batteries should be investigated for utilization on the FREEDOM;
- iv.) Wires are shielded to avoid unexpected environmental conditions and any shortages.

21. CLASS II SIZING OF RECOVERY SYSTEMS

This chapter outlines the recovery process if the FREEDOM is missed by the defense system targeting it. Based on Reference 58, there is a set plan of action for safely bringing the FREEDOM down in a reusable state.

21.1 DESCRIPTION OF MAJOR RECOVERY SYSTEM COMPONENTS AND DISPOSITION

As described in Chapter 18, the FREEDOM rotates between 10 to 17.5 Hertz during the terminal flight phase at sea level. An advantage of this rotating orientation is the motion of the short period and long period/phugoid modes. The short period mode caused the FREEDOM to "wobble" in a small circle. The long period mode caused a helix type motion around an arbitrary point, which made contacting the FREEDOM difficult. Figure 21.1 displays the short period and long period/phugoid motions.

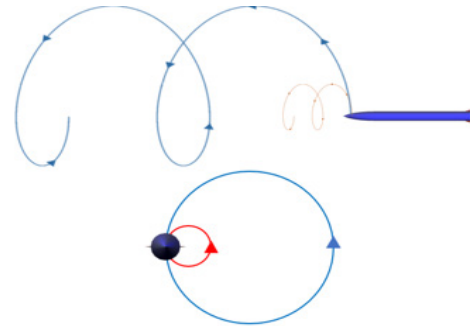


Figure 21.1: Short Period Mode (Red) and Long Period/Phugoid Mode (Blue)

The design team mandated that the interception attempt with the FREEDOM occurs when the weight would be between 10,200 and 6,000 pounds. This gives a sufficient amount of propellant to perform the recovery procedure and activate the recovery mode. This mode commands an immediate pull up at 10 degrees per second. After achieving vertical flight for 10 seconds, the engine would burn for one additional verification second. Engine shut down would occur 11 seconds after recovery mode activation, allowing the FREEDOM to coast straight up until perigee. If it is

necessary, the engine could continue to burn to achieve the minimum altitude for parachute deployment (5,000 feet). Figure 21.2 shows the worst-case flight profile for the position. A blue line displays when the engine is operational while the red line is after engine shutdown.

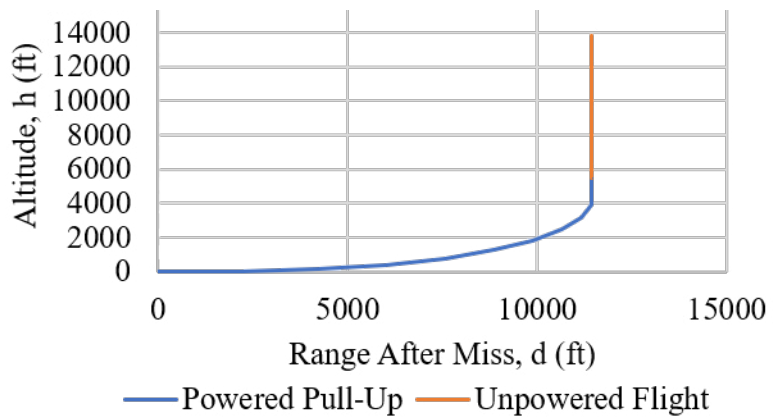


Figure 21.2: Recovery Position Flight Profile

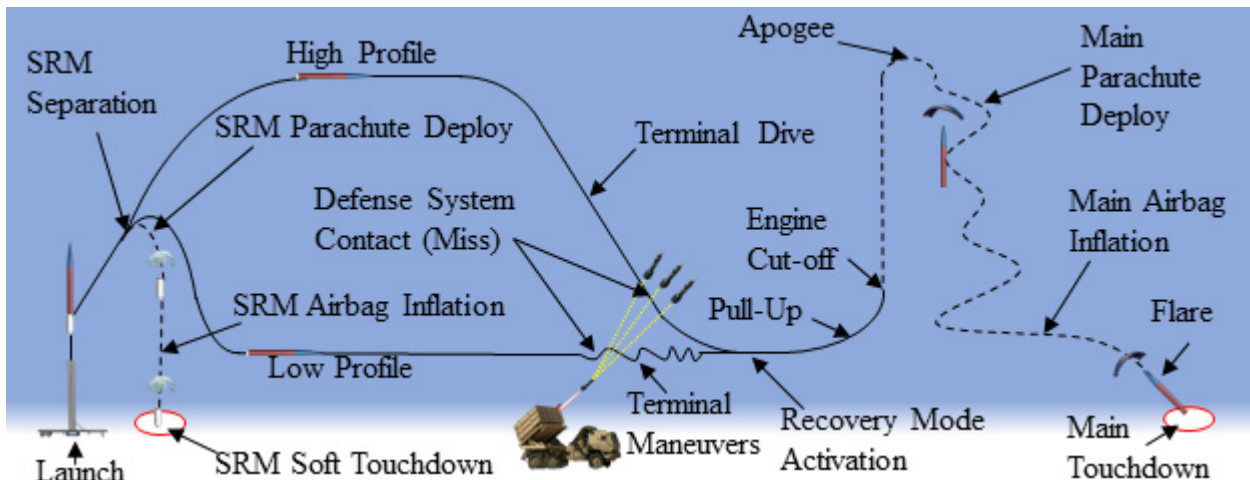


Figure 21.3: The Recovery Storyboard

Above, Figure 21.3 depicts the storyboard of the recovery plan. After the modified Northrop Grumman Orion 50XL booster has spent all of the solid fuel, it decouples from the main terminal stage falling back toward Earth. The team prescribed that the booster cut off must be at an altitude of 3,000 feet to deploy all recovery systems. The parachute chosen for the boost stage was the Airborne Systems Unicross Low-Cost Cargo Delivery Parachute. This thin, cost-effective parachute could arrest between 1,000 to 3,200 pounds and safely land the payload on the ground. This parachute, like the booster, is safely reusable for five flights. It would deploy a few moments after the booster reaches flight apogee. This recovery system arrests the booster, impacting the hard deck at 28 feet per second (Ref. 59). An airbag at the base of the booster would inflate before impact to further protect the booster and increase the likelihood of reusability. Airborne Systems North America made this selected airbag as well (Ref. 61).

For the FREEDOM body, the recovery system chosen for this flight stage was the Airborne Systems Dragonfly Guided Precision Aerial Delivery System. The parachute system would be guided using a GPS sensor. A terrain map of the outer surroundings is programmable onboard parachute internal computer. The computer requires only a landing coordinate and a weight of the system. The landing coordinate would be preselected and can adapt to new landing coordinates. With this system, the flight range safety officer could take over manual control of the navigation. This also provides a means of communication between the ground controller and the FREEDOM. The Dragonfly provided a lift to drag ratio of 3.5:1, so the minimum height that could be achieved after a miss is 13,800 feet. This height allowed for the Dragonfly to fly the FREEDOM 48,300 feet

in ranges. The Dragonfly automatically flares to reduce the impact speed by a minimum of 50% using the preprogrammed terrain map and GPS. This would reduce the maximum impact velocity of 8.54 to 4.27 feet per second at 10,000 pounds. At 5,030 pounds, it also reduces the minimum impact speed of 6.06 to 3.03 feet per second.

Just before landing, an airbag produced by Airborne Systems would inflate at the aft of the FREEDOM to provide additional protection for reusability. Figure 21.4 displays the terminal impact velocity just before the flare with relation to all possible allowable weights. The popup presents the hand calculations for the maximum and minimum weights.

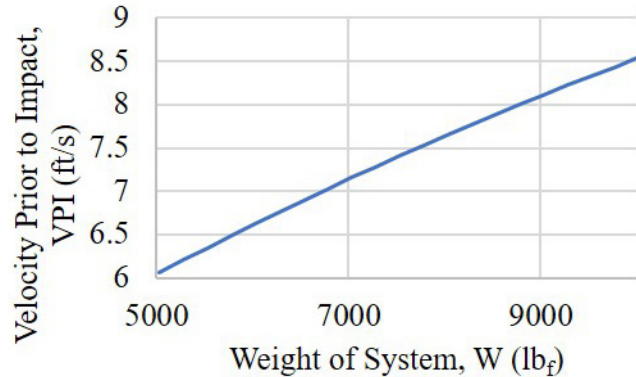


Figure 21.4: Impact Velocity to Weight

21.2 CAD OF RECOVERY SYSTEM

If the FREEDOM diverts from the desired flight profile, it can be detonated using an embedded deflagration line in the skin. When activated, the line heats up and breaks the FREEDOM apart. This heat would ignite the additional fuel and detonate the entire system. Based on Reference 58, this detonation would break all of the components into small pieces and cause minimal damage below. An additional

failsafe is the manual override by the range safety officer for the deflagration line. Fig-

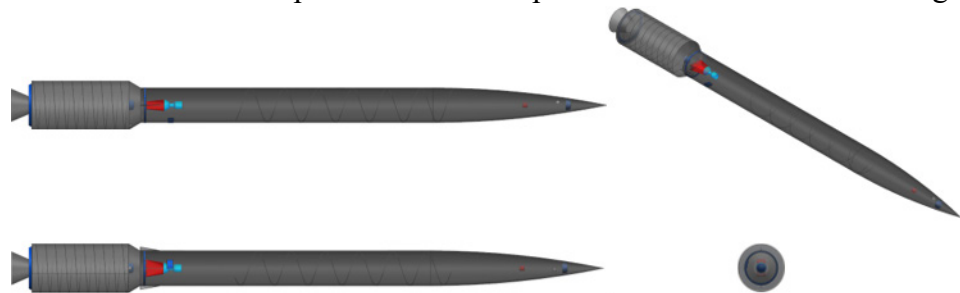


Figure 21.5: Deflagration Line: 3-View and Isometric (Scale 1:200)

21.3 CONCLUSIONS AND RECOMMENDATIONS

The authors conclude that:

- i.) The calculated impact speeds are show in Table 21.1.

The authors recommend that:

- ii.) Airborne Systems develops a custom airbag.

Nose Detail (Click) **Booster Detail** (Click)

Table 21.1: Impact Speeds

Weight (lb _f)	Impact Speed (ft/s)
10,000	4.27
5,030	3.03

22. INITIAL STRUCTURAL ARRANGEMENT

The following chapter discusses the design choices behind the layout, material, and thicknesses for the structure of the FREEDOM. Design choices and techniques were determined from methods shown in Reference 26 and discussed in Reference 60. Preliminary manufacturing processes for each component are discussed in this chapter, but a more detailed layout of manufacturing processes will be discussed in Chapter 28.

22.1 LAYOUT OF STRUCTURAL COMPONENTS

The structural components for the target drone consist of the airframe, bulkheads, attachment ring frames, nose cone, fuel and oxidizer tanks, fins, and booster attachment. The team based the material selection of the components for the high-temperature abilities and weight of the material. The target drone has three points that are the location of extremely high temperatures due to the high Mach mission profile: nose cone, fin leading edges, and rocket engine area. The team calculated the temperature at these hot spots at sea level for Mach 3.5 as 1,600 degrees Fahrenheit (Ref. 26). The designers also considered manufacturing, transportation, storage, ground handling, launch platform carriage, launch, and terminal maneuvering conditions when sizing the substructure for the target drone (Ref. 26). The launch loads, loads on the pressurized vessel, impact loads, loads from propulsion systems are the load cases considered for structural design.

Figure 22.1 shows the spacing between the bulkheads and their attachment points to the airframe. Due to the large size of the FREEDOM, the designers selected the airframe to be mono-coque with bulkhead dividers. Based on Reference 60, the thickness of each structural component should be between

0.25 to 0.375 inches, where the maximum thickness is at the nose. There were three 0.25 inch thick bulkhead dividers in the target drone. The

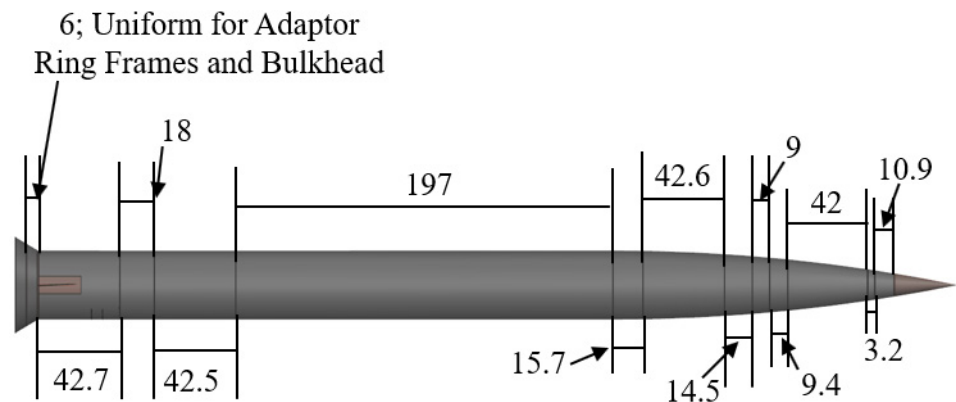


Figure 22.1: Frame and Bulkhead Spacing: Side View
All Dimensions in Inches (Scale 1:100)

most forward bulkhead was used for the attachment of the nose cone section that detaches for the parachute recovery system. The second bulkhead divided the payload bay and fuel system. The most aft bulkhead divided the fuel system with the rocket engine to reduce interference. The nine 0.25 inch thick ring frames provided attachment points for fixing the internal components into place. The designers chose carbon fiber as the material used for the bulkheads and ring frames because of its high strength and low deflection abilities. The low-cost manufacturing process to make the bulkheads and ring frames were filament winding. The bulkheads and ring frames attach to the airframe skin with epoxy that would be spun to cover the entire attach location.

The inside of the nose cone contained the payload and batteries. This area was also one of the points with the hottest temperatures from the high Mach mission profiles; therefore, the team chose 0.375 inch-thick reinforced carbon-carbon as the material for the two sections of the nose cone (Ref. 60). Reinforced carbon-carbon has high-temperature capabilities of up to 3,630 degrees Fahrenheit (Ref. 62), which would keep the payload safe from the maximum temperature of 1,600 degrees Fahrenheit. The manufacturing method of the reinforced carbon-carbon nose cone added resin to the fibers into a mold where the material was heated to retain the shape (Ref. 62). Since the nose cone portion contains the payload, the designers chose to make it removable at all times for easy access into the payload bay. The tip of the nose cone used four stainless steel exploding bolts from Ensign-Bickford Aerospace and Defense to detach for the parachute recovery system (Ref. 57).

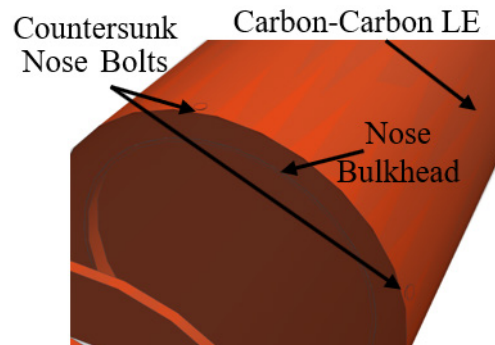


Figure 22.2: Nose to Bulkhead (Not to Scale)

Figure 22.2 shows the attachment point that hold the tip nose cone in place at the forward bulkhead. The second nose cone portion holds the payload bay, so the team decided to epoxy the nose cone end to a ring frame in the fuselage section.

Figure 22.3 shows the attachment point of the fins to the airframe. The primary purpose

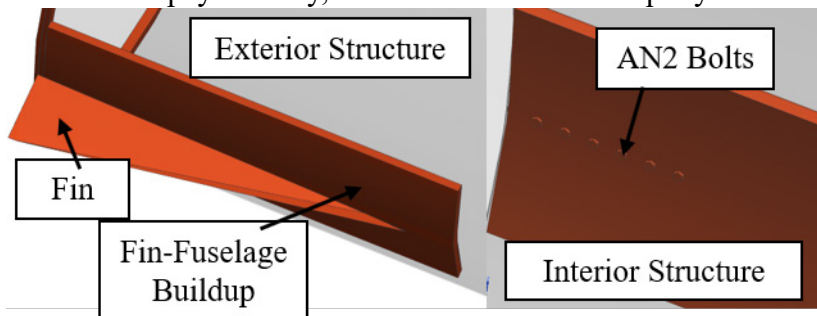


Figure 22.3: Exterior and Interior Fin (Not to Scale)

of the fins was to provide roll control for the target drone. The fins are in the boundary layer and experience the highest temperatures on the target drone. Therefore, the designers chose to manufacture the fins as 0.2 inches thick of solid reinforced carbon-carbon components. The fins do not carry any of the structural loads, so the fins do not need any substructure. The fins used a manufacturing process similar to the nose cone and attached to the airframe with six steel AN2 bolts each.

The rocket engine area was another high-temperature location. This rocket engine had regenerative cooling from the fuel and oxidizer, which cooled down this hot area. Therefore, 0.025 inches and 0.01 inches thick carbon fiber was used as the material for both the fuel and oxidizer tanks. The tanks were filament wound as a low cost and simple manufacturing method (Ref. 26). The designers sized the fuel and oxidizer tanks to be accessible for refueling by using four removable steel AN8 bolts at the bottom bulkhead. Then, the fuel and oxidizer tanks attached to the airframe with eight steel AN8 bolts per ring frame. Figure 22.4

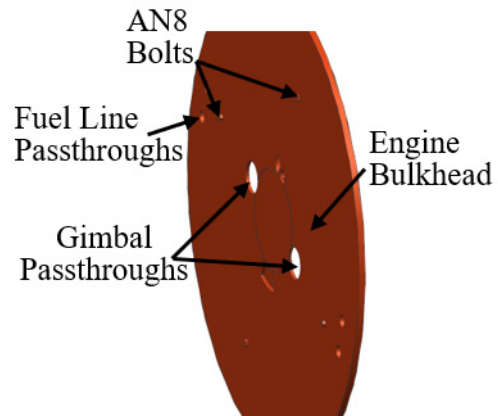


Figure 22.4: Engine Bulkhead (Not to Scale)

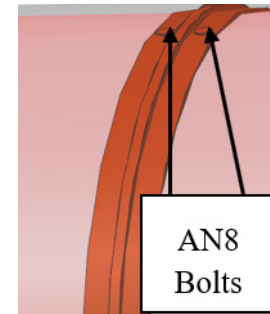


Figure 22.5: Ring Frame Bolts (Not to Scale)

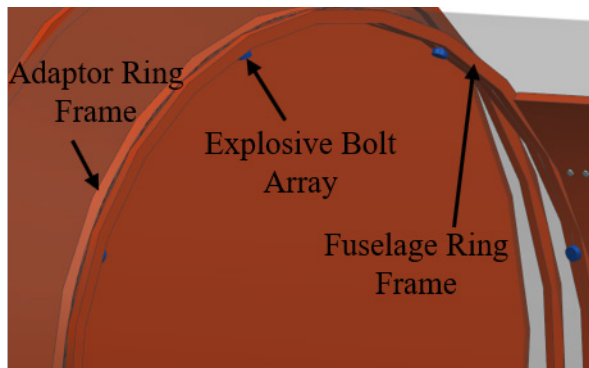


Figure 22.6: Fuse-adapter Ring (Not to Scale)

shows the removal of the bottom bulkhead for refueling access. Figure 22.5 shows a closeup on the attachment points on one of the ring frames.

Northrop Grumman’s Orion 50 XL SRM and the 0.5 inches thick adaptor ring were made from an aluminum alloy and manufactured at Northrop Grumman. The SRM adaptor ring was attached to the bottom airframe ring frame with eight stainless steel exploding bolts from Ensign-Bickford Aerospace and Defense (Ref. 57). After the FREEDOM reaches the target altitude of the mission profile, the booster needs to detach from the main vessel through exploding bolts. Figure 22.6 shows the attachment point for the booster adaptor ring to the bottom ring frame.

Table 22.1 summarizes the materials selected and thickness for each of the structural components. The overall assembly consisted of inserting each component or sliding in bulkheads and ring frames into the airframe through one end of the target drone. Composites materials are more expensive than metallic; however, the designers chose to make the trade-off of higher cost for the thermal capabilities and high strength to low weight ratios that the composite materials provided. The thicknesses for each component are sized based on the terminal maneuver loads in the critical flight profile. The popup shows the calculations for the maximum temperature needed to size the structure.

Table 22.1: Structural Components

Component	Material Selection	Thickness (in)
Airframe	Graphite Composite	0.25
Bulkheads/ Ring Frame	Carbon Fiber	0.25
Nose Cone	Reinforced Carbon-Carbon	0.375
Fins	Reinforced Carbon-Carbon	0.2
Fuel Tanks	Carbon Fiber	0.025
Oxidizer Tanks	Carbon Fiber	0.01

22.2 CAD DRAWINGS OF STRUCTURAL LAYOUT

The layout of each structural component is shown in Figure 22.7. The popup displays a magnified isometric view with labeled substructure components.

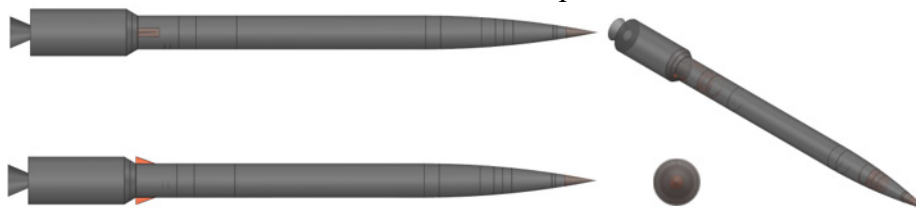


Figure 22.7: Structure Schematic: 3-View and Isometric (Scale 1:200)

22.3 CONCLUSIONS AND RECOMMENDATIONS

The authors conclude that:

- i.) The nose cone and fins use reinforced carbon-carbon at thicknesses of 0.375 and 0.2 inches;
- ii.) The bulkheads, ring frames, fuel tank, and oxidizer tank use carbon fiber at thicknesses of 0.25 inches, 0.25 inches, 0.025 inches, and 0.01 inches, respectively;
- iii.) The airframe is made from graphite composite and is 0.25 inches thick.

Labeled Isometric View
(Click)

The authors recommend that:

- i.) The factor of safety used for the structure be reduced with structural testing to determine the over-designed and under-designed parts of the target drone.

Hand Calculations
(Click)

23. CLASS II WEIGHT AND BALANCE

A Class II weight and balance was performed using methods from Reference 3. The CAD of the FREEDOM assisted with finding the weight and position of each component.

23.1 CLASS II WEIGHT AND BALANCE CALCULATIONS

The positions and weights were used to determine the location of the overall C.G. These components, their weight, and their position are shown in the popup image below. The components were broken up into the 11 major subcategories: payload systems, main parachute, missile airbag, skin structure, fin system, engine system, helium system, LOX and RP-1 tank system, adaptor system, booster system and propellants. Using the procedure described in Chapter 14, the C.G. position in the X, Y, and Z-axis were found for each component. These are also shown in the popup image.

X_{C.G.} Hand calculations
(Click)

Component with Weight and Position
(Click)

23.2 CLASS II CG POSITIONS ON THE AIRFRAME, CG EXCURSION

The values in the popup window above were combined using the same method as used in Chapter 14 to calculate the C.G. position of the FREEDOM at any point during the flight. The C.G. excursion for the first stage is shown in Figure 23.1. The C.G. excursion for the 2nd stage is shown in Figure 23.2. The position of each subcomponent C.G. location is shown in Figure 23.3.

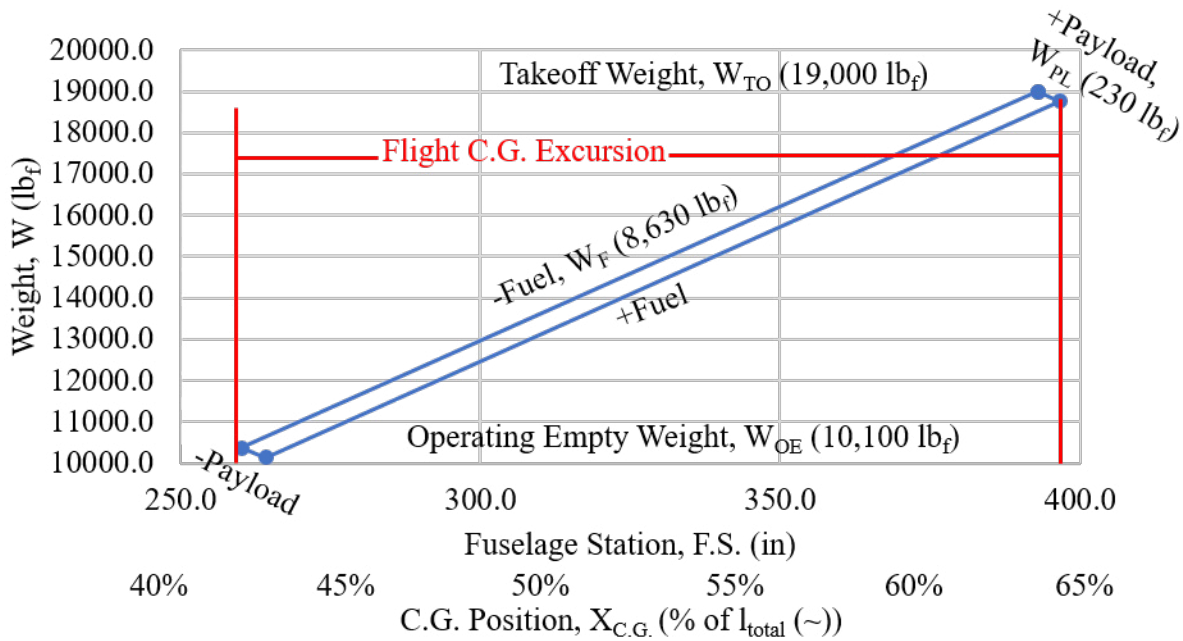


Figure 23.1: Class II C.G. Excursion Diagram: Booster Phase

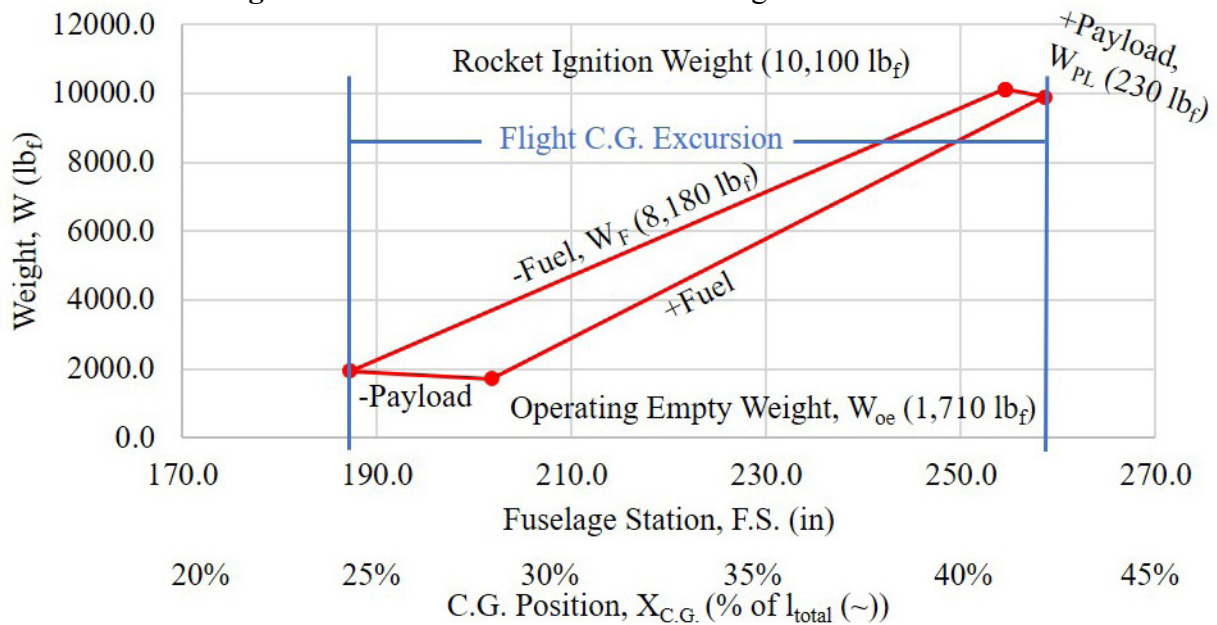


Figure 23.2: Class II C.G. Excursion Diagram: Rocket Engine Phase

23.3 CONCLUSIONS AND RECOMMENDATIONS

The authors conclude that:

i.) Table 23.1 shows the C.G. excursion results.

The authors Recommend that:

ii.) More Iterations are performed to mitigate C.G. excursion.

Table 23.1: C.G. Excursion Results

Flight Condition	C.G. Ex-cursion (in)	C.G. Excur-sion (%)
Booster Phase	137	22
Rocket Engine Phase	57	12

Label	Category	Weight (lbf)	F.S. (in)	B.L. (in)	W.L. (in)
1	Payload System	536	67	0	0
2	Main Parachute	503	41	0	0
3	Missile Landing Airbag	30	476	0	0
4	Skin Structure	288	189	0	0
5	Fin System	15	469	0	0
6	Engine System	428	446	0	0
7	Helium System	25	99	0	0
8	LOX and RP-1 Tank Systems	120	291	0	0
9	Adaptor	121	490	0	0
10	Booster	113	517	0	0
11	Solid Rocket Propellant	8630	552	0	0
12	RP-1	2260	271	0	0
13	LOX	5920	271	0	0
C.G.	Total	18990	393	0	0

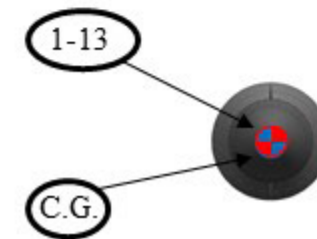
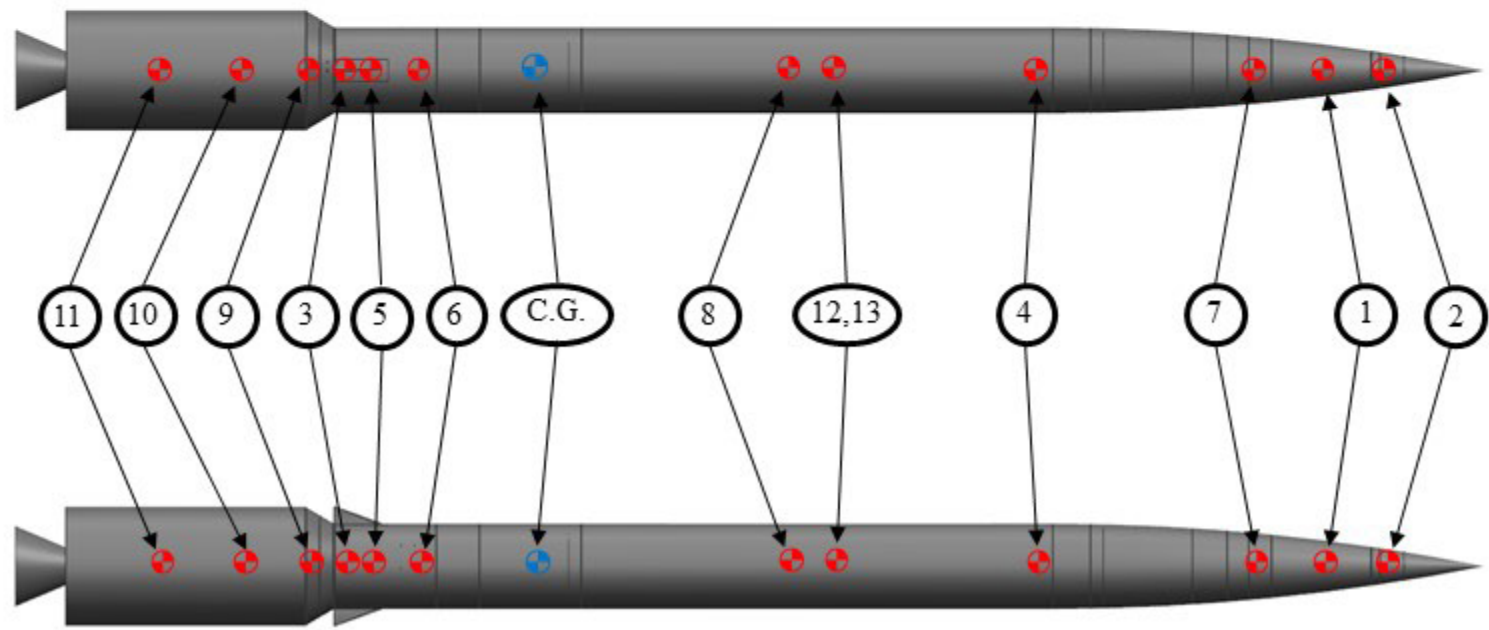


Figure 23.3: FREEDOM C.G.: 3-View and Isometric (Scale 1:80)

24. CLASS II WEIGHT AND BALANCE

This chapter investigates the C.G. excursion results from Chapter 23.

24.1 CLASS II WEIGHT AND BALANCE ANALYSIS

The change in C.G. for the terminal phase of the mission allows for a C.G. shift of 57 inches, which is an additional 1.6 percent more than it was for the preliminary estimations. This was caused by a reduction in the structural weight of the FREEDOM. This was also caused by increasing the accuracy of the specific weights of the FREEDOM sub-components. Several fixed equipment components were moved forward to shift the C.G. forward at earlier points during the flight; however, this causes a more substantial shift as more propellant aft of the C.G. is burned during flight. This was favorable because it shifts the C.G. forward, which reduces the distance to the aerodynamic center, decreasing instability. Additional C.G. shift was mitigated by converting the liquid propellant tanks to coaxial. Missiles are inherently unstable due to the aerodynamic center being at the tip of the tangent ogive nose. This confirms that the C.G. excursion of the FREEDOM is within the acceptable range for operation (Ref. 63). The FREEDOM also demonstrates sufficient controllability with a bandwidth of 100 Hertz. This allows for the missile to be controllable even when at maximum roll frequency of 19.5 Hertz.

24.2 CONCLUSIONS AND RECOMMENDATIONS

The authors conclude that:

- i.) A 100 Hertz bandwidth is sufficient for controlling the FREEDOM;
- ii.) The C.G. excursion is reasonable and acceptable for both flight profiles of the FREEDOM.

The authors recommend that:

- i.) Different aerodynamic additions to shift the C.G. aft should be implemented to reduce instability further;
- ii.) The FREEDOM should be restructured to have the C.G. of the liquid propellant tanks in the terminal phase match the overall FREEDOM C.G., so the C.G. excursion is mitigated as more fuel is burned.

25. UPDATED 3-VIEW AND AIRCRAFT FAMILY SUMMARY

25.1 UPDATED 3-VIEW AND SALIENT CHARACTERISTICS

Figure 25.2 depicts the final three-view of FREEDOM, while Table 25.1 shows the final design characteristics of the missile. Both are displayed on the page below.

25.2 THE FREEDOM MISSILE FAMILY

As the FREEDOM enters service, it was assumed that potential adversaries of the United States would introduce more advanced missiles that the FREEDOM cannot either emulate or out-match in performance. This is why the two future variants of the FREEDOM, the FREEDOM-B and the FREEDOM-C, would be produced.

The FREEDOM-B would improve on the original design by adding actuators to the fins. FREEDOM-B operators could then tune the roll rate, which would affect the precession and nutation of the target in flight. This would make FREEDOM-B a more difficult target to hit, as the fins could be adjusted to produce a unique flight path for each launch. The FREEDOM-C was designed as an improvement from the FREEDOM-B design. By changing the materials of the missile structure to a low-observable composite, the material would further lower the RCS of the FREEDOM missile family. This design change would make it difficult to target and intercept. This would help prepare the DoD for intercepting against potential low-observable supersonic missiles. The FREEDOM, FREEDOM-B, and FREEDOM-C are shown below in Figure 25.1.

25.3 CONCLUSIONS AND RECOMMENDATIONS

The authors conclude that:

- i.) The FREEDOM-B adds actuators to the fins;
- ii.) The FREEDOM-C changes the material of the structure to a LO composite.

The authors recommend that:

- i.) A third export variant is created, so the missile can be sold overseas to United States allies.

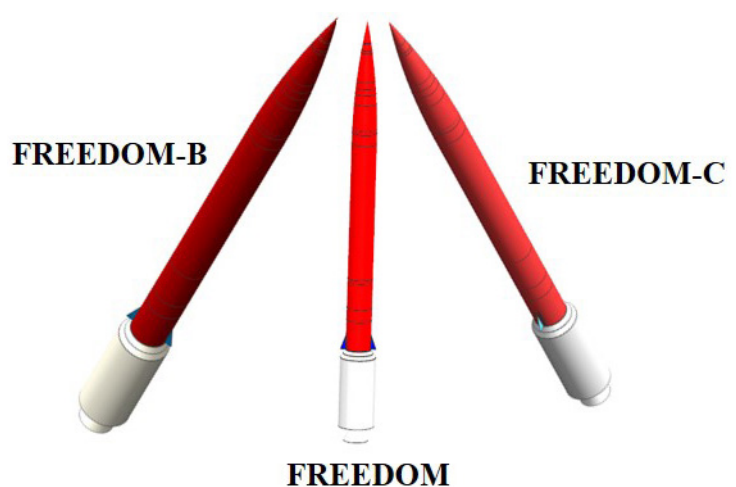


Figure 25.1: The FREEDOM Family (Not to Scale)

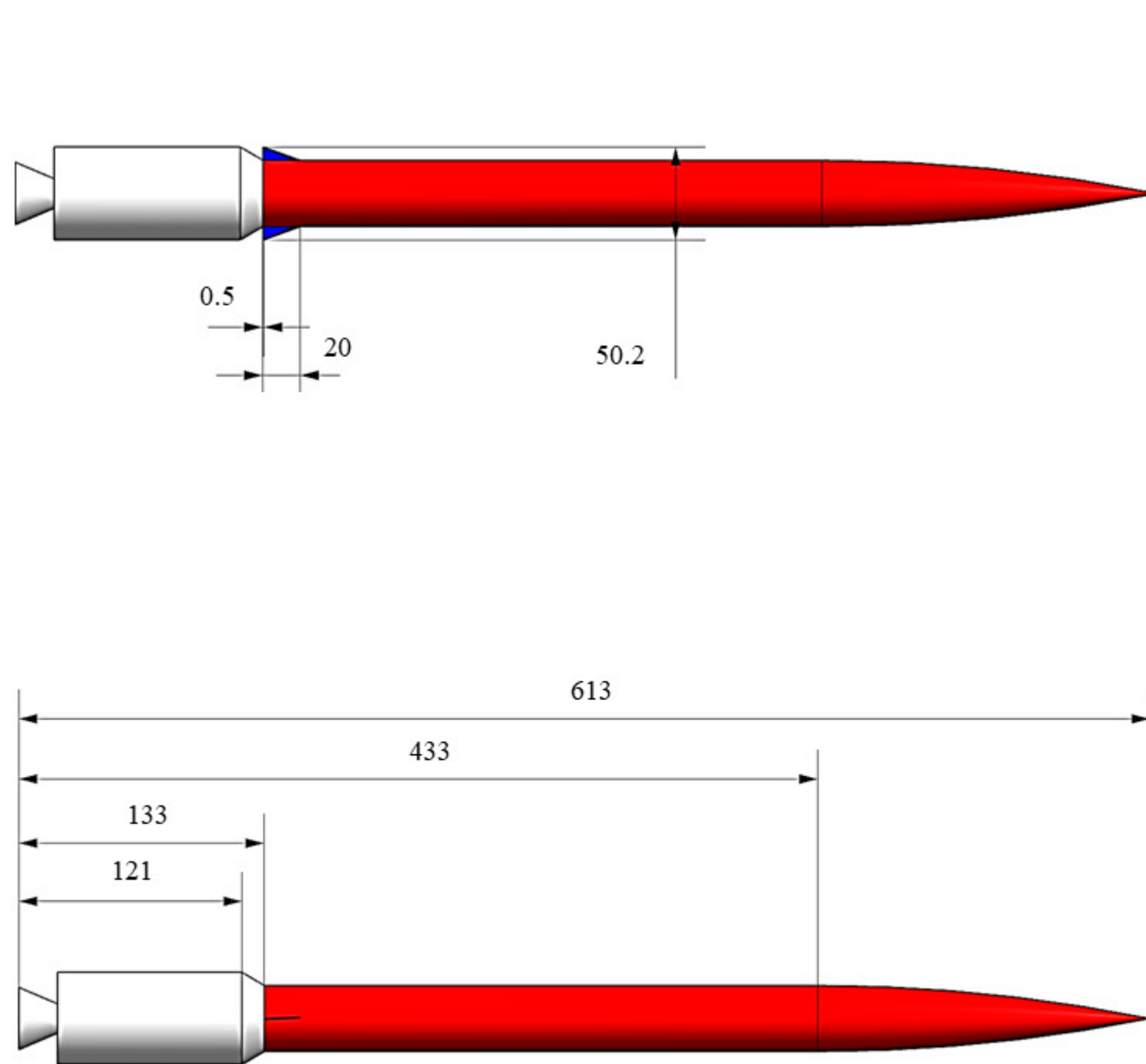


Table 25.1: Salient Characteristics

S_{fin}	0.96 (ft ²)
Aspect Ratio	1.46 (~)
b/2	0.59 (ft)
Taper Ratio	0.18 (~)
C	1.67 (ft)
C	1.11 (ft)
L.E. Thickness Angle	5.00 (degrees)
t/c	1.00 (~)
Λ	70.00 (degrees)
i	2.73 (degrees)
ϵ	0.00 (degrees)
Γ	0.00 (degrees)
Fuselage Length	40.00 (ft)
Fuselage Diameter	3.00 (ft)
Maximum Length	51.10 (ft)
Maximum Diameter	1.39 (ft)
Maximum Takeoff Weight	19000 (lb _f)
Range (nmi)	150 (nmi)

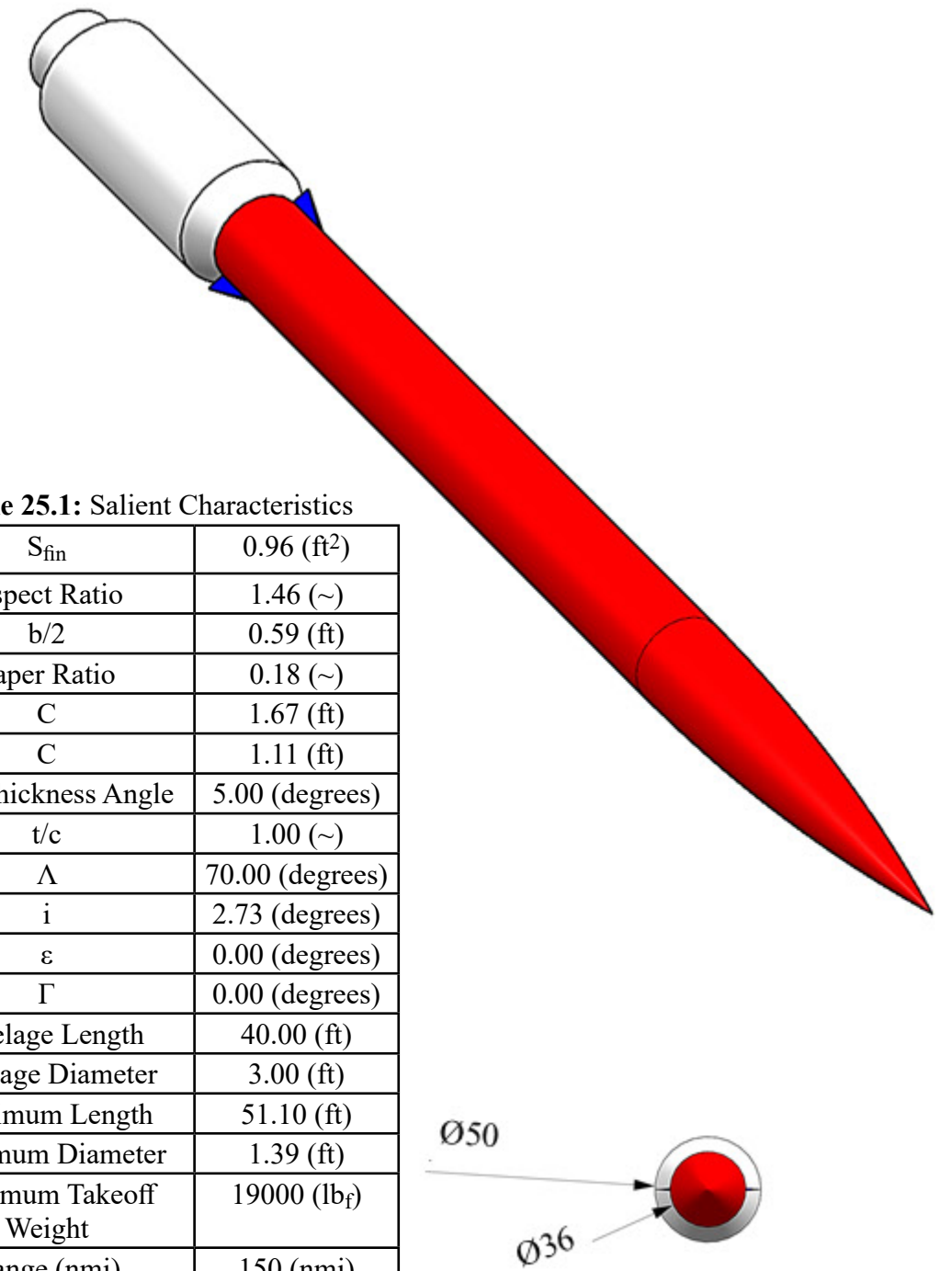


Figure 25.2: Updated 3-View: All Dimensions in Inches (Scale 1:80)

26. ADVANCED TECHNOLOGIES

The following chapter covers the advanced technology the team designed for the target drone that differentiates the FREEDOM compared to other target drones on the market based on recommendations from Reference 60.

26.1 ADVANCED TECHNOLOGY SWEEP

The designers implemented an advanced flight control system to avoid intercepting missiles. The missile uses a cant angle on the fins to achieve a constant roll rate during the flight. Since the target drone does not have an actuator controlling the fins, the overall cost and complexity of the system were reduced. The system achieves the desired roll rate depending on the velocity of the missile. During the higher Mach flight, the target drone rolls at a faster rate than during lower Mach flight. The constant roll rate of the flight system determines the precession and nutation modes of the target drone. Using the precession and nutation modes instead of the standard long period and short period modes allow the team to simulate the flight modes of a butterfly. These insects are designed to fly in random fluttery patterns to avoid potential predators (Ref. 60). Similar to this flight mode, a derivative of the FREEDOM model would add an actuator on each fin to tune the roll rate to match the precession and nutation frequencies of the intercepting missile. The target drone would use this advanced flight control technique to miss intercepting missiles effectively.

26.2 CONCLUSIONS AND RECOMMENDATIONS

The authors conclude that:

- i.) The advanced technology of the FREEDOM is a flight control system that determines the precession and nutation modes with the roll rate;
- ii.) The flight control system of the FREEDOM avoids interception by tuning the roll rate to match predator vehicles.

The authors recommend that:

- i.) The advanced flight control system is developed with flight test procedures.

27. RISK MITIGATION

The following chapter discusses the procedures and systems put in place to ensure the risk associated with the operation of the FREEDOM was mitigated. These systems were designed based on the recommendations from Reference 60.

27.1 RISK MITIGATION SUMMARY

The significant risk related to the target drone was a lost round. Missiles are inherently unstable systems that increase the risk of becoming uncontrollable during the mission profile. The team decided on three methods to ensure the safety of the public is not compromised. The FREEDOM would use a high bandwidth actuator of 100 Hz to control the missile effectively (Ref. 60). A higher bandwidth actuator makes the missile controllable even with its inherently unstable nature. On the small chance this actuator fails, the team decided to implement two systems depending on the weight of the target drone at that point in the mission profile. If the missile weighs less than 10,000 pounds, the FREEDOM would perform a pull-up maneuver, cut the engine, and activate the parachute recovery system. Chapter 21 discusses the details of the parachute recovery system. If the missile becomes uncontrollable earlier in the mission profile and has not burned off enough fuel to weigh less than 10,000 pounds, the team designed a deflagration system that would activate and break the missile into small pieces through detonation (Ref. 60). To ensure the safety of the public, the missile should stay within the test range during all mission profiles. An onboard flight computer could detonate the target drone if it begins to leave the testing range. On-site at the test range, a range safety officer could detonate the target drone when deemed necessary to maintain the safety of the public.

27.2 CONCLUSIONS AND RECOMMENDATIONS

The authors conclude that:

- i.) The FREEDOM is controlled with a 100 Hz actuator;
- ii.) A parachute recovery system and deflagration line mitigate the risk of the FREEDOM.

The authors recommend that:

- i.) Prototypes of the parachute system and deflagration line are developed and tested.

28. MANUFACTURING PLAN

This chapter describes the manufacturing plan and purchases from suppliers required for assembling the FREEDOM. The manufacturing plan details the fabrication, assembly, building layout, and part flow required for producing the target missile.

28.1 EXPLODED VIEW

The exploded view in Figure 28.1 below shows the major subassemblies and components of the FREEDOM. These major components would be assembled in the facilities described in Section 28.3.

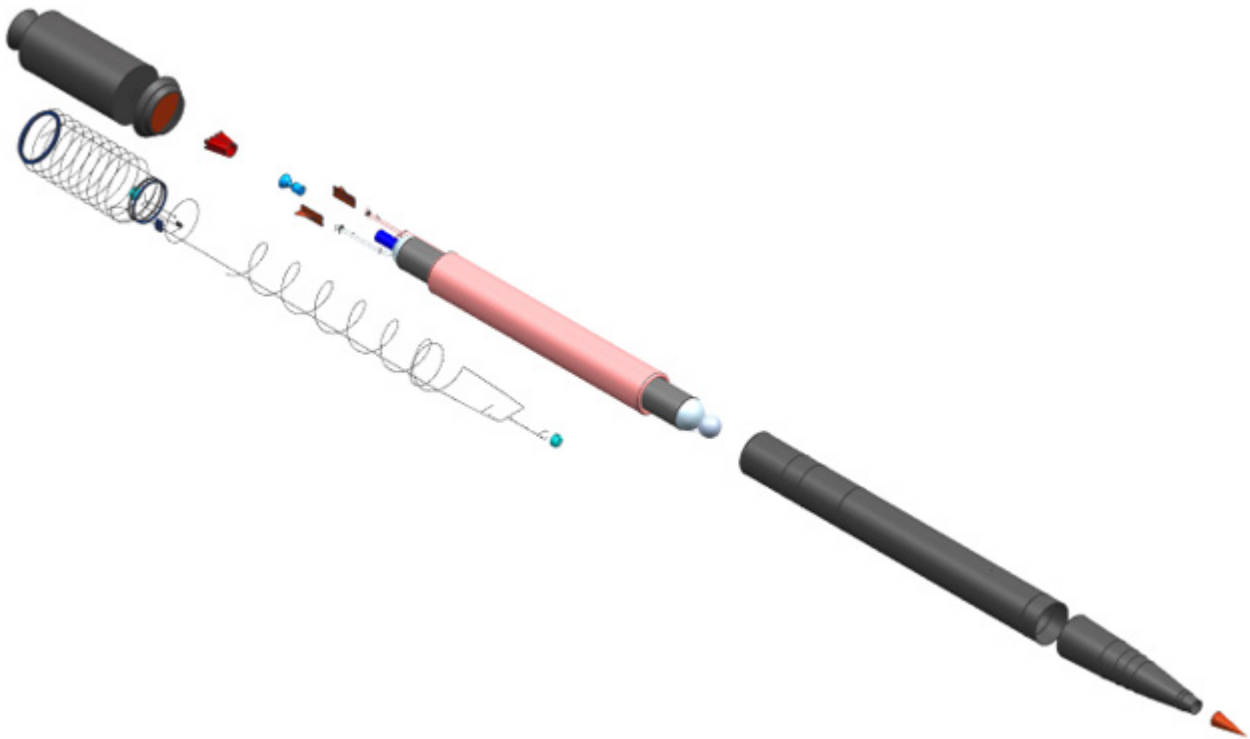


Figure 28.1: FREEDOM Exploded View (Not to Scale)

28.2 BILL OF MATERIALS

A bill of materials was required for determining which components must be procured to assemble the FREEDOM. The bill of materials was used to determine the manufacturing facility layout. The popup below shows the bill of materials for the FREEDOM. This table displays the components, the number of components required, and the supplier.

Bill of Materials
(Click)

28.3 FABRICATION AND ASSEMBLY PROCESS

The manufacturing process begins by procuring and shipping all the components listed in the Bill of Materials to the assembly facilities. All components are purchased from third party vendors or specialized manufacturers. This includes, but is not limited to, all fuselage and adaptor ring bodies, bulkheads, frames, fuel tanks, fuel lines, fins, engines, transition ducts, and payload capsules. At the cost of increasing procurement costs from outsourcing, the company developing the FREEDOM would reduce labor costs by only needing to hire assembly technicians. Because the FREEDOM was intended to be developed and produced by a final integrator, the fabrication and assembly process only discusses the final assembly of the missile.

Figure 28.2 below shows the different buildings and their uses in the assembly process. Each major mating or integration process uses its own building to minimize collateral damage in the event

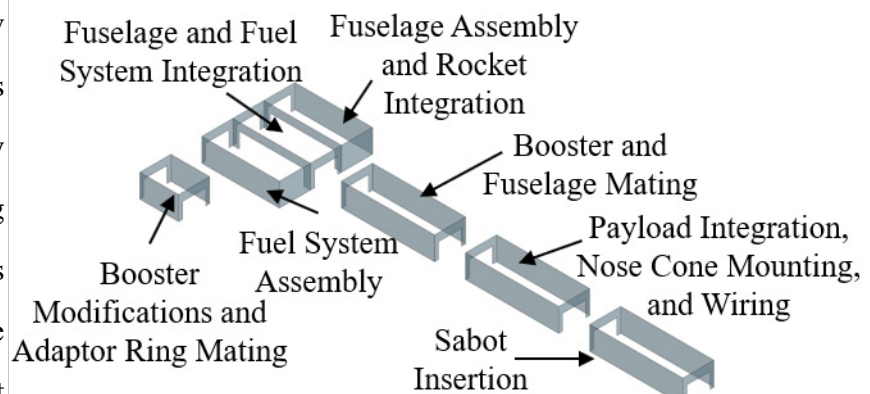


Figure 28.2: FREEDOM Assembly Facility Layout (Not to Scale)

of a catastrophic failure on the assembly line. To further reduce the risk of damage occurring to adjacent buildings, all openings in Figure 28.2 feature retractable doors that shut when subassemblies are not being moved from building to building.

The assembly process first begins with a delivery of parts ordered to the assembly facility. The booster modification and adaptor ring mating building are where workers mate the Orion 50 booster to the adaptor ring. At this time, the workers also install the booster airbag, transponder, parachute, and battery. The battery is fully discharged at this time and has coverings over its terminals to prevent sparking. The fuselage and fuel system integration building is where the fuel system and fuselage are assembled in side rooms. It is important to note that while the carbon-carbon nose cone is delivered to the fuselage assembly room, it is not installed at this time. This gives workers access to the payload area of the fuselage. The Thruster E-2 engine is also installed at this time.

Once both the fuel system and fuselage subassemblies are finished, the two are brought together in the center room. The integrated fuselage and fuel system is then brought to the next building down the assembly line, where it is mated with the booster with explosive bolts. The second to last building in the assembly line is where the payload capsule is mounted to the fuselage, all wiring is completed, and the reinforced carbon-carbon nose cone is assembled. As with the booster building, the batteries present in the missile fuselage are fully discharged to prevent sparking. This finishes the assembly of the FREEDOM. It is then brought to the last building of the assembly line, where it is inserted into a sabot and awaits transit to a warehouse of the U.S. military. Figure 28.3 below summarizes the flow of parts and subassemblies through the facilities.

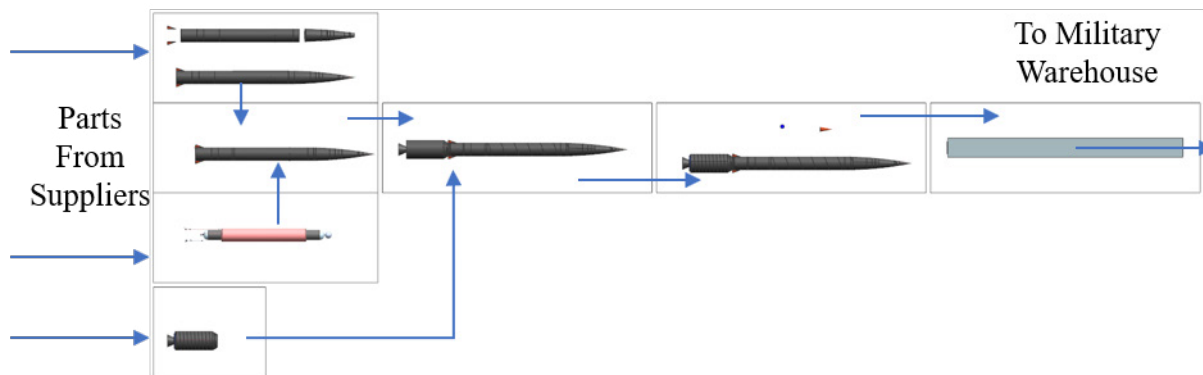


Figure 28.3: Assembly Flow (Not to Scale)

28.4 FUTURE VARIANT ASSEMBLY CONSIDERATIONS

In the FREEDOM-B and FREEDOM-C future variants, additional actuators must be assembled and joined with the fins of the missile. This would be done in the fuselage assembly and rocket integration room. For the FREEDOM-C variant, the change in selected composite materials would not change the process at the assembly facilities in Figure 28.2, as the composite pultrusions are not manufactured on-site.

28.4 CONCLUSIONS AND RECOMMENDATIONS

The authors conclude that:

- i.) All components of FREEDOM will be purchased prefabricated to minimize labor costs;
- ii.) The FREEDOM will be assembled in separate buildings to minimize damage.

The authors recommend that:

- i.) Research assembly facility locations that are near transportation hubs to reduce costs.

29. COST ANALYSIS

The following chapter discusses the cost analysis for the FREEDOM. The cost analysis was performed using AAA.

Table 29.1: Cost Analysis Value

Price Component	Amount (\$)
Research, Development, Test, and Evaluation Cost	2.77*10 ⁹
Acquisition Cost	7.23*10 ⁹
Total Manufacturing Cost	6.58*10 ⁹
Program Production Cost	5.62*10 ⁹
Flight Test Operation Cost	3.97*10 ⁵
Airframe Engineering Design Cost	3.00*10 ⁸
Operating Cost	1.00*10 ⁴
Disposal Cost	1.01*10 ⁸
Life Cycle Cost	1.01*10 ¹⁰
Estimated Price Per Target Drone	2.86*10⁷

29.1 COST ANALYSIS SUMMARY

Table 29.1 shows the costs obtained from the AAA model. The popups below show the cost calculations. The following costs were based on the production run of 350 units in addition to 15 developmental testing units (Ref. 1).

Figure 29.1 shows the price per target drone versus the units in production. A red point on the graph shows the estimated price per target drone for the specified production run of 350 units. The graphs follow an inverse and asymptotic trend because as fewer units are produced, the price per target drone increases significantly

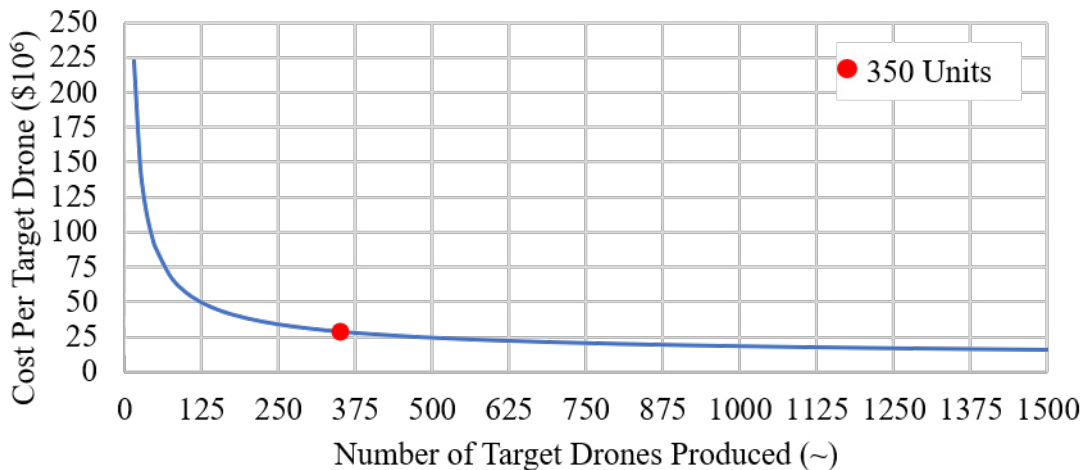


Figure 29.1: Cost vs. the Number of Target Drones Produced

29.2 CONCLUSIONS AND RECOMMENDATIONS

The authors conclude that:

- i.) The cost for one FREEDOM missile is 28.59 million dollars.

The authors recommend that:

- i.) A more specific price for the Launcher engine is used for the analysis.

RDTE Cost
(Click)

Acquisition Cost
(Click)

LCC Cost
(Click)

30. CLASS II STABILITY AND CONTROL

This chapter utilized Roskam method from Reference 8 to analyze the FREEDOM in the context of Class II stability and control. Also, the authors scrutinized the ethical nature and all aspects of the stability and control demanded by the RFP (Ref. 1). This investigation primarily related to compliance with MIL-standards and C.G. excursions throughout the analysis.

30.1 CLASS II STABILITY AND CONTROL ANALYSIS

The authors analyzed the static longitudinal, lateral, and directional stability in Chapter 16. Chapter 30 augments the stability analysis by examining the dynamic longitudinal and lateral-directional stability as well as the spin characteristics. This missile belonged in Category A, which encompasses nonterminal flight phases that require rapid maneuvering, precision tracking, or precise flight-path control. Also, Category B with an accurate flight-path control applied to the climb and cruise phases of the FREEDOM.

Upon the calculations of the dynamic modes, the FREEDOM resulted in unstable longitudinal modes while the missile is de-facto stable. The calculated nutation damping ratio placed the handling quality of the missile in Level 1. Also, Category A and B flight phases of the freedom result in a Level 1 handling quality through the value of precession. The authors concluded the results mentioned above upon performing a sensitivity analysis on the precession mode; the precession damping ratio and natural frequency are sensitive to C_{mq} and $C_{m\alpha}$, respectively.

30.2 CONCLUSIONS AND RECOMMENDATIONS

The authors conclude that:

i.) The Class II precession and nutation mode results are shown in Table 30.1;

ii.) A feedback system is not necessary because of the handling qualities are Level 1.

The authors recommend that:

i.) A analysis should be completed with the USAF Stability and Control DATCOM manual.

Table 30.1: Class II Stability and Control Results

Mode	ω_n (Hz)	ζ (~)	Handling Quality
Precession	5.16	0.62	Level 1
Nutation	0.03	0.05	Level 1

**Class II Stability and Control
Hand calculations
(Click)**

31. ADVANCED PERFORMANCE

This Chapter illustrates the advanced performance of the FREEDOM throughout the flight profile. Roskam method from Reference 8 was used to determine the climb rate, thrust performance, cruise range, and maneuver rates.

31.1 ADVANCED PERFORMANCE ANALYSIS

The authors verified the performance of the FREEDOM, which required mission and airworthiness performance verifications. Table 31.1 shows that the FREEDOM meets and

Table 31.1: FREEDOM Rate of Climb

Ceiling Type	Current Climb Rate (ft/min)	Minimum Required Climb Rate (ft/min)
Supersonic Combat Ceiling	36,000	1,000
Supersonic Cruise Ceiling	29,000	1,000

exceeds the minimum rate of climb needed, including a supersonic combat ceiling at 1000 ft/min and supersonic cruise ceiling at 1000 ft/min. Figure 31.1 demonstrates the rate of climb of the FREEDOM throughout the mission profile, which is an indicator of satisfactory values.

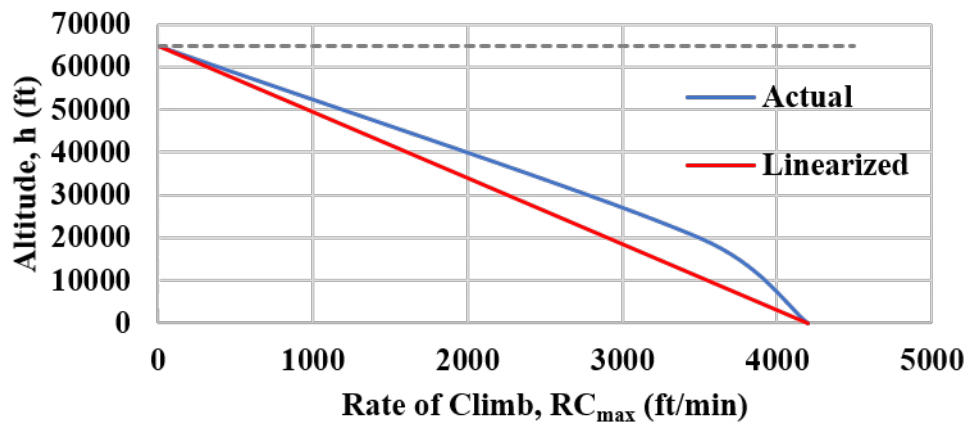


Figure 31.1: Rate of Climb of the FREEDOM

The team researched a missile in the market that possessed comparable characteristics and capabilities. Ultimately, the team selected the GQM-163 Coyote to emulate and reverse engineer the drag polar and thrust profiles. The purpose of this analysis was to develop an available power chart for the chosen missile and the FREEDOM. The two excess power charts were overlaid on top of one each other to reveal comparative insights. Figure 31.2 and Figure 31.3 demonstrate the comparative analysis between the FREEDOM and the GQM-163 Coyote from the lens of altitude versus Mach number and thrust versus speed, respectively.

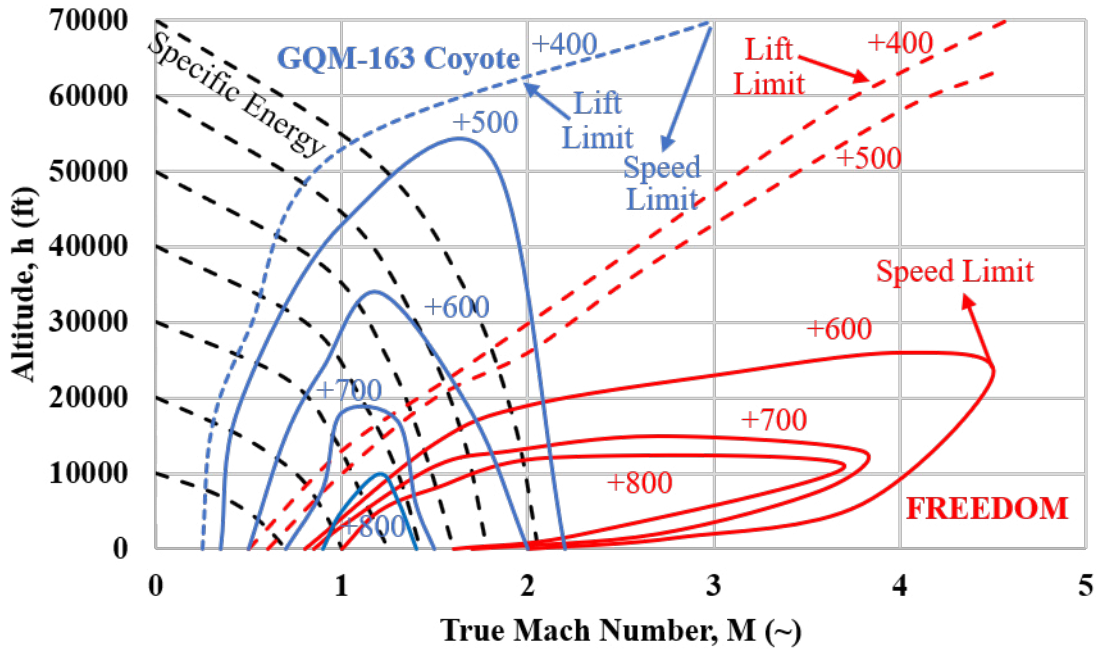


Figure 31.2: Altitude vs. Mach: The FREEDOM and GQM-163 Coyote

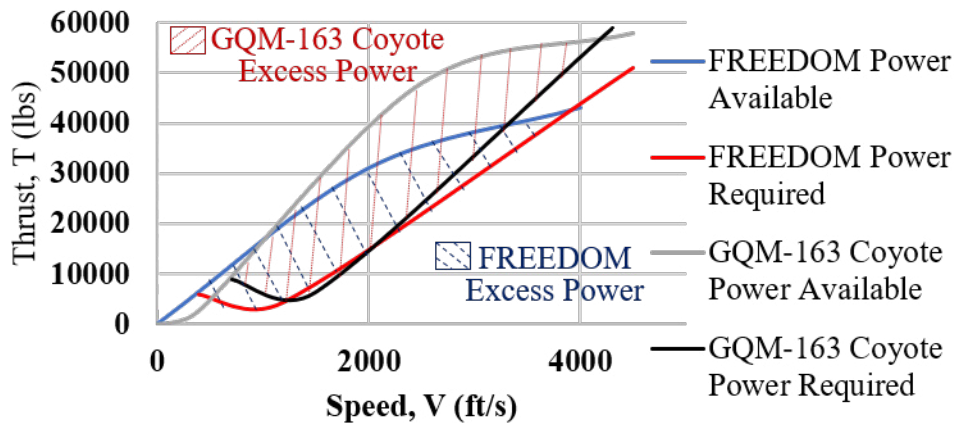


Figure 31.3: Thrust vs. Speed: The Freedom and GMQ-163 Coyote

The authors examined typical mission cruise specifications, including cruise speed, cruise altitude, range and payload, fuel reserves at the end of the mission, maximum cruise speed, corresponding altitude and payload, and finally, payload expended. Table 31.2 contains these specifications according to the Brequet equation, which are indicators of the absence of discrepancy between specified and predicted range performance. Therefore, any type of design change is not necessary at this stage.

Table 31.2: : FREEDOM Cruise Data

Altitude (ft)	V (ft/s)	Payload (lbs)	C_j (lb _f /lb _f /hr)	R (nmi)	Breguet Equation Range Capability
0	3910	500	12	199	Meets requirement of 150 nmi
65,000	3680	500	12	196	Meets Requirement of 150 nmi

Military regulations govern the diving aspect of the FREEDOM. Reference 8 lays out two different methods to examine dive profiles, including finding the dive for a known speed or angle. The team selected the former approach due to the known speed. Then equations 5.52 and 5.53 from Roskam Part VII (Ref. 8) determined γ and α , respectively. Finally, the authors drew a conclusion that validated the diving scenario based on calculated and assumed values of α . Table 31.3 presents the information pertinent to the dive profile in the low and high altitudes cases and justifies that no design changes are necessary.

Table 31.3: Dive Profile Calculations

Altitude (ft)	Assumed α (degrees)	γ (degrees)	α (degrees)	α and assumed α are within 0.1 degree?
0	-15.00	-14.83	-14.98	Yes
65,000	-18.00	-17.71	-17.96	Yes

The FREEDOM experiences instantaneous maneuvers that must oblige military regulations. As Dr. Barrett advised in Reference 63, the missile was abstained from pull-up maneuver due to the lack of information on the maneuver mode in the AIAA specification (Ref. 1). Instead, the team was guided to analyze the maneuver profile in a steady level turn with sinusoidal peaks along the path. It is important to note that the instantaneous g's in this context was the 15 g's, which dropped the total power required. The following graph in Figure 31.4 demonstrates the turn rate versus calibrated airspeed in knots.

Advanced Performance Hand Calculations 1
(Click)

Advanced Performance Hand Calculations 2
(Click)

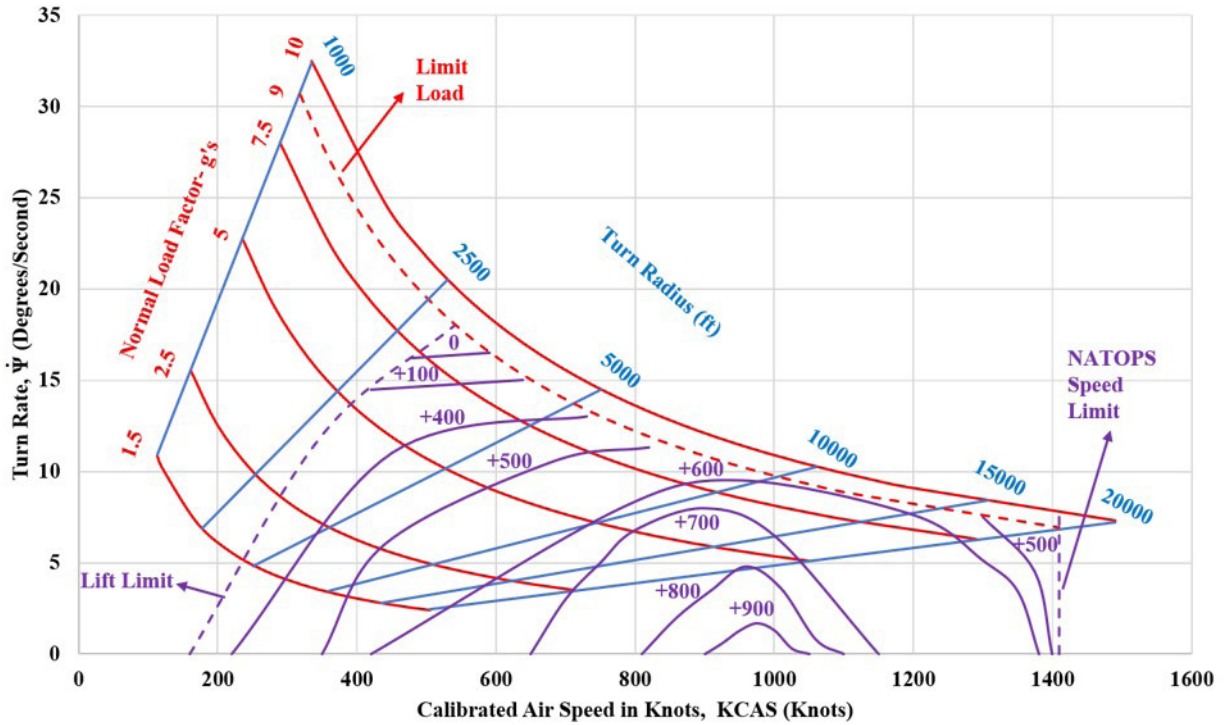


Figure 31.4: Turn Rate vs. Calibrated Air Speed

31.2 CONCLUSIONS AND RECOMMENDATIONS

The authors conclude that:

- i.) The climb rates for each ceiling type is shown in Table 31.4;
- ii.) The cruising range and dive profile results are show in Table 31.5;
- iii.) The FREEDOM meets the RFP (Ref. 1) requirements for the advanced performance.

The authors recommend that:

- i.) More missiles are reverse engineered to compare a multitude of thrust and drag profiles to the FREEDOM;
- ii.) The future missile that is compared to the FREEDOM should be more similar in configuration;
- iii.) A consultation with the U.S. military should occur to discuss what specific performance characteristics should be considered.

Table 31.4: Climb Rate Results

Ceiling Type	Current Climb Rate (ft/min)
Supersonic Combat Ceiling	36,000
Supersonic Cruise Ceiling	29,000

Table 31.5: Cruise and Dive Profile Results

Altitude (ft)	Cruise R (nmi)	Dive α (degrees)
0	199.00	-14.98
65,000	196.00	-17.96

32. SPECIFICATION COMPLIANCE

Table 32.1 displays the RFP (Ref. 1) compliance of the FREEDOM and page numbers the requirement is met.

Table 32.1: RFP Specifications Compliance

Profile	RFP Specification	Predicted Missile Performance	Is the Requirement met?	Page #
General	A threshold range of 60 nmi	67 nmi	Yes	25
General	An objective range of 150 nmi at the end of the terminal phase	196 nmi	Yes	81
General	Determined range to complete the launch phase	199 nmi	Yes	81
General	Launch altitude is 0-3,500 ft with a 0° to 90° elevation angle	Launch system is apart of a mobile, standard trailer with an elevating sabot	Yes	33
General	GNC system maintains course $\pm 1,500$ ft of programmed trajectory during cruise	maintains course within $\pm 2,000$ ft	Yes	79
General	A 50 ft CEP is achieved at the end of the terminal phase	50 ft	Yes	82
General	Fuel and Propellant is safe for at least 10 years during storage, transportation, and handling	10 years	Yes	6
General	Payload module is 3.5 ft long by 10 in diameter with a maximum weight of 500 lb	3.5 ft long by 10 in diameter with a weight of 500 lb	Yes	15
High Profile	Cruise speed is between Mach 2.0 and Mach 4.5 at 5,000 to 65,000 ft.	Mach 4.5	Yes	81
Low Profile	Cruise speed is between Mach 2.0 and 3.5 at 15 to 200 ft. above the launch elevation	Mach 3.5	Yes	81
High Profile	Terminal dive angle between 10° to 75° at Mach 0.9 to Mach 3.5	17.96°	Yes	81
Low Profile	Maximum High-g maneuvers are 15-g in the lateral plane and 7-g in the longitudinal plane	15-g in the lateral plane and 7-g in the longitudinal plane	Yes	81
Low Profile	High-g maneuvers occur over the final 20nmi of the flight for 45 seconds	15-g maneuvers occur over the final 20nmi of the flight for 45 seconds	Yes	82
Low Profile	Terminal impact speed is between Mach 2.0 to Mach 3.5	3.5	Yes	82

33. MARKETING PLAN AND PATH FORWARD

33.1 MARKETING PLAN

The FREEDOM program brings an innovative approach to the target drone market. To meet the needs of the military, the team designed the FREEDOM to simulate an aerial threat. This simulation allows the military to develop forward-thinking systems to protect the United States and its allies. The FREEDOM uses a high bandwidth actuator to emulate the frequencies of intercepting missiles. The advanced flight control system of the FREEDOM allows the military to develop more advanced systems with the ability to overcome this type of advanced system. Defense technology improves each year, so the military of the United States and its allies should adopt the FREEDOM program to move forward with new technology.

33.2 PATH FORWARD

For the first few years of production, the FREEDOM program will include the initial FREEDOM variant and market towards the United States military. After the initial purchases and first years in production, the program will move towards making FREEDOM variants B and C to improve upon the first design of the target drone. Eventually, the team will design an export target drone for marketing towards the militaries of allied countries. In the future, when the program grows, the production units will increase from 350 target drones to a higher predetermined amount of target drone. This increase in production units will reduce the overall cost per target drone and help the team to market the missile to more potential allied militaries. Continuing to improve the FREEDOM target drone with new variants and manufacturing an export missile for allied militaries will increase the overall profit for the FREEDOM program.

33.3 CONCLUSIONS AND RECOMMENDATIONS

The authors conclude that:

- i.) The FREEDOM is a marketable design with an advanced control system;
- ii.) To increase production, the FREEDOM program should develop a series of variant models.

The authors recommend that:

- i.) A research and development team is assembled to continue the FREEDOM program.

REFERENCES

1. Anon., "2019-2020 Graduate Team Missile Systems Design Competition – Supersonic Aerial Target," AIAA, [https://www.aiaa.org/designcompetitions/], Reston, VA 20191, 1 September 2019.
2. Roskam, J., "Airplane Design; Part I: Preliminary Sizing of Aircraft," DARcorporation, Lawrence, KS, 1991.
3. Roskam, J., "Airplane Design; Part II: Preliminary Configurations Design and Integration of the Propulsion System," DARcorporation, Lawrence, KS, 1991.
4. Roskam, J., "Airplane Design; Part III: Layout Design of Cockpit, Fuselage, Wing, and Empennage: Cutaways and Inboard Profiles," DARcorporation, Lawrence, KS, 1991.
5. Roskam, J., "Airplane Design; Part IV: Layout Design of Landing Gear and Systems," DARcorporation, Lawrence, KS, 1991.
6. Roskam, J., "Airplane Design; Part V: Component Weight Estimation," DARcorporation, Lawrence, KS, 1991.
7. Roskam, J., "Airplane Design; Part VI: Preliminary Calculation of Aerodynamic, Thrust and Power Characteristics," DARcorporation, Lawrence, KS, 1991.
8. Roskam, J., "Airplane Design; Part VII: Determination of Stability, Control and Performance Characteristics: FAR and Military Requirements," DARcorporation, Lawrence, KS, 1991.
9. Roskam, J., "Airplane Design; Part VIII: Airplane Cost Estimation: Design, Development, Manufacturing and Operating," DARcorporation, Lawrence, KS, 1991.
10. Anon., Advanced Aircraft Analysis, version 4.0, Lawrence, KS: DARCorporation, 2019.
11. Anon., "V-2 MISSILE," Britannica, Available: <https://www.britannica.com/technology/V-2-missile>.
12. Anon., "A-4/V-2 Makeup - Tech Data & Markings," V2Rocket.com, Available: <http://www.v2rocket.com/start/makeup/design.html>
13. Anon., "File: Fusé V2.jpg," Wikimedia Commons, Web Site [https://commons.wikimedia.org/wiki/File:Fus%C3%A9_V2.jpg], Wikimedia Foundation, 24 August 2004.
14. Anon., "XSM-64 NAVAHO MISSILE," Boeing History Products, Available: <https://www.boeing.com/history/products/xm-64-navajo-missile.page>
15. Anon., "North American SSM-A-2,4,6/B-64/SM-64 Navaho," Directory of U.S. Military Rockets and Missiles, Available: <http://www.designation-systems.net/dusrm/app1/sm-64.html>
16. Michals, K. "SM-64 Navaho Nuclear Missile," Flickr, Web Site [https://www.flickr.com/photos/rocbolt/8174481029], SmugMug, 4 November 2012.
17. Anon., "BQM-34 Firebee," Northrop Grumman Unmanned Systems, Available: <https://www.northropgrumman.com/Capabilities/BQM34Firebee/Documents/Firebee-DS-05.pdf>
18. Krutein, W., "Ryan Bqm-34 Firebee Target Drone Missile," Pixels.com, Web Site [https://pixels.com/featured/ryan-bqm-34-firebee-target-drone-missile-wernher-krutein.html], Pixels.com, 20 July 2016.
19. Anon., "GQM-163A Coyota," Jane's by IHS Markit, Available: <https://janes.ihs.com/Janes/Display/juav9295-juav>
20. Anon., "GQM-163A Coyota Supersonic Sea Skimming Target," Northrop Grumman, Available: https://www.northropgrumman.com/Capabilities/SupersonicMissileTargets/Documents/Coyote_Factsheet.pdf
21. Keller, J., "Orbital to build 18 GQM-163A Coyote supersonic sea skimming target drones for U.S. Navy and allies," Military & Aerospace Electronics, Web Site [https://www.militaryaerospace.com/unmanned/article/16726795/orbital-to-build-18-gqm163a-coyote-supersonic-sea-skimming-target-drones-for-us-navy-and-allies] Endeavor Business Media, LLC., 5 July 2018.

22. Keshmiri, S., Colgren, R., Farokhi, S., and Mirmirani, M., "Ramjet and Scramjet Engine Cycle Analysis for a Generic Hypersonic Vehicle," 14th AIAA/AHI SPHST Conference, AIAA 2006-8158, 2006, Canberra, Australia.
23. Keshmiri, S., Colgren, R., and Mirmirani, M. "Development of an Aerodynamic Database for a Generic Hypersonic Air Vehicle," AIAA MST Conference, AIAA-2005-35352, San Francisco, California
24. Keller, J., "Orbital to build 18 GQM-163A Coyote supersonic sea skimming target drones for U.S. Navy and allies," Military & Aerospace Electronics, Web Site [<https://www.militaryaerospace.com/unmanned/article/16726795/orbital-to-build-18-gqm163a-coyote-supersonic-sea-skimming-target-drones-for-us-navy-and-allies>] Endeavor Business Media, LLC., 5 July 2018.
25. Lt. Nowell Jr., John B., USN, "Missile Total And Subsection Weight And Size Estimation Equations," Defense Technical Information Center, DTIC, pdf, [<https://apps.dtic.mil/dtic/tr/fulltext/u2/a256081.pdf>], United States Navy, June 1992.
26. Fleeman, E. L., "Missile Design and System Engineering," AIAA Education Series, edited by J. A. Schetz, AIAA, Reston, Virginia, 2012
27. Anon., "Propulsion Products Catalog" Northrop Grumman, PDF, [https://www.northropgrumman.com/Capabilities/PropulsionSystems/Documents/NGIS_MotorCatalog.pdf], northropgrumman.com, June 2018
28. Brown, C., "Elements of Spacecraft Design," American Institute of Aeronautics and Astronautics, Inc., Reston, VA, 2002.
29. Barrett, R. M., "Technical Discussion on Determination of Missile Recovery," The University of Kansas Aerospace Engineering Department, 4:30-5 pm, 5 October 2019.
30. Farokhi, S., "Technical Discussion on Missile Aerothermal Management," The University of Kansas Aerospace Engineering Department, 3:30 - 3:55 pm, 4 October 2019.
31. Anon., "Launch Rail Image," Shopify, Available: https://cdn.shopify.com/s/files/1/0093/8940/8315/products/ZLL-Render-Small_300x300.png?v=1549156593
32. Anon., "Flatbed Truck Image", Clipart, Available: https://www.clipartwiki.com/iclip/xiTiom_semi-truck-png-flatbed-semi-truck-png/
33. Sutton, G., Biblarz, O., "Rocket Propulsion Elements," John Wiley & Sons, Inc., Hoboken, New Jersey, 2017.
34. Farokhi, S., "Technical Discussion on Propulsion System Selection," The University of Kansas Aerospace Engineering Department, 5:15 - 5:30 pm, 3 October 2019.
35. Farokhi, Saeed, "Aircraft Propulsion," The University of Kansas, 2nd ed., Wiley, New York, 2014.
36. Anon., "Launcher Engine - 2" Launcher Space, Available: [<https://launcherspace.com/engine-2>].
37. Caywood, W., Ravello, R., Weckesser, L., "Tactical Missile Structure and Materials Technology," Johns Hopkins APL, Technical Digest, 2006.
38. Abott, J. M., Anderson, B. H. ,and Rice, E. J., "Inlets, Ducts, and Nozzles," NASA CR-2523, February 1990.
39. Shandor, M., Stone, A. R., Walker, R. E., "Injection Vector Control," Johns Hopkins APL, Technical Digest, 1963.
40. Beebe, S. I., "Hole-Type Aerospike Compound Nozzle Thrust Vectoring," California Polytechnic State University, Master of Science Thesis, San Luis Obispo, CA, 2009.
41. Barrett, R. M., "Technical Discussion on Determination of High Lift Device Requirements," The University of Kansas Aerospace Engineering Department, 1:00 - 2:00 pm, 30 September 2019.
42. Barrett, R. M., "AE521_SSAT_RB3_Master," Vimeo, Web Site, [<https://vimeo.com/364696979>], accessed 9 October 2019.
43. Fleeman, E. L. "Tactical Missile Design, TMD, Spreadsheet," [Excel Spreadsheet], 29 August 2012, available for

download at <https://arc.aiaa.org/doi/suppl/10.2514/4.869082>.

44. Anon., “Federal Size Regulations for Commercial Motor Vehicles,” U.S. Department of Transportation Federal Highway Administration, Web Site, [https://ops.fhwa.dot.gov/freight/publications/size_regs_final_rpt/index.htm#c-mv], accessed 25 October 2019.
45. Barret, R. M., “Technical Discussion on Supersonic Missile V-n Diagrams,” The University of Kansas Aerospace Engineering Department, 12:30 - 12:50 pm, 24 October 2019.
46. Roskam, J., “Airplane Flight Dynamics and Automatic Flight Controls; Part II: Chapters 7 Through 15,” Roskam Aviation and Engineering Corporation, Lawrence, KS, 1979.
47. Roskam, J., “Airplane Flight Dynamics and Automatic Flight Controls; Part I: Chapters 1 Through 6,” Roskam Aviation and Engineering Corporation, Lawrence, KS, 1979.
48. Barrett, R. N., “AE521_SSAT_RB4_movie,” Vimeo, Web Site, [<https://vimeo.com/370004970>], accessed 30 October 2019.
49. Darling, J. A., “Handbook of Blunt-Body Aerodynamics Volume 1: Static Stability,” Naval Ordnance Laboratory, NOLTR 73-225, White Oak, Silver Spring, MD, December 1973.
50. Jorgenson, L. H., “A Method for Estimating Static Aerodynamic Characteristics for Slender bodies of Circular and Noncircular Cross Section Alone and With Lifting Surfaces at Angles of Attack from 0° to 90°,” NASA TN D-7228, April 1973.
51. Ross, M. N., Sheaffer, P. M., “Radiative Forcing Caused by Rocket Engine Emissions,” American Geophysical Union, Washington, District of Columbia, 28 April 2014.
52. Anon., “Overview of Greenhouse Gases,” Environmental Protection Agency, Web Site [https://www.epa.gov/gh-gemissions/overview-greenhouse-gases/carbon_dioxide_emissions/], United States Environmental Protection Agency, 11 April 2019.
53. Moog Inc., Aerospace Products, “Gimbals”, document, Available: <https://www.moog.com/products/space-mechanisms/gimbals.html>.
54. Clinton, F. E., “Thrust Vector Control for Nuclear Thermal Rockets,” NASA TM D-2180, April 2013.
55. Taghavi, R., “Technical Discussion on Propulsion System and Thermal Management,” The University of Kansas Aerospace Engineering Department, 2:00 - 2:45 pm, 21 November 2019.
56. Anon., “Outriggers,” Liftmoore, Inc., Web Site [<http://liftmoore.com/outriggers/>], accessed 28 November 2019.
57. Anon., “Bolt, Explosive ”Ensign-Bickford Aerospace & Defense Company Web Site: [<https://www.eba-d.com/products/bolt-explosive/>], accessed 1 December 2019.
58. Barrett, R. M., “Technical Discussion on End Game Procedures and Recovery Options,” The University of Kansas Aerospace Engineering Department, 4:00 - 5:30 pm, 22 November 2019.
59. Potvin, J., “Calculating the Descent Rate of a Round Parachute,” Parks College Parachute Research Group, Web Site [pcprg.com/rounddes.htm], accessed 24 November 2019.
60. Barrett, R. M., “Technical Discussion on Structural Design and Advanced Technologies,” The University of Kansas Aerospace Engineering Department, 4:00 - 4:45 pm, 6 December 2019.
61. Anon., “Airborne Systems: Product Line, Cargo Delivery Systems,” Web Site [<https://airborne-sys.com/products/cargo-delivery-systems/>], accessed 7 November 2019.
62. Mouritz, A. P., Introduction to aerospace materials, Reston, VA: American Institute of Aeronautics and Astronautics, 2012.
63. Barrett, R. N., “Report_Block6_secs1&2,” Vimeo, Web Site, [<https://vimeo.com/379174658>], accessed 12 December 2019.